Magma processes of the Younger and Older granites in the Yanai district of the Ryoke belt, southwest Japan

Eri AKASAKI

Graduate School of Science and Engineering
Yamaguchi University
Doctoral dissertation

Abstract

The Cretaceous granitic rocks in the Chugoku district, Southwest Japan arc, are divided into three groups; Older Ryoke granites, Younger Ryoke granites and San'yo granites. The Kibe Granite, representative Younger Ryoke granite in the Yanai district, Yamaguchi Prefecture, occurs as an elliptic suite accompanied by a coeval Himurodake Quartz diorite, and intrudes the high-grade part of Ryoke metamorphic rocks. The lithology of the Kibe granite generally shows a homogeneous biotite-granite including euhedral K-feldspar as phenocrysts and locally containing micro-magmatic enclaves. The granite shows migmatitic structures involving pelitic gneisses at the marginal part of the suite. On the other hand, mixing and mingling structures are recognized in the contact zone between the Kibe Granite and the Himurodake Quartz diorite. The major and trace element variations of the Kibe Granite seem to be explained by subtraction of plagioclase with minor biotite and K-feldspar from a single parental magma. In addition to the fractional crystallization process, the results of Sr isotopic studies reveal that the Kibe Granite was influenced by interaction among the granitic magma, pelitic gneisses and/or the Himurodake Quartz dioritic magma. The Kibe Granite would, therefore, be derived from the complicated magma processes including assimilation of the pelitic gneisses, magma mixing with the Himurodake Quartz diorite and fractional crystallization. These magma processes probably occurred during the exhumation stage of the Ryoke metamorphic belt along its isothermal decompression path. The Gamano-Obatake Granodiorite locally shows migmatite structures, and the boundary with the Kibe Granite is obscure. The corroded plagioclase coexisting with quartz and K-feldspar can be observed in the migmatite structure. This texture is regarded as mixture of a residual plagioclase and anatectic melt under the eutectic situations. The epsilon Sr and Nd isotopic compositions of the Gamano-Obatake Granodiorite are plotted within the Kibe Granite. The field occurrence and petrographical features suggest that the partial melting probably took place in the Gamano-Obatake Granodiorite. The isotopic data combined with occurrence and petrography of these granitic rocks suggests that the partial melting probably took place in the Gamano-Obatake Granodiorite, giving rise to the Kibe Granite magma. The Himurodake

Quartz diorite is thought to be a heat source at this event. Consequently, the Ryoke granitoids continuously intrude the crust from the Older Ryoke granite to the Younger Ryoke granite with strong connection related to their petrogenesis.

Contents

Figure and table list

Chapter 1. Introduction

1-1. Previous studies

Mesozoic to Paleogene Tertiary granitic rocks occur in the continental margin of the circum Pacific region. These granitic rocks are widely exposed in the Southwest Japan where the granitic rocks are divided into the Ryoke, San'yo and San'in belts in terms of their lithologies, geochemical compositions, accompanied ore deposits and formation ages (Ishihara, 1971). On the other hand, Kagami et al. (1992) divided the granitic rocks into the North, Transitional and South Zones based on their Sr isotopic compositions. In addition, they claimed that the Sr isotopic compositions should reflect those of upper mantle to lower crust, where is regarded as a source region of dioritic to granitic magmas. The boundary of each zone defined by Kagami et al (1992) is almost parallel to sub-parallel to the boundaries between San'in, San'yo and Ryoke belts.

The Ryoke belt consists of Cretaceous granitic rocks and low-P/high-T type metamorphic rocks. The granitic rocks from the Ryoke belt (the Ryoke granitoids hereafter) are widely exposed in the belt rather than the metamorphic rocks. The Ryoke granitoids are mainly exposed in three districts: the Chubu district, the Kinki district and the Chugoku distridt.

Koide (1958) investigated the Ryoke granitoids in the Dando area, Aichi Prefecture, and classified these granitoids into the Older Ryoke granite and the Younger Ryoke granite. According to Koide (1958), the Older Ryoke granite undergoes regional metamorphism with pervasive foliation, whereas the Younger Ryoke granite gives the thermal effect to the surrounding metamorphic rocks. Sakai et al. (1965) and Yamada (1966) redefined the term "Older and Younger Ryoke granties". They discovered that the Inagawa-Sumikawa granite belonging to the Younger Ryoke granite intruded into the Nohi Ryolites, and gave the contact metamorphism to the Nohi Ryolites. Therefore, they proposed that the magma activity of the Younger Ryoke granite occurred after eruption of the Nohi Ryolite. On the other hand, the mutual relationships between the Older granite and the Nohi Ryolite is not confirmed at that time (Yamada, 1971; Ryoke Research Group, 1972). Harayama et al. (1985) revealed that the

magma activity of Nohi Ryolites was prolonged. In addition, they claimed that the rhyolite and the Younger Ryoke granite occurred as a volcano-plutonic complex. Therefore, the magma activity of Nohi Rhyolites cannot be used as the time marker of the boundary between the Older and Younger Ryoke granites.

Okamura (1957) studied both the Ryoke metamorphic rocks and granitoids from the western part of Chugoku district. He explained that the Paleozoic sediments were undergone by metasomatism introducing the alkai-alumina emanation, and were progressively transformed into the following metamorphic series; biotite schists → banded gneisses → migmatites → granites from shallower to deeper level of the crust. After this metasomatic event, the granitic magmas intruded into the metamorphic rocks. Okamura (1957) and Higashimoto et al. (1983) defined the Older and Younger Ryoke granites in this region in terms of occurrence and microstructures because there are no any volcanic rocks such as the Nohi Rhyolite in this region. The Older Ryoke granite consistently intrudes into the metamorphic rocks and shows gneissose structures. On the contrary, the Younger Ryoke granite discordantly intrudes the structures of metamorphic rocks.

According to Yokoyama (2009), the Ryoke granitoids were divided into the Older and Younger granites in terms of their structural elements. He defined that the Older Ryoke granite shows a sheet-like suite with pervasive foliations parallel to those of the host-metamorphic rocks. The Younger Ryoke granite are subdivided into three types, Types 1 ~ 3, but all types of the Younger Ryoke granites discordantly intrude the host-metamorphic rocks. Types 1, 2 and 3 granites are characterized by individual structural features; discordant-disharmonic granites, discordant-harmonic granites and discordant-massive granites, respectively.

Okano and Honma (1983) reported Rb-Sr isotopic ratios of the Older and Younger Ryoke granites in the Yanai district, Yamaguchi Prefecture, and they expressed that the Older Ryoke granite was resulted from process of contamination between the granitic magma and the host gneisses. On the other hand, Moutte and Iiyama (1984) and Moutte (1990) inferred that the quartz diorites accompanied by the Older and Younger Ryoke granites could be of the parental magma of the granitic rocks because these intrusive rocks formed monotonous trends on the

variation diagrams. However, they did not show any reasons for the compositional changes among these rocks. Suzuki et al. (1996) and Suzuki and Adachi (1998) determined the monazite CHIME ages for the Older and Younger Ryoke granites from the Yanai district. They revealed that the intrusive ages show the period from 95Ma to 90Ma.

In the final decade of 20th century, the petrological and geochronological studies were performed on the individual granite suites mainly from the Chubu district (Kutsukake,1993; Yuhara 1994; Kutsukake, 1997; Yuhara and Kagami 1999; Yuhara et al. 2000; Kutsukake, 2002; Yuhara, 2008). For instance, Sr and Nd isotopic studies revealed the petrological character of the granitic magma and newly defined the classification of the petrological province (Kagami et al., 1992; Yuhara 1994; Yuhara and Kagami 1999; Yuhara 2000; Yuhara et al. 2000). The geochronology for the CHIME method confirmed that the magma activity of the Ryoke granitoids sifted toward the east of the belt (Suzuki et al. 1996; Suzuki and Adachi, 1998). In addition, Yuhara et al. (1999, 2000) and Kutsukake (2002) investigated the Ryoke granitods from the Chubu district and reported the petrogenesis of granitic magma. They claimed that the Ryoke granitoids would be derived from the partial melting of mafic lower crust and subducted oceanic crust.

1-2. Aim of this study

According to the previous researches, there is still remaining big problem regarding the Ryoke granitoids; 1) magma process of the granite and 2) classification of the granite. Okano and Honma (1983) revealed that the contamination of the Ryoke metamorphic rocks is an important process to produce the Ryoke granitoids. On the other hand, Moutte (1990) claimed that the chemical variation of the Ryoke granitoids in Yanai district is mainly controlled by the fractional crystallization. Both studies, however, do not show the enough evidence regarding the magma processes and petrogenesis of granitic magma.

The Ryoke granitoids were classified into the Older and Younger Ryoke granites. Harayama (1985) claimed that it is not suitable terms because of the following reasons. The magma activity of the Younger Ryoke granite overlaps with that of the Nohi Rhyolite and the

field relationship between the Older Ryoke granite and the Nohi Rhyolite is still unclear. In addition, there are no volcanic equivalents to the Nohi Ryolites in the Yanai district (Imaoka et al., 1994).

The Yanai district is one of the typical areas of the Ryoke metamorphic belt. The very low- to high-grade metamorphic rocks appear in this area and both the Older and Younger Ryoke granites widely crop out. In other words, all rock types consisting of the Ryoke metamorphic belt can be observed in the Yanai district. Therefore, the detail petrological investigation of intrusive rocks in this area can analyze the typical magma processes in the Ryoke metamorphic belt.

To resolve the above-mentioned problem, the author addresses geology, petrography and geochemisty of the Ryoke granitoids. The Kibe Granite belonging to the Younger Ryoke granite is associated with the Himurodake Quartz diorite. This mode of occurrence gives us good opportunity to analyze the chemical variation of intrusive rocks through the process of magma mixing and/or mingling. Furthermore, the Gamano-Obatake Granodiorite, one of the typical Older Ryoke granites, is also investigated regarding the petrogenitic relationships between the Older and Younger Ryoke granite. Finally, the author discusses the magma process of the Kibe Granite and shows the schematic model for the formation of granitic magma. The magma process of the granitic rocks provides us the valuable information for the growth and differentiation of continental crust (Gromet and Silver, 1987; Wedepohl, 1991, 1995; Kagami et al., 1999; Kutsukake, 2002; Kamei, 2002; Jahn et al., 2004). Therefore, it is further expected that the study should fundamentally clarify the formation of continental crust in the active continental margin.

Chapter 2. Geological outline

The Yanai district, the eastern part of Yamaguchi Prefecture, is underlain by the Ryoke metamorphic rocks and granitic rocks of the Ryoke and San'yo belts (Fig. 2-1). The Ryoke metamorphic rocks are composed mainly of schists and genisses, and their protoliths are considered to be the Kuga Group corresponding to the Jurassic accretionary complexes including pelitic rocks, sandstones and cherts with trace amounts of limestones (Higashimoto et al., 1983). The metamorphic grade in this region progressively increases from north to south (Okudira et al., 1993, 2001; Ikeda, 1998).

The granitic rocks of the Ryoke belt (the Ryoke granitoids, hereafter) are divided into the Older and Younger granites. These granites intrude the medium- to high-grade portions of the Ryoke metamorphic rocks. The Ryoke granitoids studied here are the Gamano Granodiorite, the Obatake Granodiorite, the Kibe Ganite and the Namera Granite (Fig. 2-1). The Gamano and the Obatake Granodiorites belong to the Older granite, whereas the Kibe and Namera granites are of the Younger granite (Okamura, 1957). In this paper, the author newly defines "the Gamano-Obatake Granodiorite" and "the Himurodake Quartz diorite". The Gamano-Obatake Granodiorite is defined as gathering both the Gamano and the Obatake Granodiorites because there are little difference of lithofacies and constituent minerals. The Himurodake Quartz diorite is used to be called as "the quartz diorite in the Himurodake area" by Moutte (1990). The Himurodake Quartz diorite re-defined here is characterized by occurring as stocks and dikes with medium to fine grained massive structure.

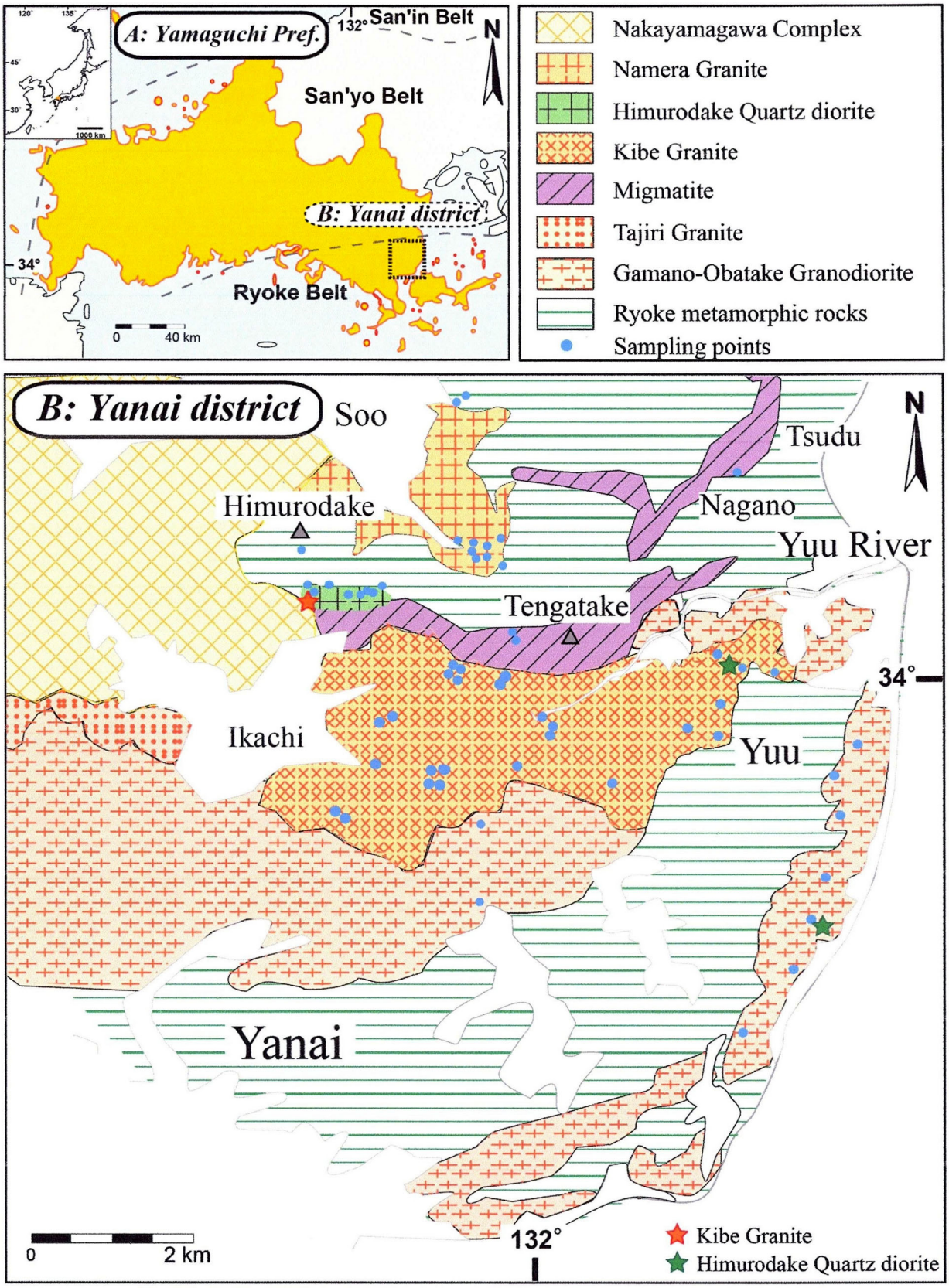

Fig. 2-1 Geological map of the Yanai district. A: Index map of the Ryoke, San' yo and San' in Belts. B: Geological map of studied area. The data are compiled from Higashimoto et al. (1983), Okudaira (1993) and Suzuki et al. (1996).

Chapter 3. Geology of the Yanai district

The geology of the Yanai district consists mainly of the Ryoke metamorphic rocks and the Ryoke Granitoids. In this chapter, the mode of occurrence of the metamorphic rocks and granitoids is described. Mutual relationships among these rocks are shown in Fig.3-1.

3-1. Ryoke metamorphic rocks

The Ryoke metamorphic rocks described here are located in three areas, the Gamano-Obatake area, the Himurodake area and the Namera area. The metamorphic rocks in the Gamano-Obatake area are composed mainly of pelitic rocks and are intruded by the Ryoke granitoids (Fig. 3-1-1). The metamorphic rocks belong to the garnet-cordierite zone (Ikeda, 1998), which is recognized as the highest-grade part of the Ryoke Metamorphic Belt in the Yanai district.

The Himurodake area located in the northern end of the Kibe granite is underlain by pelitic gneisses (Fig. 3-1-2). These gneisses belong to the cordierite-K-feldspar and garnet-cordierite zones (Ikeda 1998).

The metamorphic rocks in the Namera area are composed mainly of pelitic rocks, occurring in the northern margin of the Namera Granite. These metamorphic rocks underwent the medium-grade metamorphism belonging to the K-feldspar-corderite zone (Fig. 3-1-3, Ikeda 1998).

3-2. Gamano-Obatake Granodiorite

The Gamano-Obatake Granodiorite is exposed in the Iwakuni and Yanai Cities with 24 km in E-W and 15 km in N-S (Fig. 2-1). This granodiorite occurs as a sheet-like body concordant with the Ryoke metamorphic rocks. This rock is locally associated with mafic magmatic enclaves (MMEs) and the host gneisses.

The Gamano-Obatake Granodiorite lithologicaly shows the medium- to coarse-grained

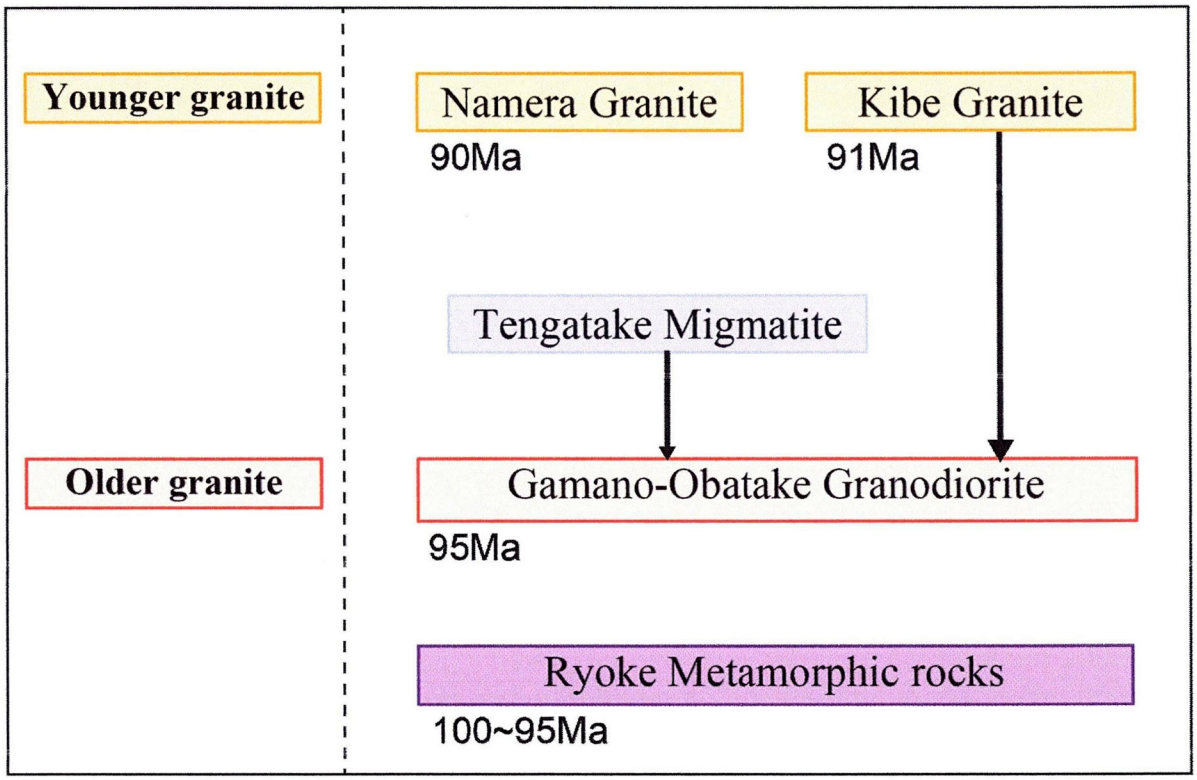

Fig. 3-1 Mutual relationships among the Ryoke granites and the Ryoke metamorphic rocks.The data are compiled from Higashimoto et al. (1983), Okudaira (1993), Suzuki et al. (1996) and Okudira et al. (2001).

Fig. 3-1-1 Occurence of the pelitic gneiss in the Gamano-Obatake area.

Fig. 3-1-2 Occurence of the pelitic gneiss in the Himurodake area.

Fig. 3-1-3 Occurence of the pelitic gneiss in the Namera area.

biotite granodiorite with light gray color and has a gneissose structure parallel to the foliation of the host rocks (Fig. 3-2-1). Garnets are locally observed.

3-3. Migmatite

The migmatite is classified into the Nagano Migmatite and the Tengatake Migmatite (Fig. 2-1). Both migmatites are considered as an injection type migmatite, but not as an in-situ anatexite (Okudaira, 1993; Okudaira and Seo, 1996). Most of paleosomes in both migmatites are of pelitic gneisses and metamorphosed cherts of the Ryoke metamorohic rocks; thereby, the migmatite has been produced by the mixture of the Ryoke metamorphic rocks and a granitic melt (Okudaira, 1993; Okudaira and Seo, 1996).

The Nagano Migmatite occurs in the northeastern side of the Kibe Granite and the northern end of the Gamao-Obatake Granodiorite (Fig. 2-1). This migmatite possesses the specific structures, *e.g.*, agmatitic, venitic and nebulitic structures (Fig. 3-3-1). The Tengatake Migmatite is exposed in the northern part of the Kibe Granite (Fig. 2-1) and shows raft-like, venitic and schlieren structures (Fig. 3-3-2).

3-4. Himurodake Quartz diorite

The Himurodake Quartz diorite occurring as small stocks (Fig. 2-1) is recognized at three places of this region; the northwestern and inner parts of the Kibe Granite and the inner part of the Gamano-Obatake Granodiorite (Fig. 2-1). The rock is of medium to fine-grained with gray to dark gray color.

The Himurodake Quartz diorite shows the mingling structure at the contact zone of the Kibe Granite (Fig. 3-4-1). On the other hand, the quartz diorite occurring in the inner part of the Gamano-Obatake Granodiorite is associated with a leucocratic granite (Fig. 3-4-2), which has weak foliations similar to the Kibe Granite. The leucocratic veins intrude into the Himurodake Quartz diorite.

A

B

Fig. 3-2-1 Occurence of the Gamano-Obatake Granodiorite. A: the granodiorite including the mafic magmatic enclave. B: close up view of the granodiorite showing migmatite structure.

A

B

Fig. 3-3-1 Occurence of the Nagano Migmatite.

A

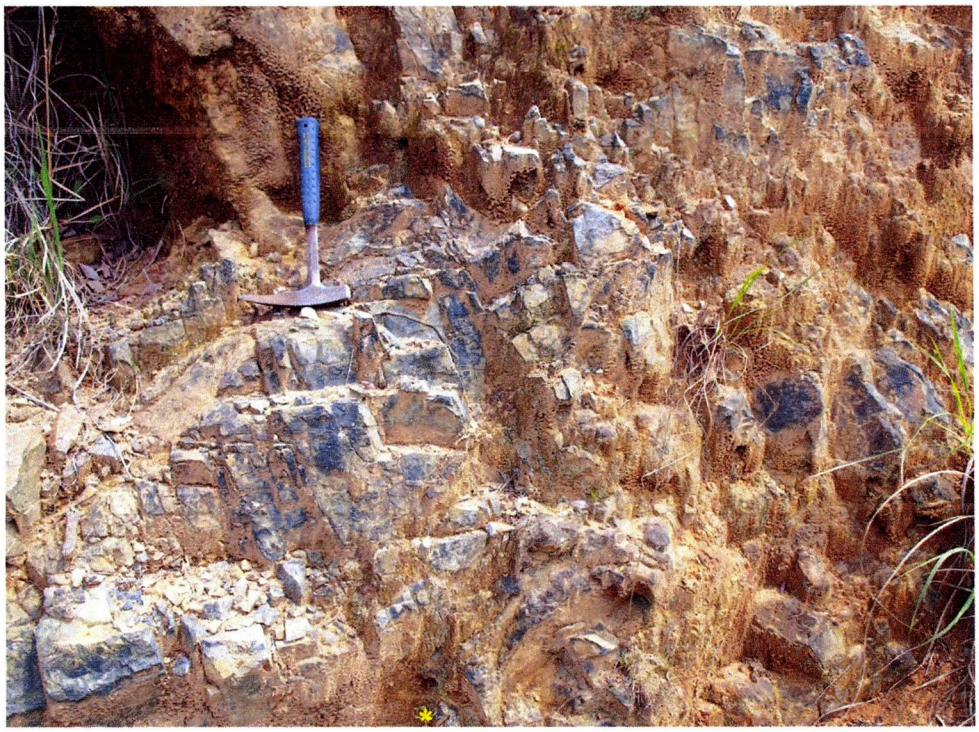

B

Fig. 3-3-2 Occurence of the Tengatake Migmatite.

A

B

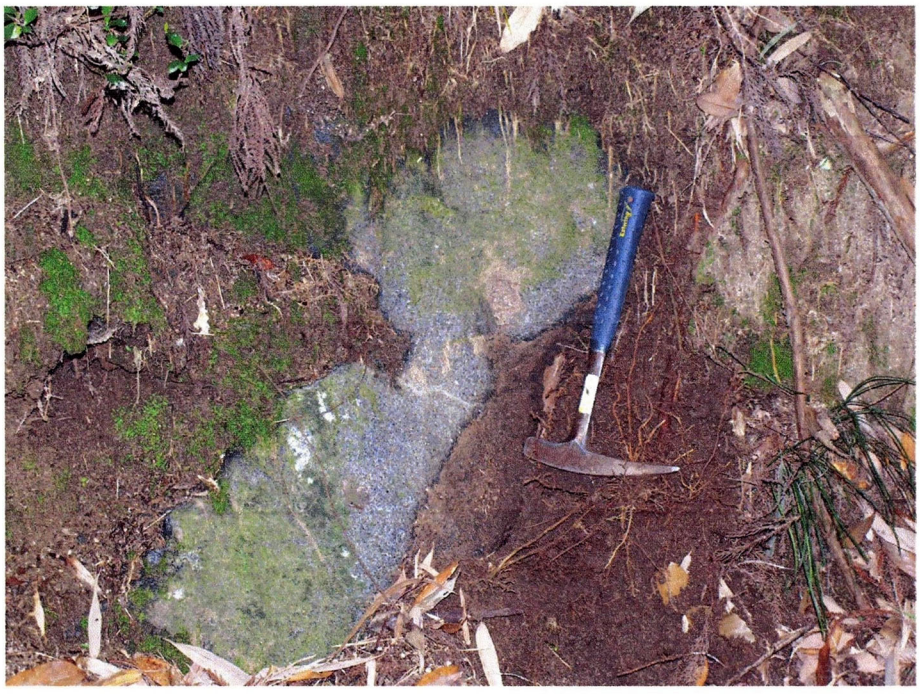

Fig. 3-4-1 Occurence of the Himurodake Quartz diorite. A: the Himurodake Quartz diorite is intruded by the granitic veins derived from the Kibe Granite. B: Contact between the Himurodake Quartz diorite (gray) and the Kibe Granite (white).

A

B

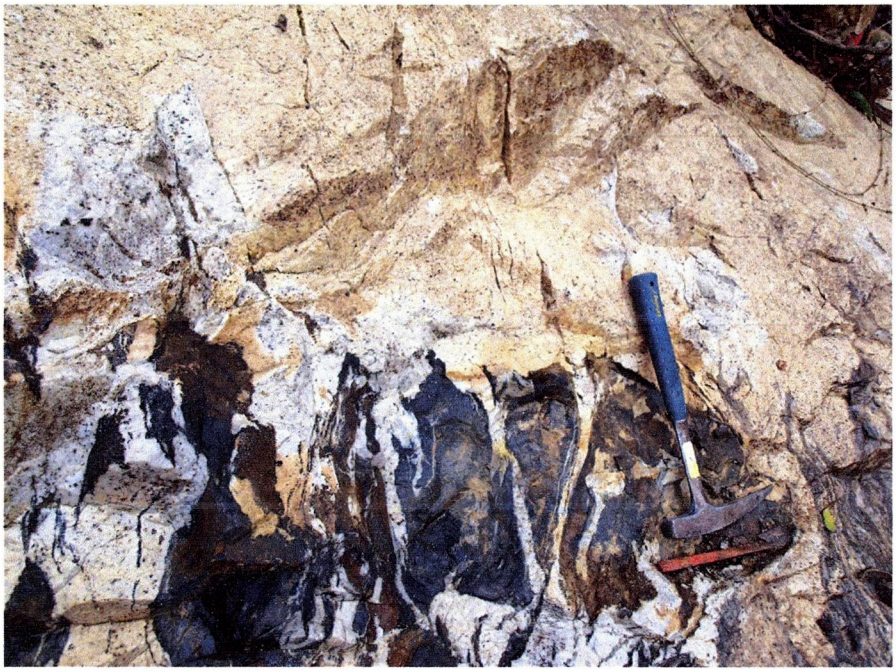

Fig. 3-4-2 Occurence of the Gamano-Obatake Granodiorite and the Himurodake Quartz diorite. Note that the Himurodake Quartz diorite (dark colored parts) intrudes the Gamano-Obatake Granodiorite. Leucocratic patches and pools appear in the Gamano-Obatake Granodiorite showing migmatite structure. The leucocratic veins derived from migmatite leucosomes intrude into the Himurodake Quartz diorite.

3-5. Kibe Granite

The Kibe Granite is situated along the Yu'u river, Iwakuni City, and occurs as an elliptic shape with 7 km long in E-W and 3 km wide in N-S (Fig. 2-1). The granite intrudes the Ryoke metamorphic rocks and the Gamano-Obatake granodiorite (Higashimoto et al., 1983). However, the Kibe granite is surrounded by the Gamano-Obatake Granodiorite on the geological map, but the boundaries between them are obscure based on the field observations.

The Kibe Granite is of biotite granite characterized by K-feldspar phenocrysts up to 9 mm (Figs. 3-5-1A and 3-5-1B). The granite shows migmatitic features at the border of the metamorphic host rocks (Fig. 3-5-1C). In places, leucocratic veins derived from the granite penetrate along the foliations of gneisses, but cut the foliations. On the other hand, the granite locally includes MMEs with a few cm to 20 cm size in the central part of suite (Fig. 3-5-1D). In addition, the Kibe Granite locally shows leucocratic and fine-granined lithofacies nearby the Himurodake Quartz diorites (Fig. 3-4-1).

3-6. Namera Granite

The Namera Granite belonging to the Younger Ryoke granite occurs at the northern part of the Kibe Granite with 3 km in E-W and 3 km in N-S (Fig. 2-1). The granite intrudes the Ryoke metamorphic rocks, and gives contact metamorphism to the host rocks (Nureki, 1974). In the western side of suite, the granite is intruded by the Soo Granodiorite (the Younger Ryoke granites) and the Nakayamagawa Complex (the San'yo granites) (Higashimoto et al., 1983).

The Namera Granite is of medium-grained biotite granite (Fig. 3-6-1). Garnets and cordierites showing greenish replaced by pinite are observed. The granite shows leucocratic containing muscovites and garnet occurring at the marginal part of the suite.

A

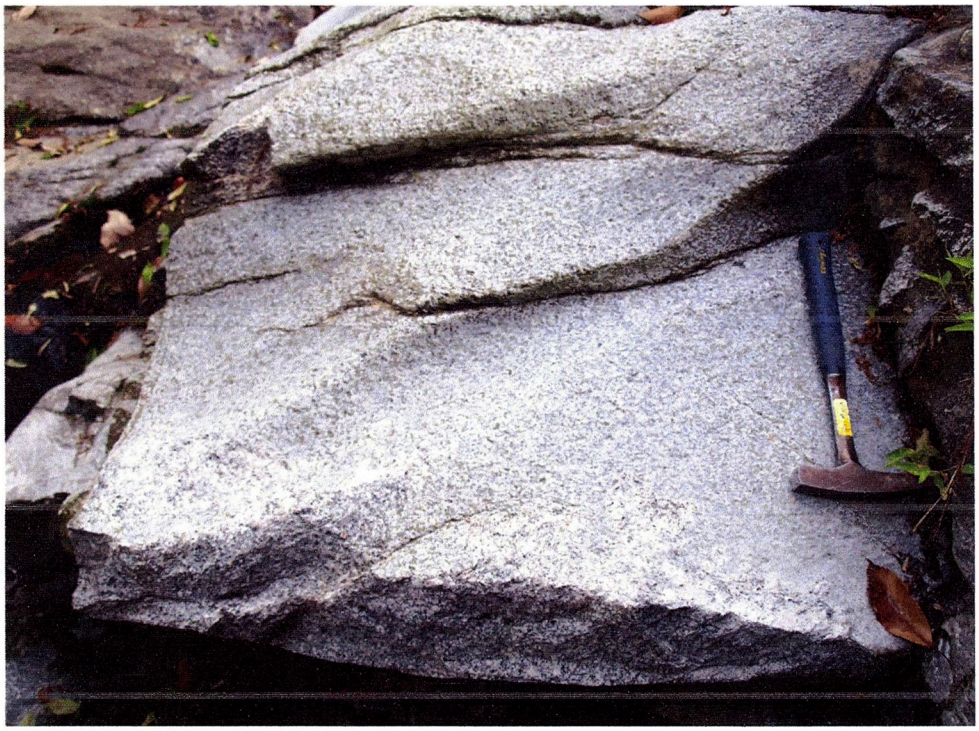

B

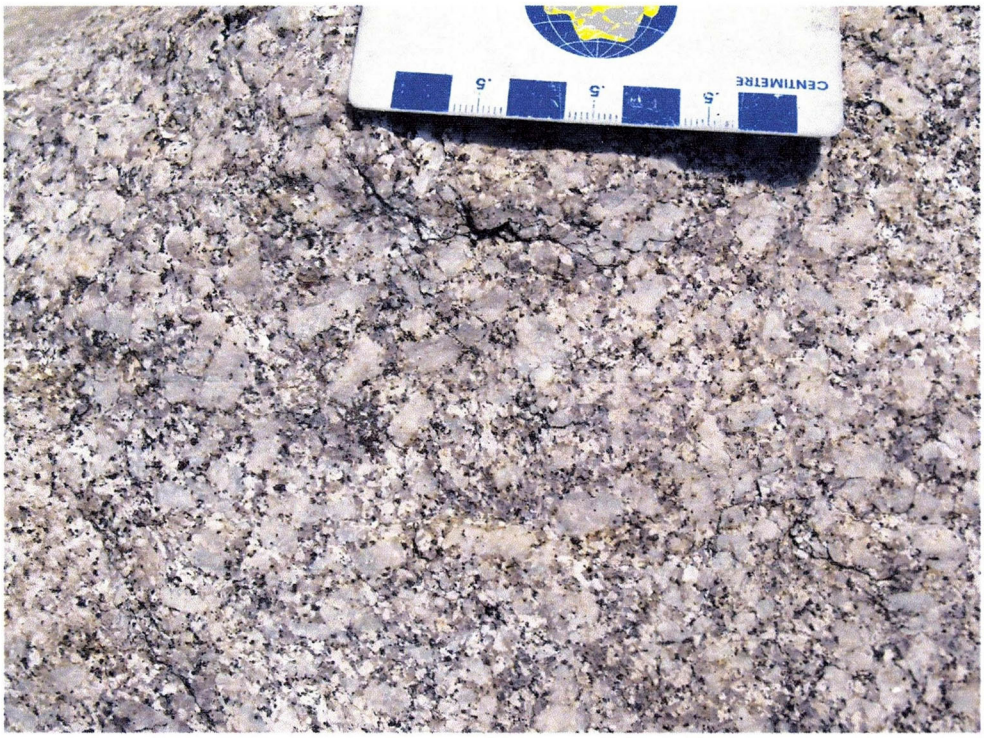

Fig. 3-5-1 Occurence of the Kibe Granite. A: the granite with massive structure. B: close up view of the granite containing K-feldspar phenocrysts.

C

D

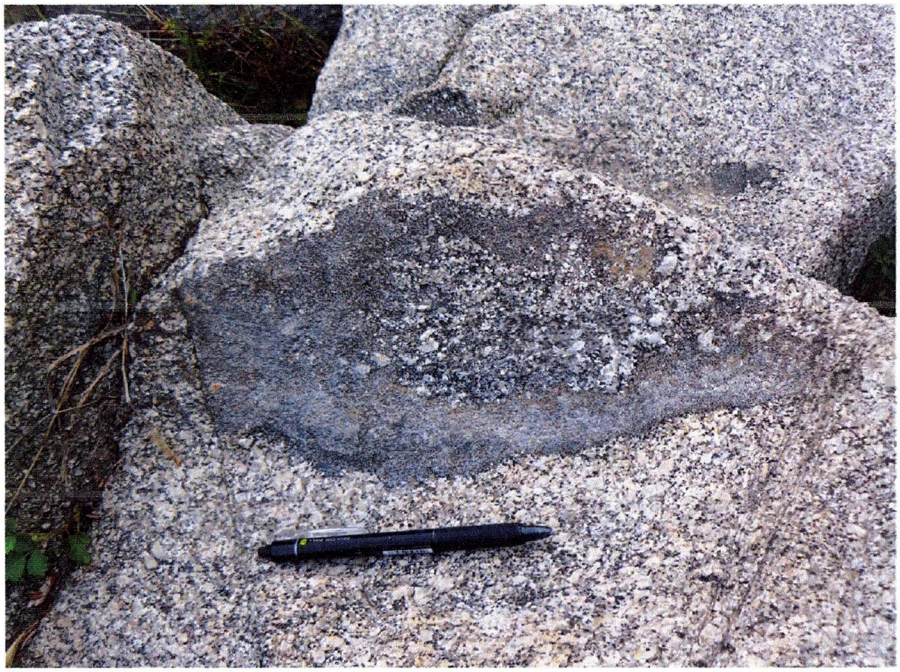

Fig. 3-5-1 Occurence of the Kibe Granite. C: relationship between the Kibe Granite and the host pelitic gneiss. This exposure shows migmatitic structure. D: occurence of a mafic enclave in the Kibe Granite. Note that the enclave generally contact with the host granite in sharp contact, whereas gradually change to the granite in some places.

A

B

Fig. 3-6-1 Occurence of the Namera Granite.

Chapter 4. Petrography

4-1. The Ryoke metamorphic rocks

As previously described, the metamorphic grade of the Ryoke metamorphic rocks in the Yanai district increases from north to south (Okudira et al., 1993, 2001; Ikeda, 1998). The author described the Ryoke metamorphic rocks on the following areas where the Ryoke granitoids studied here intruded; the Gamano-Obatake area, the Himurodake area and the Namera area. The Ryoke metamorphic rocks in these areas have mainly the pelitic compositions, thus in this section, the author has described the pelitic metamorphic rocks as a representative of the Ryoke metamorphic rocks.

4-1-1. The Gamano-Obatate area

The fine-grained biotite gneiss belonging to the garnet-cordierite zone (Ikeda, 1998) has a banded structure with melanocratic and leucocratic thin layers. It consists mainly of biotite, quartz, plagioclase, K-feldspar, cordierite and garnet (Fig. 4-1-1-1). Zircon and opaque minerals are ubiquitously included as accessory minerals. Muscovite occurs as secondary altered minerals. Biotite grains form a gneissose structure, and have bimodal grain sizes with 0.1 to 0.3 mm and 1 to 2 mm. Both biotite grains show X' = light brown, Z' = brown in pleochroism. Some biotite crystals contain zircon inclusions with pleochroic halos. Quartz has bimodal grain sizes with 0.3 to 1 mm and 1 to 3 mm. Quartz grains showing large grain size locally includes small crystals of biotite and plagioclase. Plagioclase has also bimodal grain sizes with 0.2 to 1 mm and 1 to 2 mm. Both plagioclases weakly have zoning structures and clearly show albite twin and often include small crystals of quartz and biotite. K-feldspar shows anhedral shapes with 0.5 to 2 mm. Cordierite is of 0.3 to 2 mm and is replaced by pinite. Garnet is 0.1 to 1 mm and often includes small crystals of quartz and biotite.

09032207C

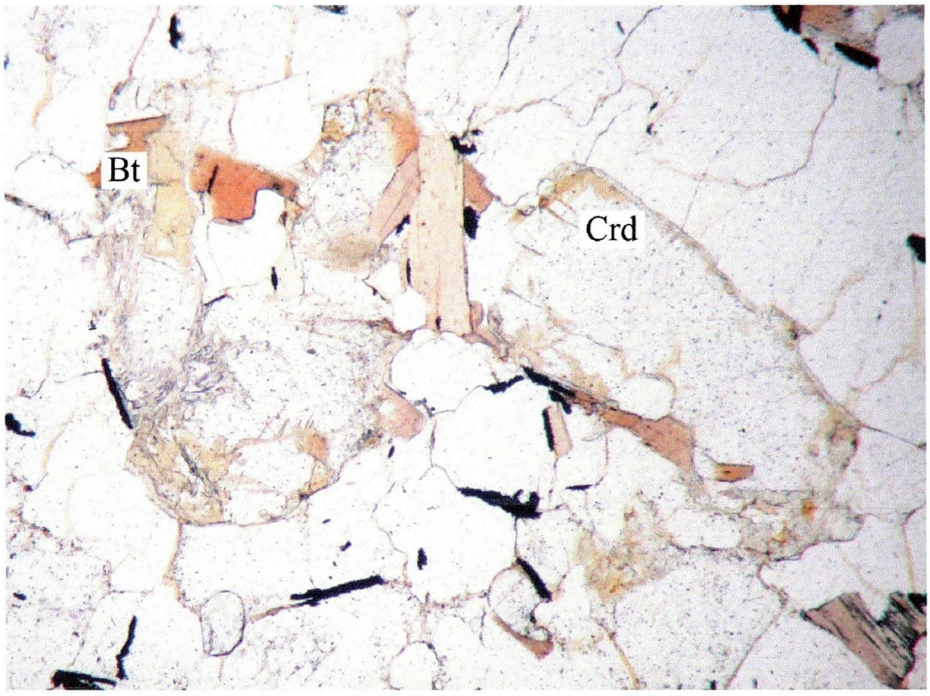

open nicol

0.75 mm

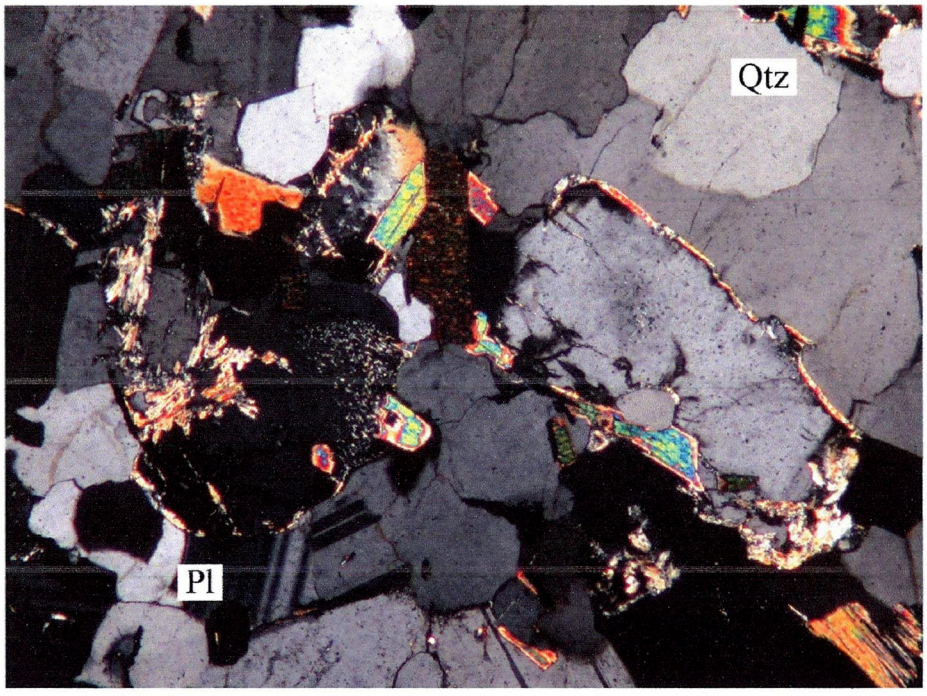

crossed nicols

0.75 mm

Fig. 4-1-1-1 Photomicrographs of the pelitic gneiss in the Obatake area. Bt: biotite, Crd: cordierite, Pl: plagioclase, Qtz: quartz.

4-1-2. The Himurodake and Namera areas

The pelitic gneiss in this area represents the metamorphic grade of the cordierite – K-feldspar zone (Ikeda, 1998). It consists mainly of biotite, quartz, plagioclase, K-feldspar and porphyroblastic cordierite (Fig. 4-1-2-1, Fig. 4-1-2-2). The mineral assemblage is similar to the pelitic gneiss from the Gamano-Obatake area but lacking garnet-cordierite paragenesis.

4-2. Gamano-Obatake Granodiorite

This suite consists mainly of plagioclase, quartz, biotite, and K-feldspar with small amount of garnet (Fig. 4-2-1). It weakly possesses foliations. Zircon, apatite, allanite and opaque minerals are ubiquitously included as accessory minerals. Plagioclase shows euhedral to subhedral shape, and weakly has zoned structures and clearly shows albite twin. The twin faces locally show curvature shapes. The plagioclase grains show bimodal size and shapes; granular crystals with 0.1 to 0.5 mm and tabular crystals with 1 to 7.5 mm. Some plagioclase grains include small crystals of biotite, quartz and zircon, and are locally replaced by sericite. Quartz shows anhedral shapes with 0.2 to 6 mm, and strongly exhibits wavy extinction. It often includes small crystals of biotite, plagioclase, zircon and apatite. Biotite shows subhedral to anhedral shape with 0.1 to 2 mm. It clearly shows X' = light brown, Z' = brown in pleochroism. Some biotite crystals include zircon and apatite with a trace amount of allanite. Pleochroic halos appear around zircon and/or allanite inclusions. Chlorite locally replaces biotite as a result of alteration. K-feldspar shows anhedral shape with 0.3 to 3 mm. Myrmekite occurs in the boundary between plagioclase and K-feldspar. Garnet shows euhedral to subhedral shape with 0.3 to 2.5 mm.

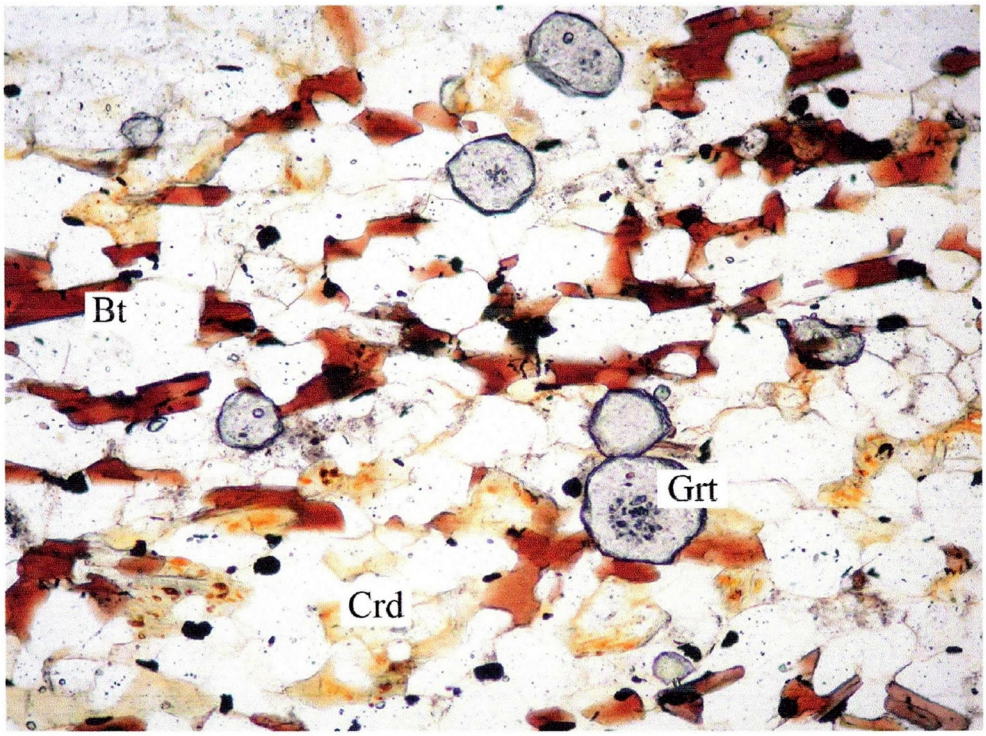

Fig. 4-1-2-1 Photomicrographs of the pelitic gneiss in the Himurodake area. Bt: biotite, Crd: cordierite, Grt: garnet.

10032102A

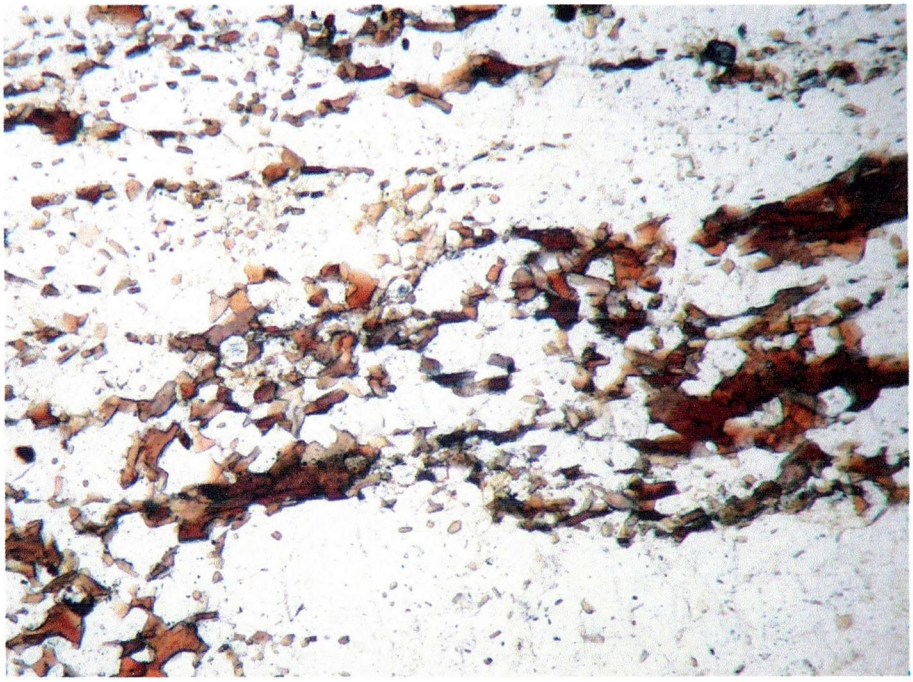

open nicol

0.75 mm

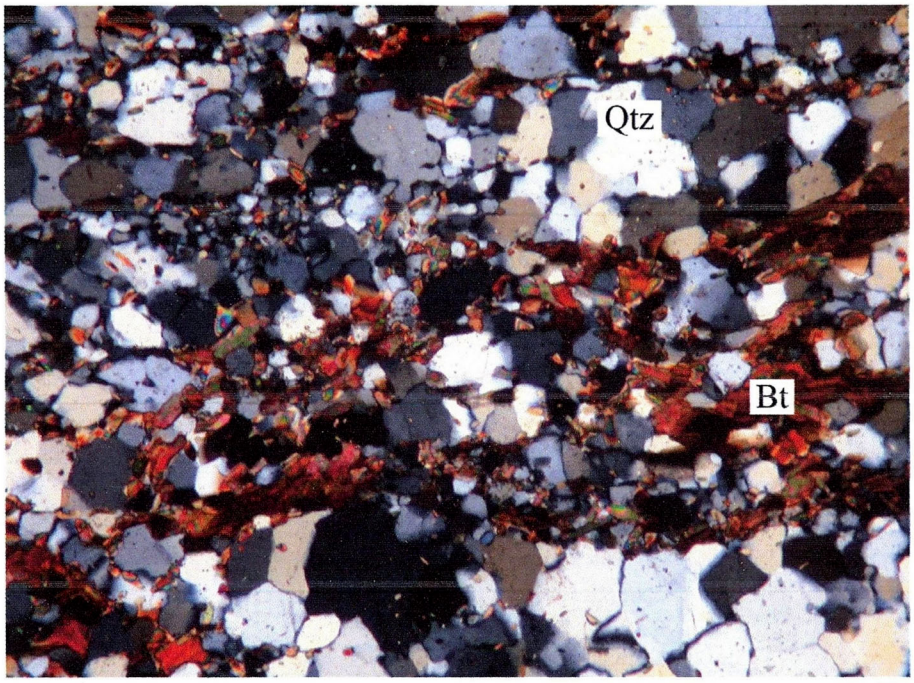

crossed nicols

0.75 mm

Fig. 4-1-2-2 Photomicrographs of the pelitic gneiss in Namera area. Bt: biotite, Qtz: quartz.

09032208B

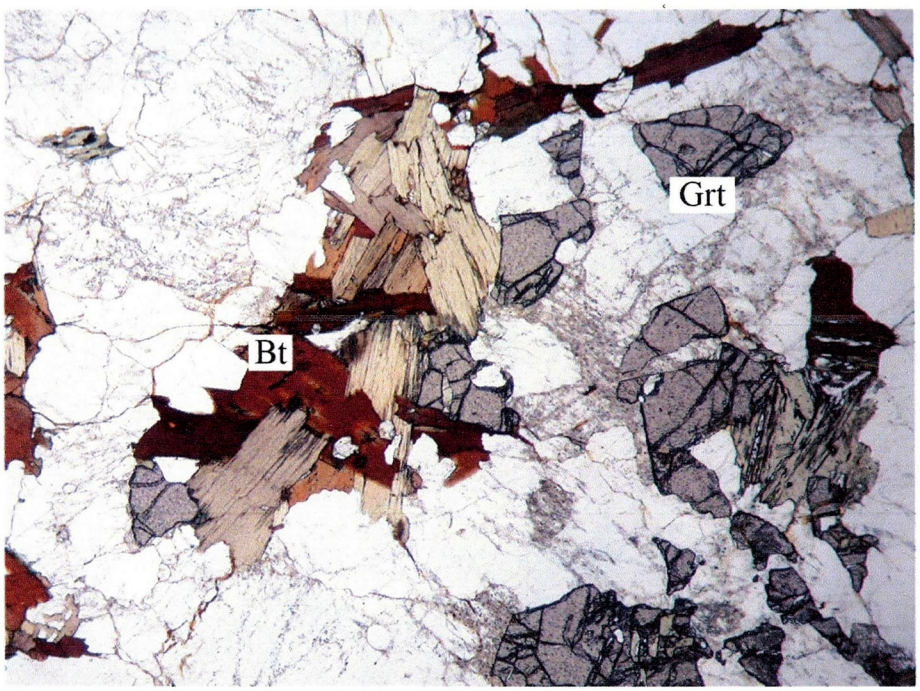

open nicol

1.5 mm

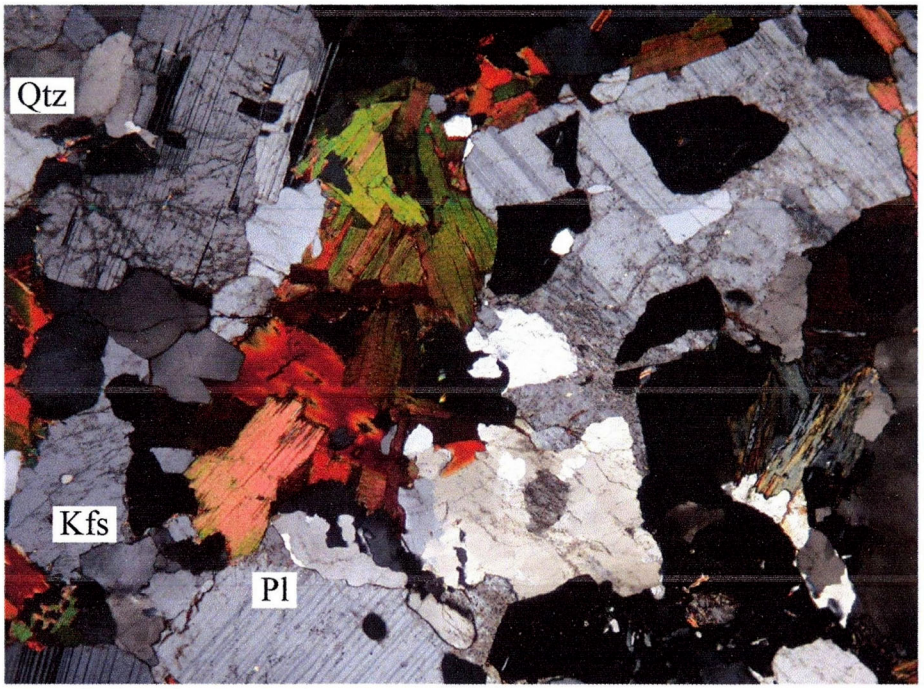

crossed nicols

1.5 mm

Fig. 4-2-1 Photomicrographs of the Gamano-Obatake Granodiorite. Pl: plagioclase, Qtz: quartz, Kfs: K-feldspar, Bt: biotite, Grt: garnet.

4-3. Migmatite

4-3-1. The Nagano Migmatite

The Nagano Migmatite shows a granoblastic texture, and consists mainly of quartz, plagioclase, K-feldspar and biotite with a trace amount of muscovite (Fig. 4-3-1-1). Zircon is ubiquitously included as accessory minerals. Quartz shows anhedral shapes with 0.1 to 0.2 mm and 1 to 2 mm in grain size, and wavy extinction. It often includes small crystals of biotite and quartz. Plagioclase shows euhedral to subhedral shapes with 0.1 to 0.6 mm. It weakly has zoning structures and clearly shows albite twin. Some plagioclase grains include small crystals of biotite. K-feldspar shows anhedral shapes with 0.9 to 1.5 mm. It includes small crystals of biotite and quartz. Biotite shows subhedral to anhedral shapes with 0.05 1 mm. It clearly shows X' = light brown, Z' = brown in pleochroism. Some biotite crystals include zircon with pleochroic halos.

4-3-2. The Tengatake Migmatite

The texture and mineral assemblage of the Tengatake Migmatite is similar to those of the Nagano Migmatite (Fig. 4-3-2-1). The Tengatake Migmatite includes garnet and cordierite paragenesis and the grain size is larger than the Nagano Migmatite, whereas the Nagano Migmatite lacks garnet and cordierite associations. The Tengatake migmatite consists mainly of quartz, plagioclase, K-feldspar, biotite and muscovite with trace amounts of garnet and cordierite. Garnet shows subhedral shapes with 0.4 to 1.5 mm. Cordierite is 0.5 to 1.5 mm and is replaced by pinite.

4-4. The Himurodake Quartz diorite

The Himurodake Quartz diorite appears at three areas, the northwestern part of the Kibe Granite, the southern part of the Kibe Granite and the inner part of the Gamano-Obatake

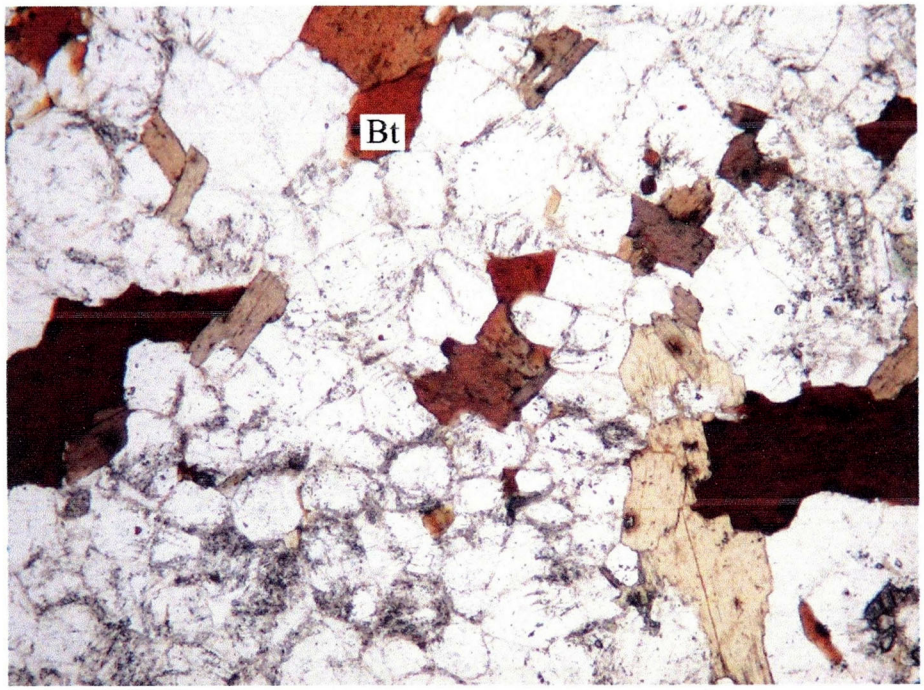

open nicol

1.5 mm

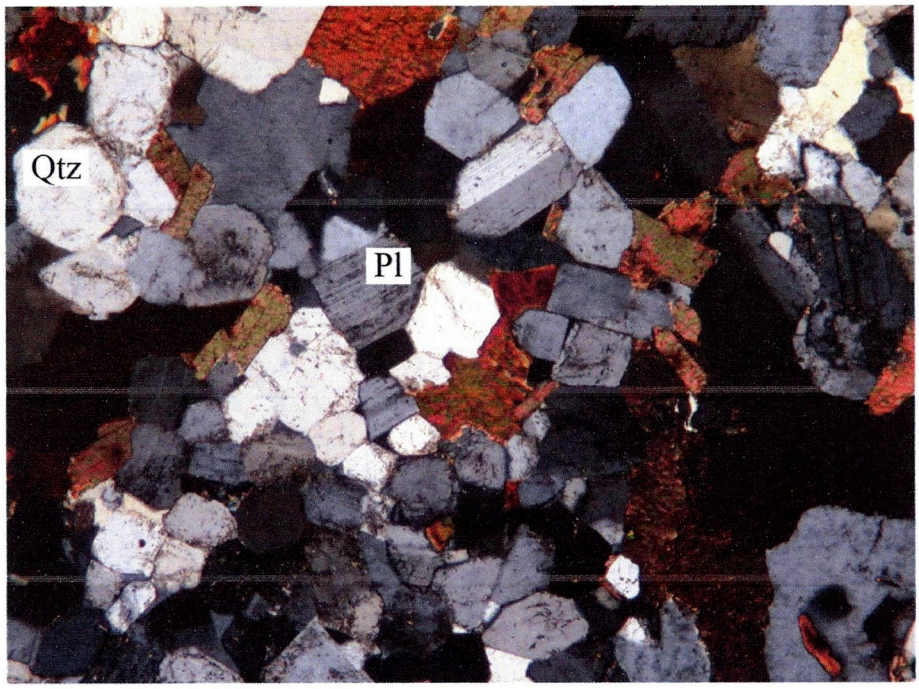

crossed nicols

1.5 mm

Fig. 4-3-1-1 Photomicrographs of the Nagano Migmatite. Bt: biotite, Pl: plagioclase, Qtz: quartz.

10050502B

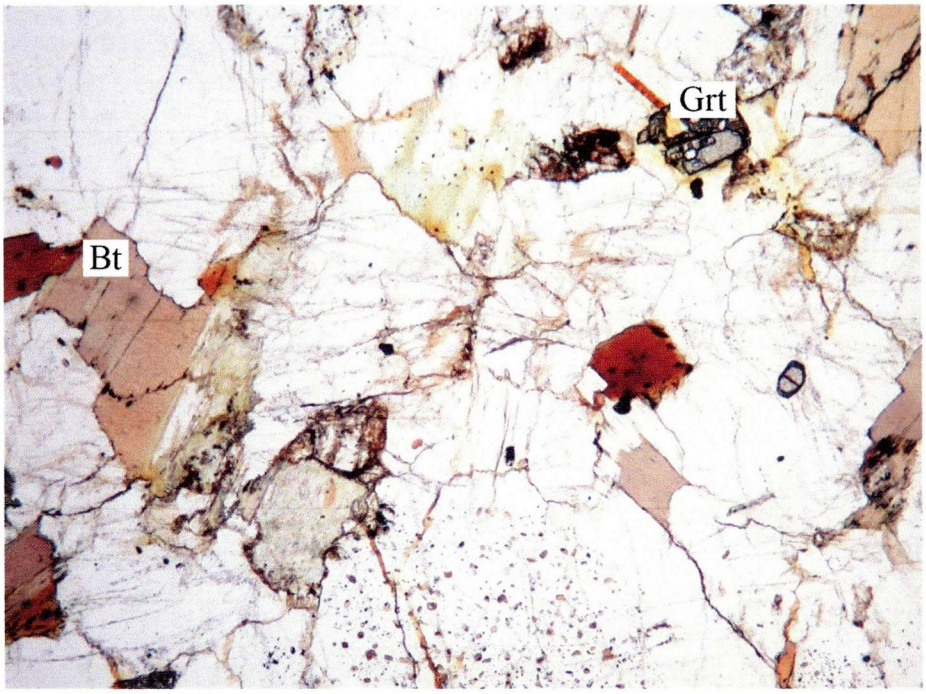

open nicol

1.5 mm

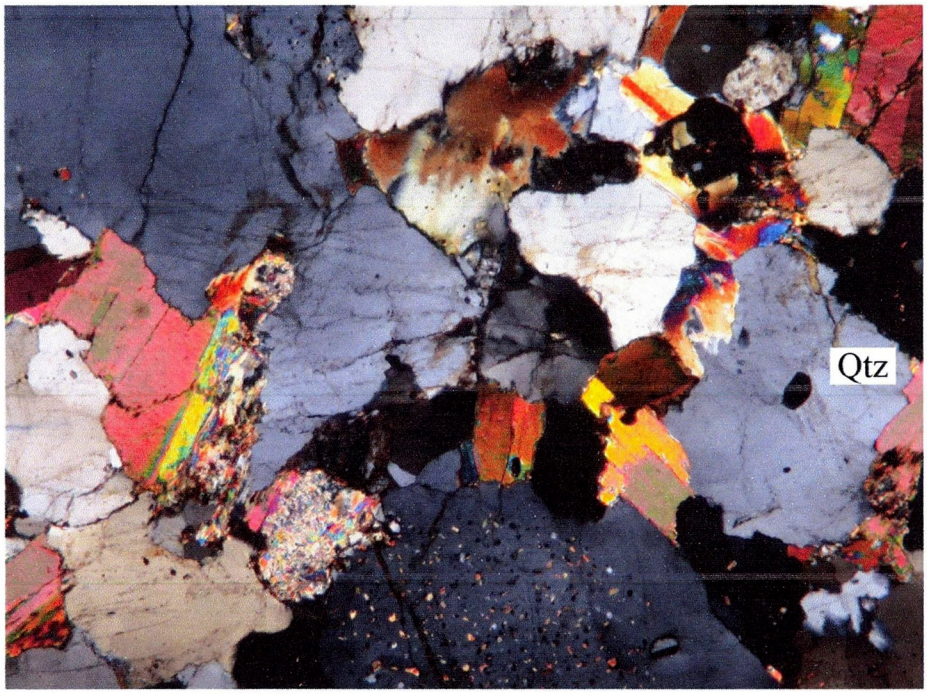

crossed nicols

1.5 mm

Fig. 4-3-2-1 Photomicrographs of the Tengatake Migmatite. Quartzs include small crystals of biotite and quartz. Bt: biotite, Qtz: quartz, Grt: garnet.

Granodiorite (Fig. 2-1). This quartz diorite generally shows dark gray to gray with medium grains. It consists mainly of plagioclase, hornblende, quartz, biotite, orthopyroxene and clinopyroxene. Apatite, zircon, and opaque minerals are ubiquitously included as accessory minerals (Fig. 4-4-1). Plagioclase shows bimodal grain size, euhedral to subhedral shape with 0.2 to 2 mm and 6 to 8 mm. Such large crystals have dusty zoning and often include small crystals of biotite, hornblende with long columnar or corrosion shapes and zircon. Hornblende shows subhedral to anbhedral shape with 0.1 to 2.5 mm. It clearly shows X' = light brown and Z' = brown in pleochroism. Some grains include small crystals of biotite, apatite and opaque minerals. Quartz shows anhedral shape with 0.2 to 5.0 mm with strong wavy extinction. Biotite shows subhedral to anhedral shape with 0.2 to 2.5 mm. It clearly shows X' = light brown and Z' = brown in pleochroism. Some biotite crystals show sword shapes. It often includes small crystals of zircon and apatite. Pleochroic halos appear around zircon. Apatite locally shows acicular shapes. Orthopyroxene and Clinopyroxene are locally surrounded by biotite and hornblende, respectively.

4-5. The Kibe Granite

The Kibe Granite consists mainly of quartz, K-feldspar, plagioclase and biotite with a small amount of muscovite. It possesses weakly foliation, and is characterized by K-feldspar phenocrysts (Fig. 4-5-1A). Zircon, apatite and opaque minerals are ubiquitously included as accessory minerals. Euhedral to subhedral allanite locally appears in this granite. Quartz shows anhedral shape with 1 to 7 mm with a strong wavy extinction and often includes small crystals of biotite, plagioclase, zircon and muscovite (Fig. 4-5-1B). K-feldspar is of a tabular shape with 4 to 9 mm, and shows remarkable perthite and microcline structures. Some K-feldspar grains show carlsbad twin. It locally includes small crystals of plagioclase, quartz and biotite, apatite, zircon and muscovite (Fig. 4-5-1C). Myrmekite occurs in the boundary between plagioclase and K-feldspar. Plagioclase shows euhedral to subhedral shape with 0.1 to 6 mm. It weakly has zoning structures and clearly shows albite twin. The twin faces locally show a curvature shape. Some plagioclase grains include small crystals of biotite, quartz,

10060601A

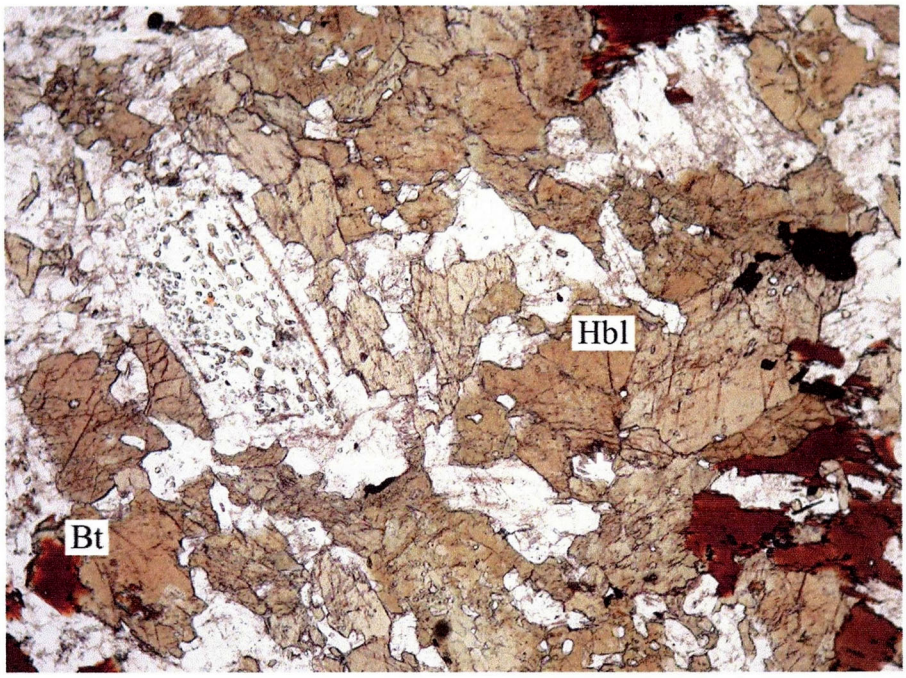

open nicol

0.75 mm

crossed nicols

0.75 mm

Fig. 4-4-1 Photomicrographs of the Himurodake Quartz diorite. Quartz diorite consisting of hornblende and plagioclase with trace amounts of biotite and quartz. Some plagioclase grains have dusty zones. Hbl: hornblende, Bt: biotite, Pl: plagioclase.

A. 09050207B

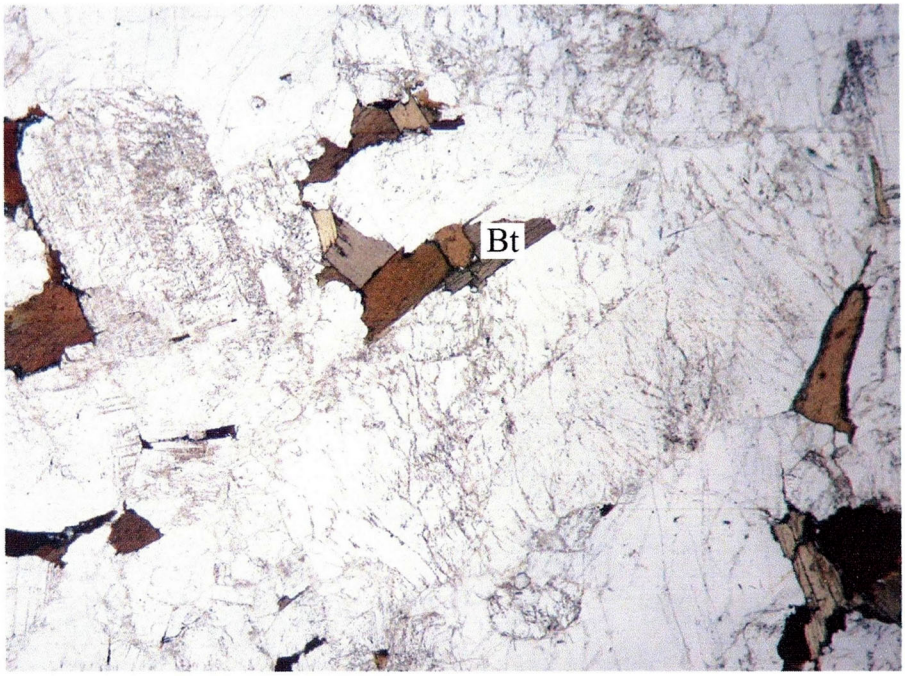

open nicol

1.5 mm

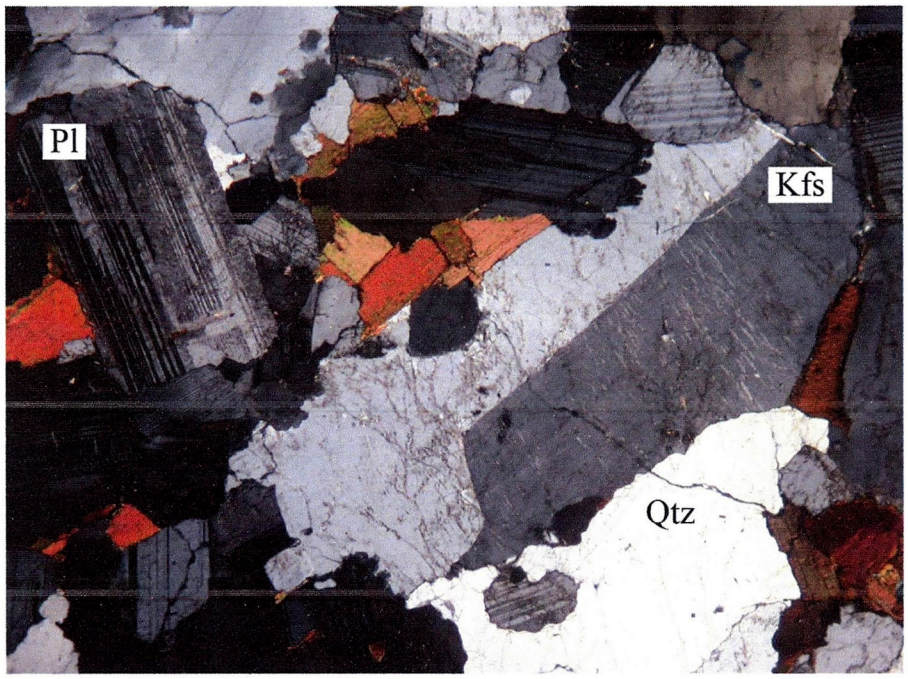

crossed nicols

1.5 mm

Fig. 4-5-1 Photomicrographs of the Kibe Granite. A: typical assemblage and texture of the Kibe Granite, containing euhedral K-feldspar. Kfs: K-feldspar, Pl: plagioclase, Qtz: quartz, Bt: biotite.

B. 09050206

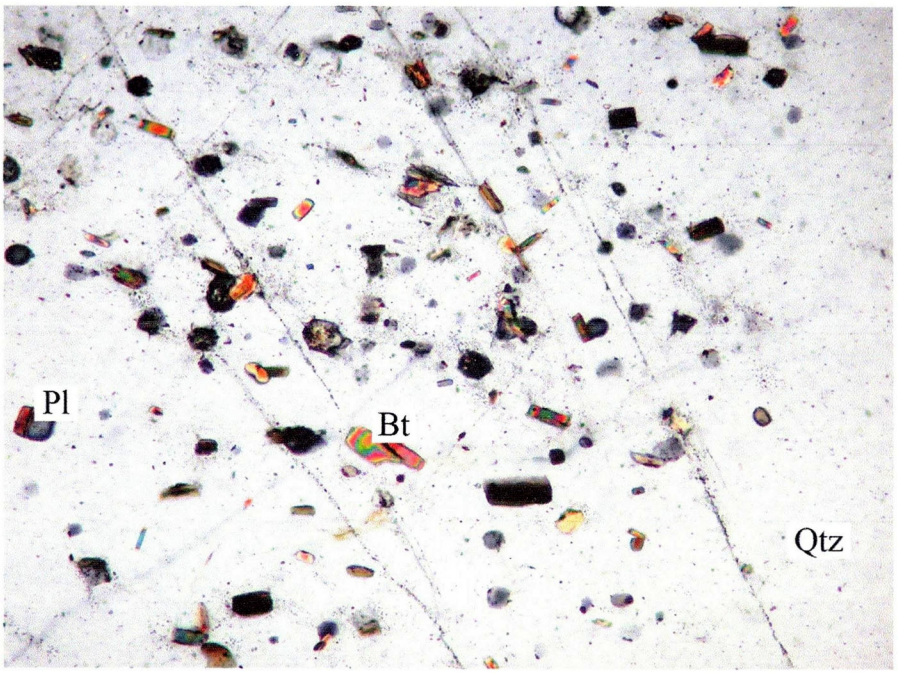

open nicol

0.15 mm

C. 09050209B

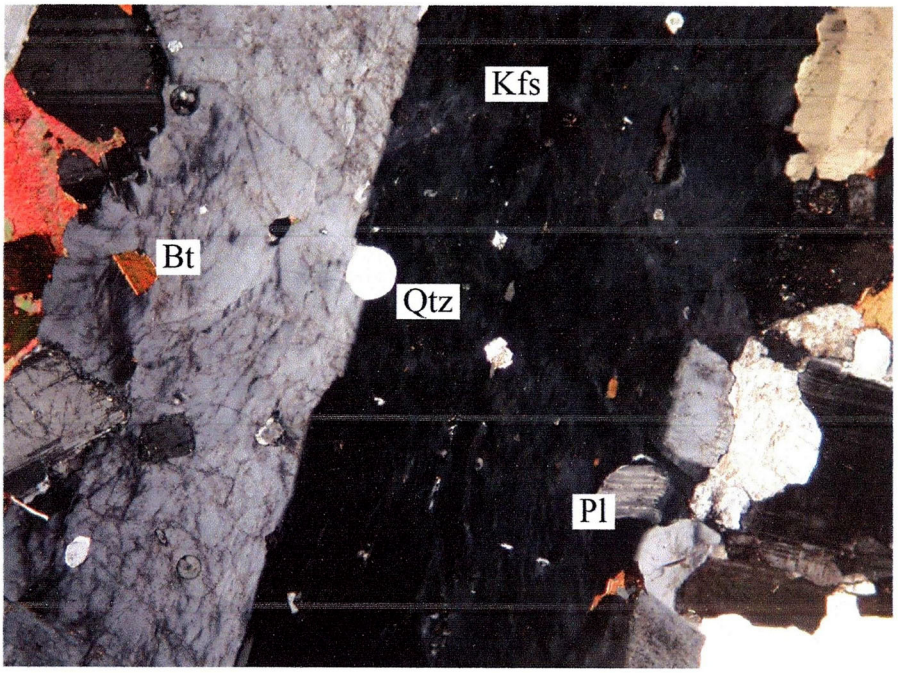

crossed nicols

1.5 mm

Fig. 4-5-1 Photomicrographs of the Kibe Granite. B: Quartz includes small crystals of biotite, plagioclase and quartz. C: K-feldspar phenocryst including anhedral plagioclase and quartz crystals. Kfs: K-feldspar, Pl: plagioclase, Qtz: quartz, Bt: biotite.

muscovite and zircon. Biotite shows subhedral to anhedral shape with 0.1 to 3 mm. It clearly shows X' = light brown and Z' = brown in pleochroism. Some biotite crystals include zircon and apatite with traces of allanite. Pleochroic halos appear around zircon and/or allanite inclusions. Muscovite occurs as a single crystal with 1 mm in grains size, or inclusion of K-feldspar, quartz and plagioclase with 0.3 to 0.1 mm (Fig. 4-5-1D). Chlorite locally replaces biotite as a result of alteration.

Although the mineral assemblage of the Kibe Granite is basically the same throughout the suite, the K-feldspar phenocrysts disappear in the marginal part of the suite. In addition, the marginal part of the suite includes garnet but lacks allanite. On the other hand, the Kibe Granite closely appearing at the Himurodake Quartz diorite locally contains hornblende but lacking muscovite.

4-6. The Namera Granite

The Namera Granite consists mainly of quartz, plagioclase, K-feldspar, biotite and muscovite with trace amounts of garnet and cordierite (Fig. 4-6-1). Some samples include sillimanite (fibrolite) as inclusions of plagioclase, K-feldspar and cordierite. Zircon, apatite and opaque minerals are ubiquitously included as accessory minerals. Quartz shows anhedral shapes with 0.3 to 5 mm in grain size, and wavy extinction. It often includes small crystals of biotite, plagioclase, muscovite and zircon. Plagioclase shows euhedral to subhedral shape with 0.1 to 5 mm, and weakly has zoning structures with albite twin. Some plagioclase grains include small crystals of quartz, biotite, muscovite and sillimanite (fibrolite). K-feldspar shows anhedral shapes with 2 to 6 mm, and shows remarkable perthites and microcline structures. It locally includes small crystals of quartz, plagioclase, biotite, muscovite and sillimanite. Myrmekite occurs in the boundary between plagioclase and K-feldspar. Biotite shows subhedral to anhedral shape with 0.1 to 4 mm. It clearly shows X' = light brown and Z' = brown in pleochroism. Some biotite crystals include zircon and apatite. Pleochroic halos appear around zircon inclusions. Garnet shows euhedral to subhedral shape with 0.2 to 1 mm. Cordierite is 0.2 to 1 mm and is replaced by pinite. Some cordierite grains include sillimanite

(fibrolite).

D. 09050204A

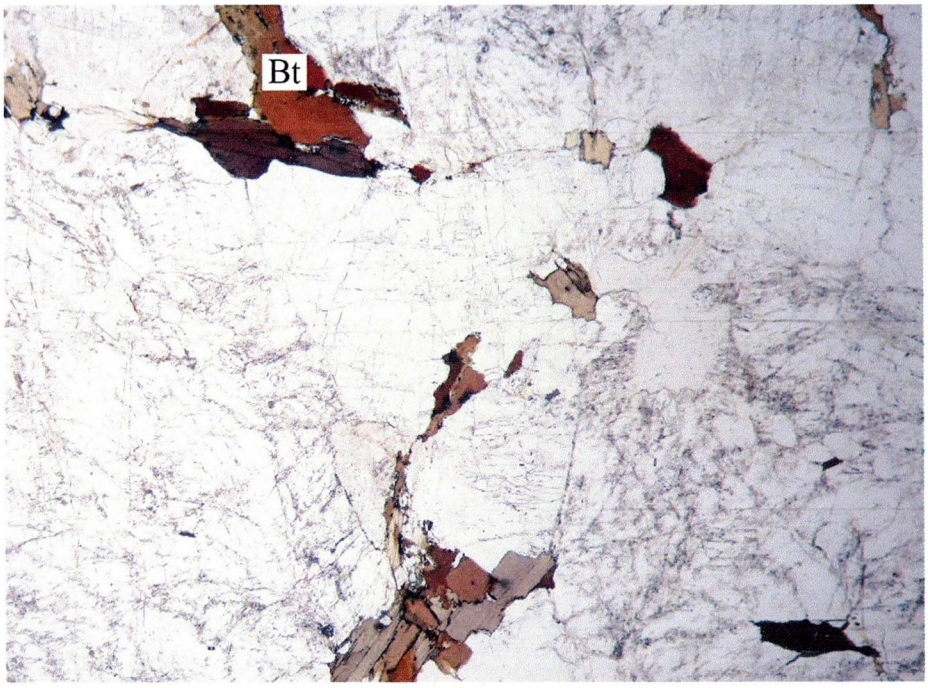

open nicol

1.5 mm

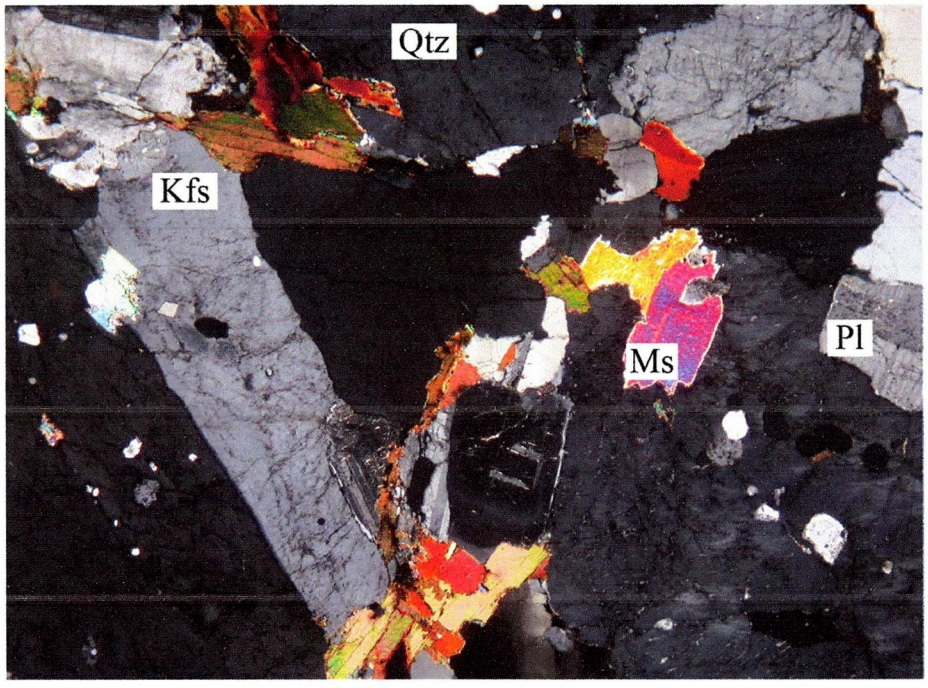

crossed nicols

1.5 mm

Fig. 4-5-1 Photomicrographs of the Kibe Granite. D: Muscovite-bearing type of the Kibe Granite. Kfs: K-feldspar, Pl: plagioclase, Qtz: quartz, Bt: biotite, Ms: muscovite.

09032202A

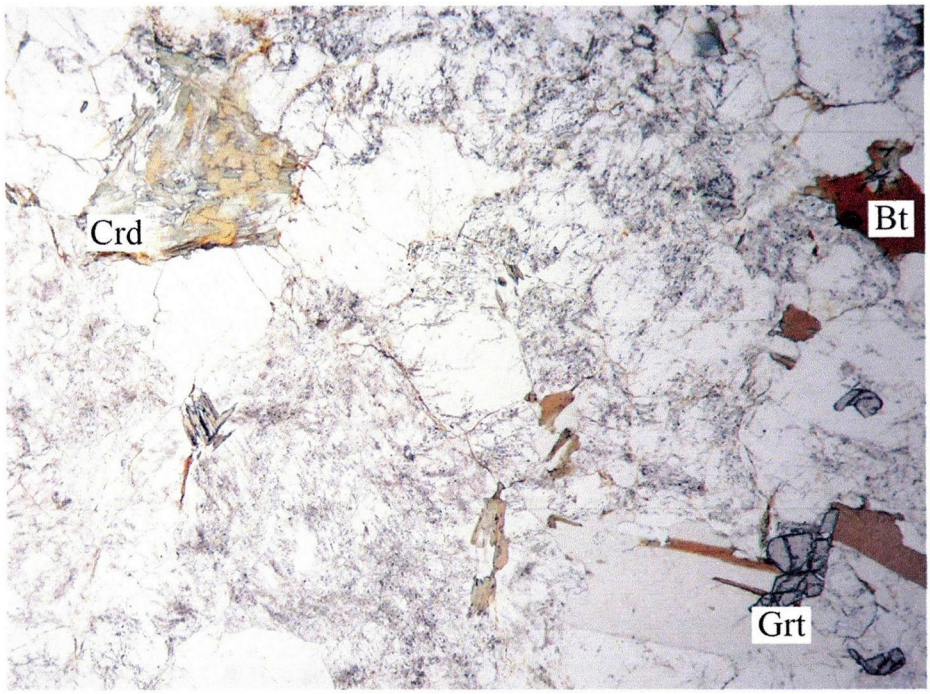

open nicol

1.5 mm

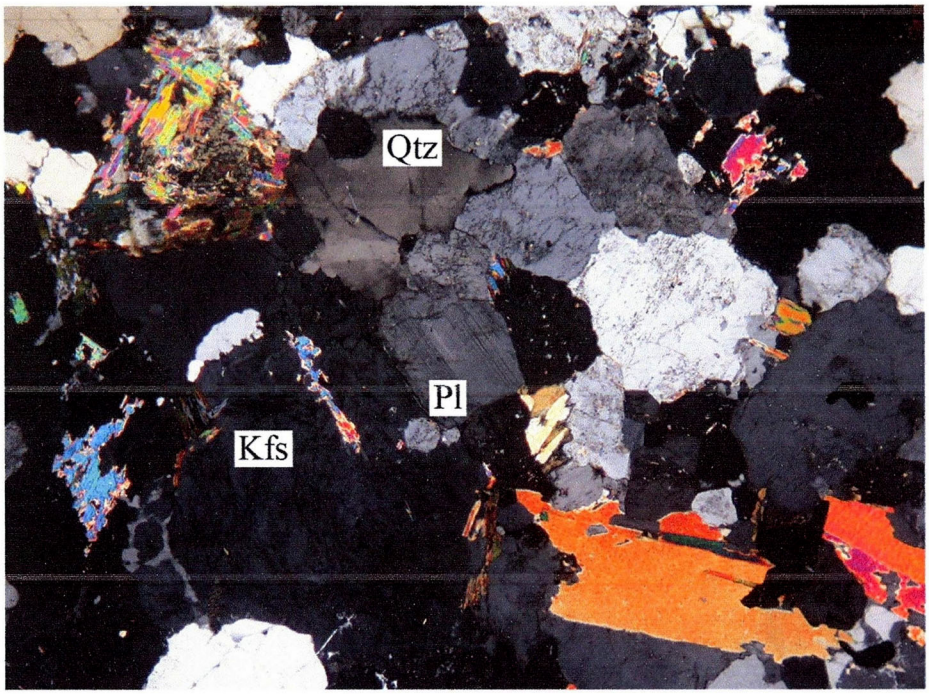

crossed nicols

1.5 mm

Fig. 4-6-1 Photomicrographs of the Namera Granite. Kfs: K-feldspar, Pl: plagioclase, Qtz: quartz, Bt: biotite, Grt: garnet, Crd: cordierite.

Chapter 5. Geochemistry

Geochemical analyses for major and some trace elements were performed by XRF installed at the Center for Instrumental Analyses, Yamaguchi University. All analyses were made on glass beads using an alkali flux comprising lithium tetraborate. The analytical procedure is described by Yamasaki et al. (1999). Trace elements including rare earth elements were determined with ICP-MS at Activation Laboratory Ltd., Canada using a lithium metaborate/tetraborate fusion technique. The results are listed in Tables 5-1 to 5-6.

5-1. The Gamano-Obatake Granodiorite

The variation diagrams of SiO_2 vs. major and trace elements for the Gamano-Obatake Granodiorite are shown in Figure 5-1-1. The SiO_2 contents are ranging from 60 to 75 wt%, and TiO_2, Al_2O_3, Fe_2O_3, MgO and CaO decrease with increasing SiO_2. K_2O slightly increases with increasing SiO_2. Alumina-saturation index (A/CNK = $100 \times Al_2O_3/(CaO+Na_2O+K_2O)$: mole) ranges from 1.04 to 1.27 indicating the peraluminous granite. Ba, Sr and Rb decrease with increasing SiO_2.

Figure 5-1-2 shows a spider diagram of the Gamano-Obatake Granodiorite normalized to N-MORB values (Sun and McDonough, 1989). The normalized patterns resemble those of the volcanic arc granite; enrichment of large ion lithophile (LIL) elements and light rare earth elements (LREE) with negative anomaly of Ta and Nb (Pearce et al., 1984). Additionally, there are little Sr and Eu depletion. Figure 5-1-3 is of chondrite normalized REE patterns of the Gamano-Obatake Granodiorite. These patterns show the enrichment of LREE and almost flat to slightly depletion of heavy rare earth elements (HREE).

5-2. The Himurodake Quartz diorite

The variation diagrams of SiO_2 vs. major and trace elements for the Himurodake Quartz diorite are shown in Figure 5-2-1. The SiO_2 contents range from 51 to 61 wt%, and Al_2O_3,

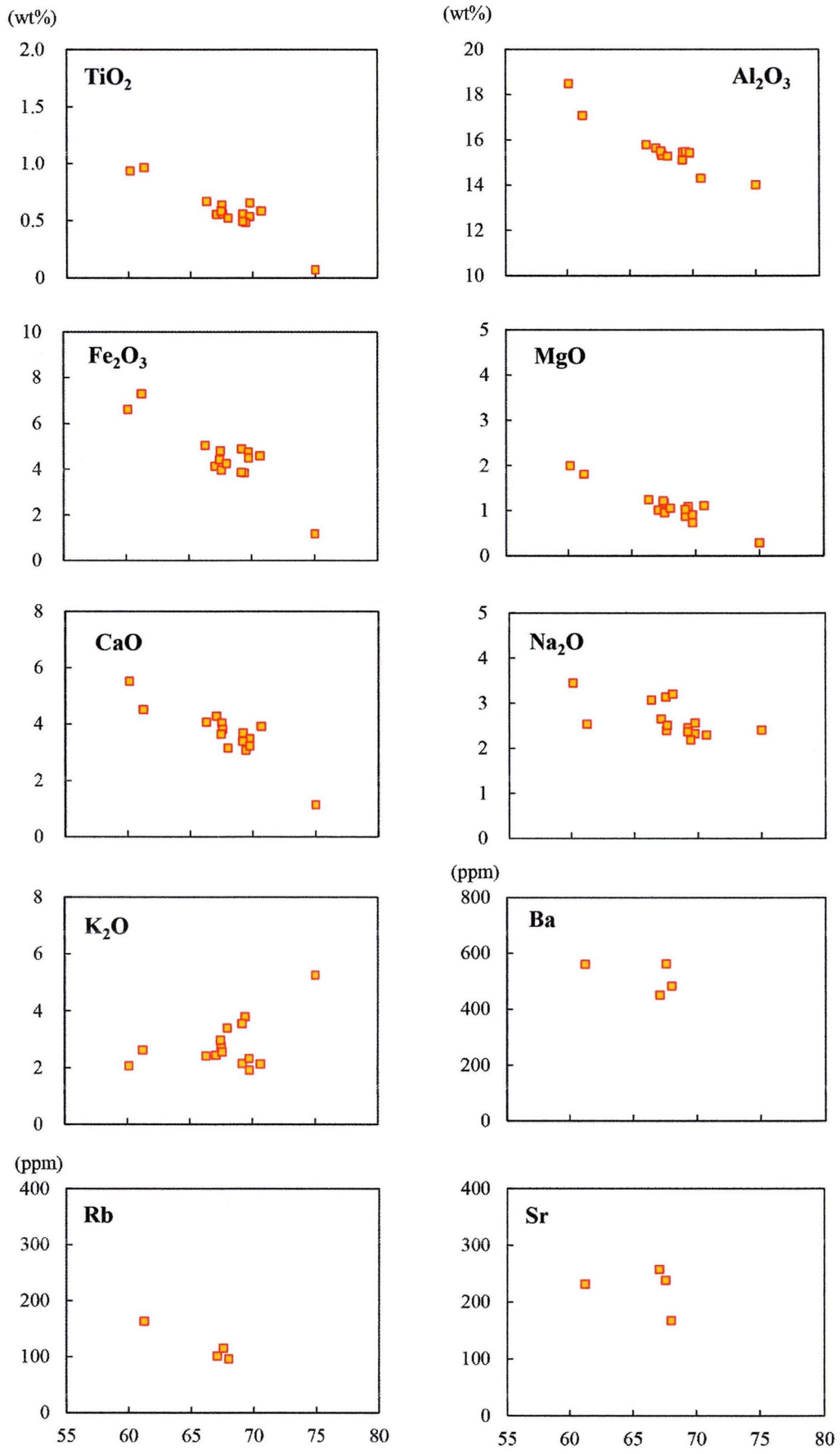

Fig. 5-1-1 Major and trace element variation diagrams of the Gamano-Obatake Granodiorite.

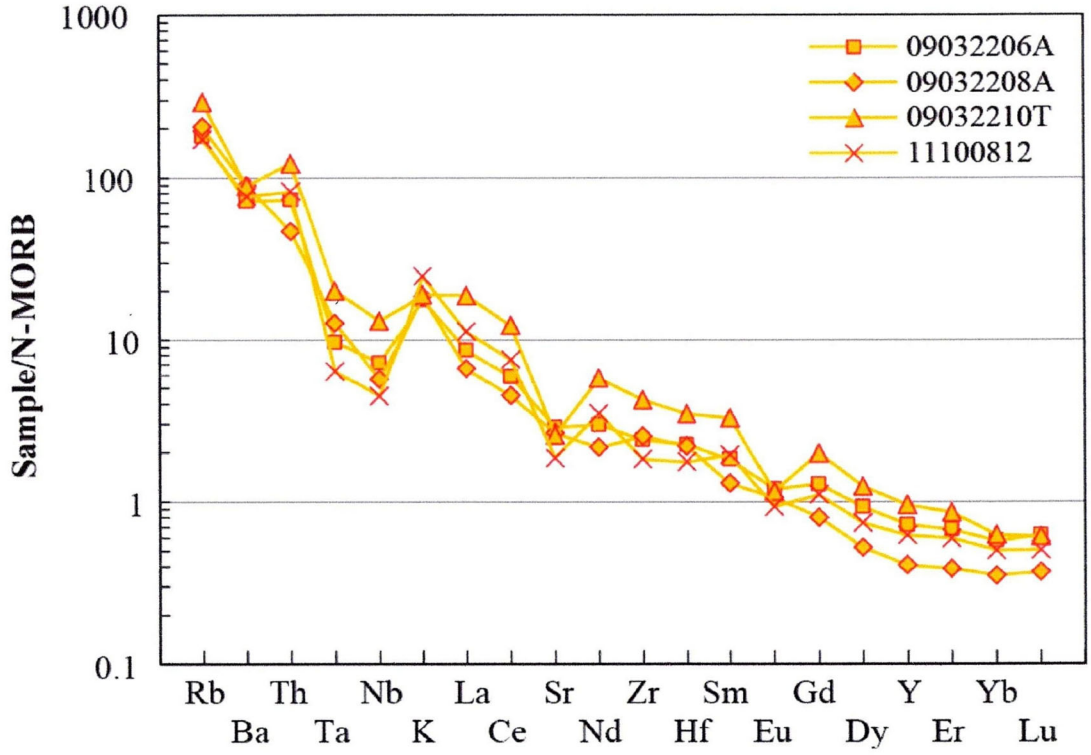

Fig. 5-1-2 Spider diagram normalized to N-MORB values for the Gamano-Obatake Granodiorite. Nomalized values are quoted for Sun and McDonough (1989).

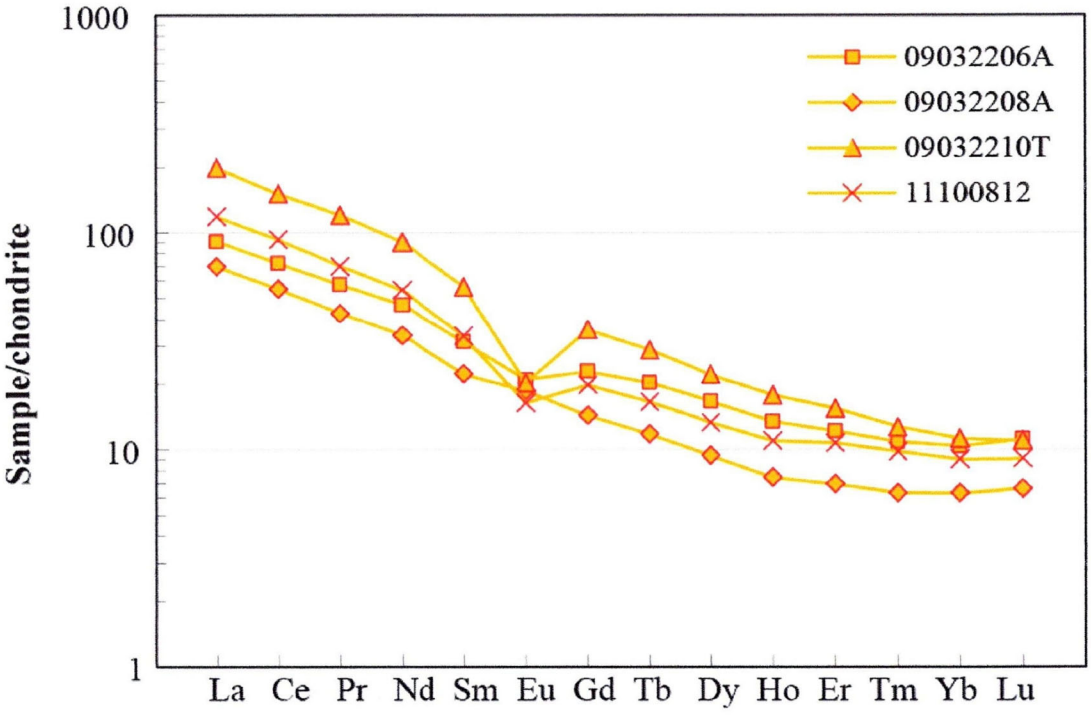

Fig. 5-1-3 Chondrite normalized REE patterns for the Gamano-Obatake Granodiorite. Nomalized values are quoted for Sun and McDonough (1989).

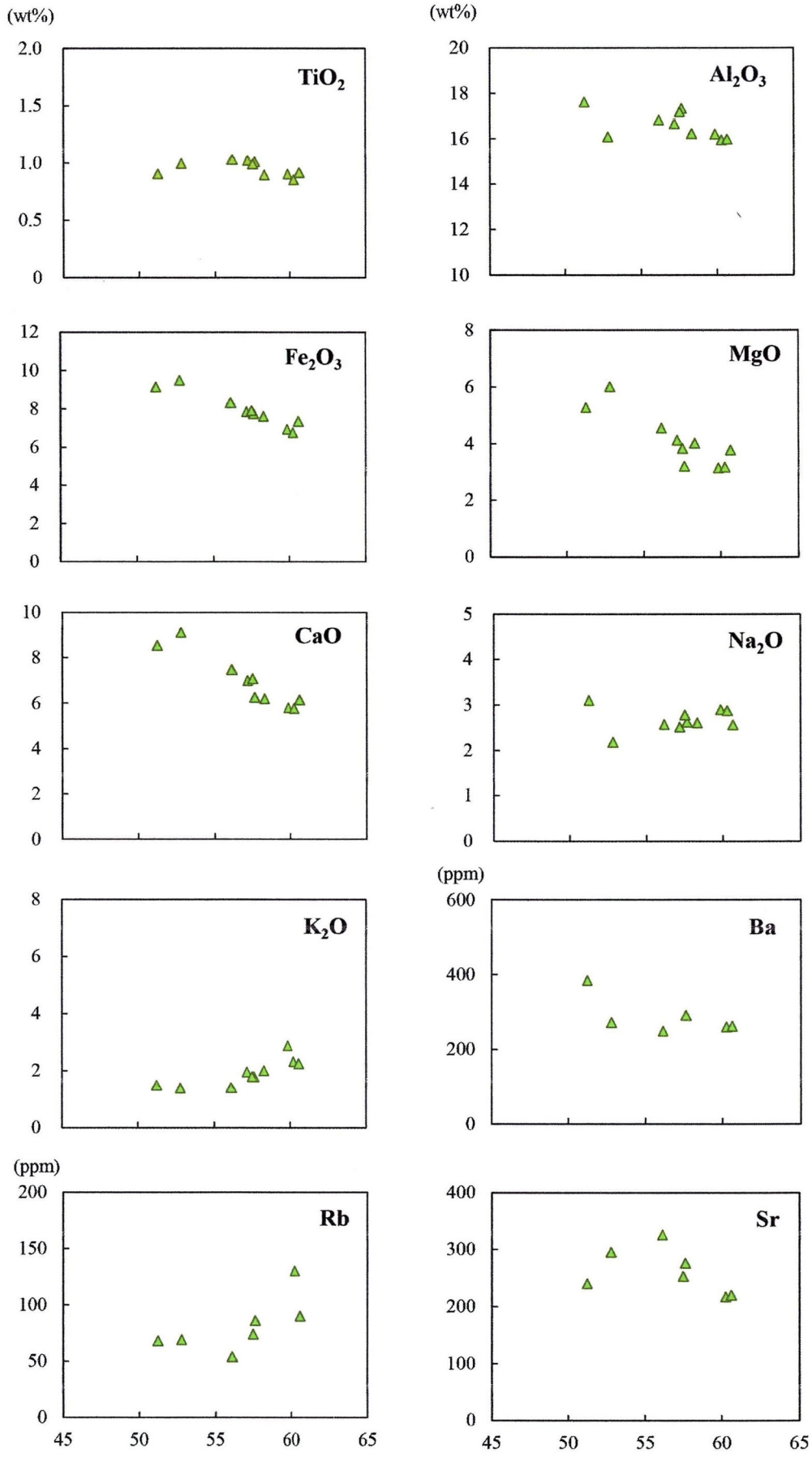

Fig. 5-2-1 Major and trace element variation diagrams of the Himurodake Quartz diorite.

Fe_2O_3, MgO and CaO decrease with increasing SiO_2. K_2O and Rb slightly increase with increasing SiO_2. Sr and Rb decrease with increasing SiO_2.

Figure 5-2-2 shows a spider diagram normalized to N-MORB values (Sun and McDonough, 1989). The normalized patterns resemble those of the volcanic arc andesite (pearce et al., 1984). Figure 5-2-3 is of chondrite normalized REE patterns. These patterns show the enrichment of LREE with negative anomaly of Eu.

5-3. The Kibe Granite

The variation diagrams of SiO_2 vs. major and trace elements for the Kibe Granite are shown in Figure 5-3-1. The SiO_2 contents are from 70 to 77 wt %. TiO_2, Fe_2O_3, MgO and CaO decrease with increasing SiO_2 contents. The other major elements somewhat vary or are tending some decrease with increasing SiO_2. A/CNK range from 1.00 to 1.17. Sr and Ba decrease with increasing SiO_2, and Rb roughly constant regardless of SiO_2 variation.

Figure 5-3-2 shows a spider diagram normalized to N-MORB values (Sun and McDonough, 1989). The normalized patterns resemble those of the volcanic arc granite (Pearce et al., 1984). Figure 5-3-3 shows chondrite normalized REE patterns. These patterns show the enrichment of LREE with negative Eu anomalies.

5-4. Namera Granite

The variation diagrams of SiO_2 vs. major and trace elements for the Namera Granite are shown in Figure 5-4-1. The SiO_2 contents range from 72 to 75 wt%, and Al_2O_3, Fe_2O_3, MgO, CaO and K_2O slightly decrease with increasing SiO_2. A/CNK is from 1.18 to 1.32. Ba decrease with increasing SiO_2.

Figure 5-4-2 shows a spider diagram normalized to N-MORB values (Sun and McDonough, 1989). The normalized patterns resemble those of the volcanic arc granite (Pearce et al., 1984). Additionally, Sr and Eu clearly show negative anomalies. Figure 5-4-3 is of chondrite normalized REE patterns. These patterns show the enrichment of LREE with

negative anomaly of Eu.

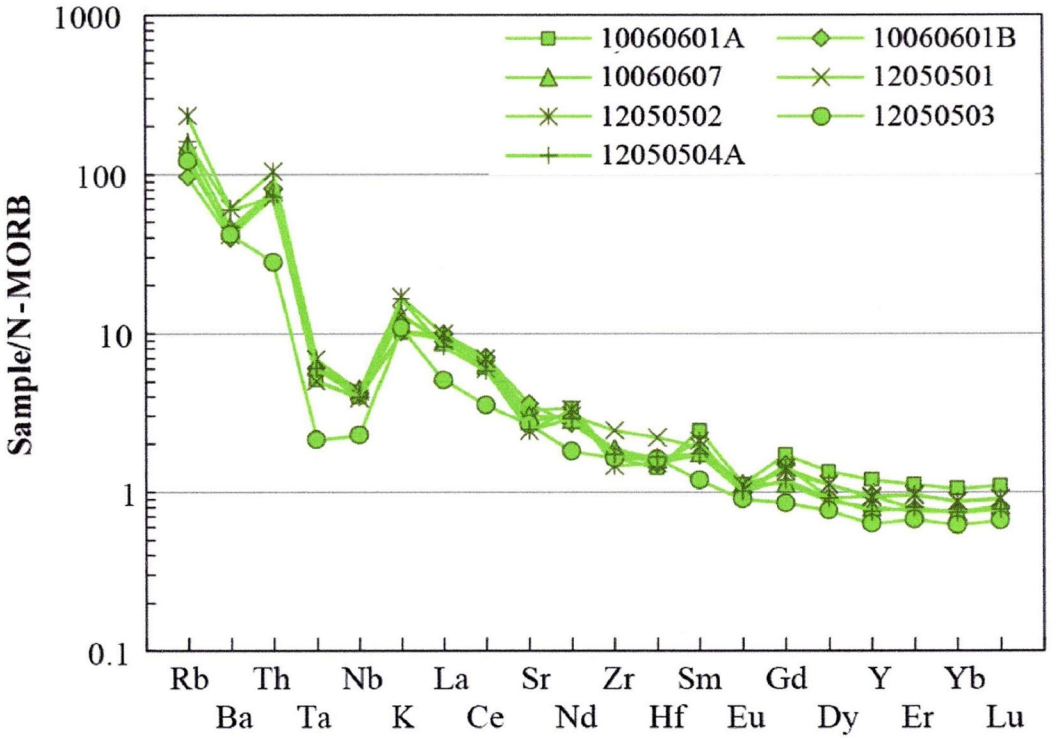

Fig. 5-2-2 Spider diagram normalized to N-MORB values for the Himurodake Quartz diorite. Nomalized values are quoted for Sun and McDonough (1989).

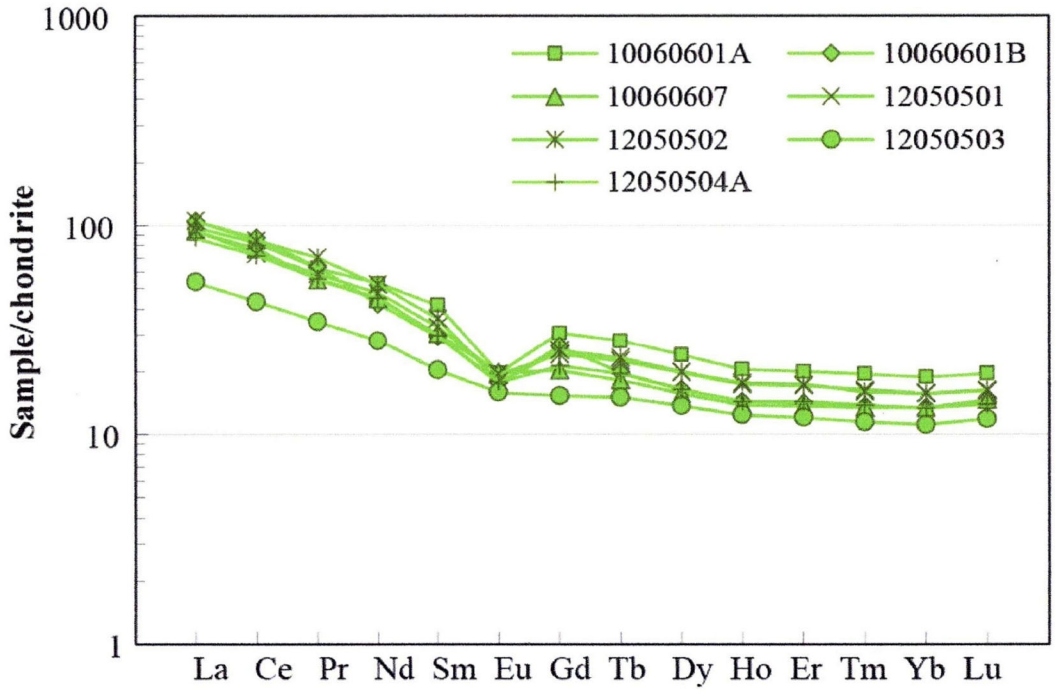

Fig. 5-2-3 Chondrite normalized REE patterns for the Himurodake Quartz diorite. Nomalized values are quoted for Sun and McDonough (1989).

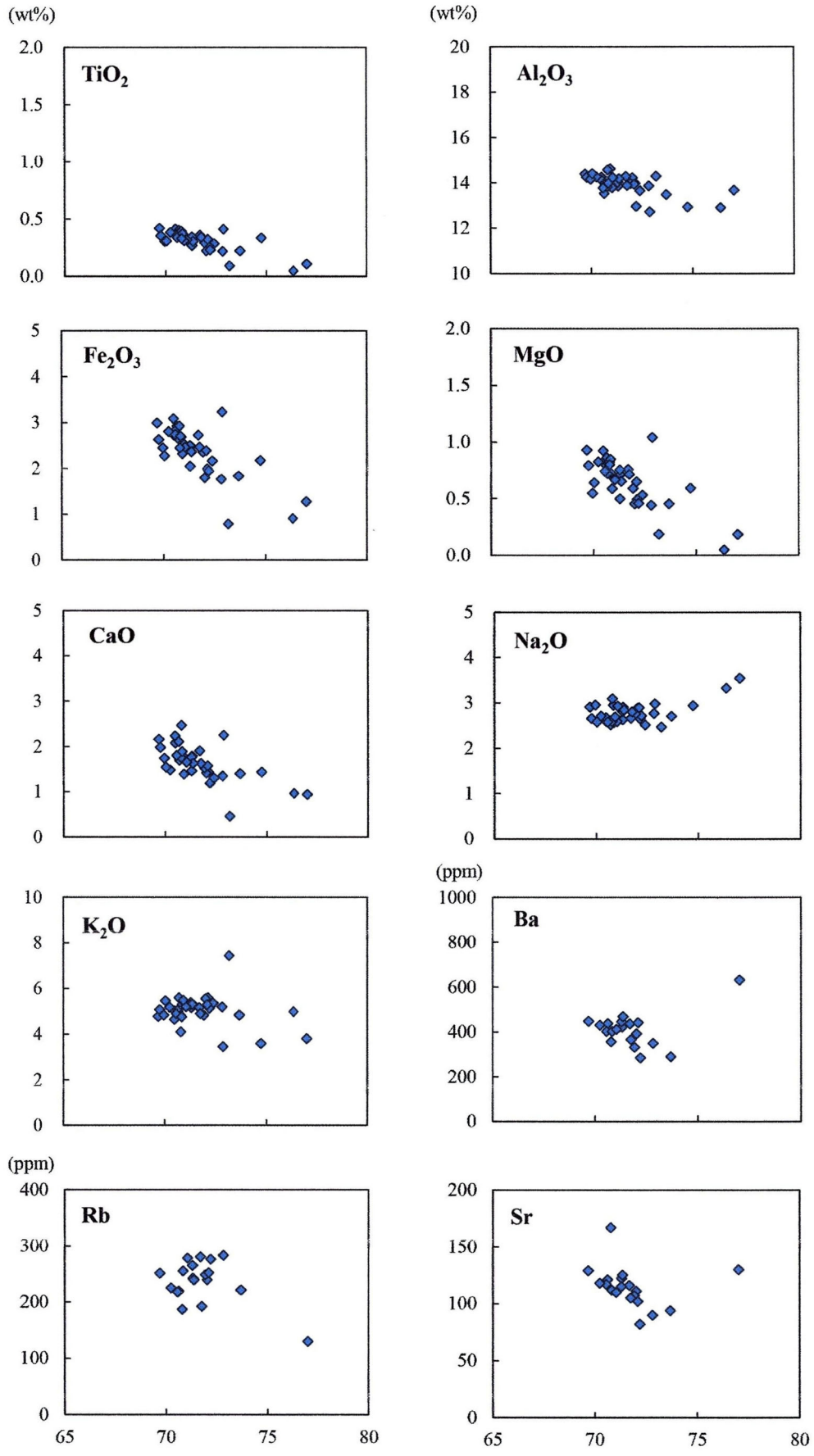

Fig. 5-3-1 Major and trace element variation diagrams of the Kibe Granite.

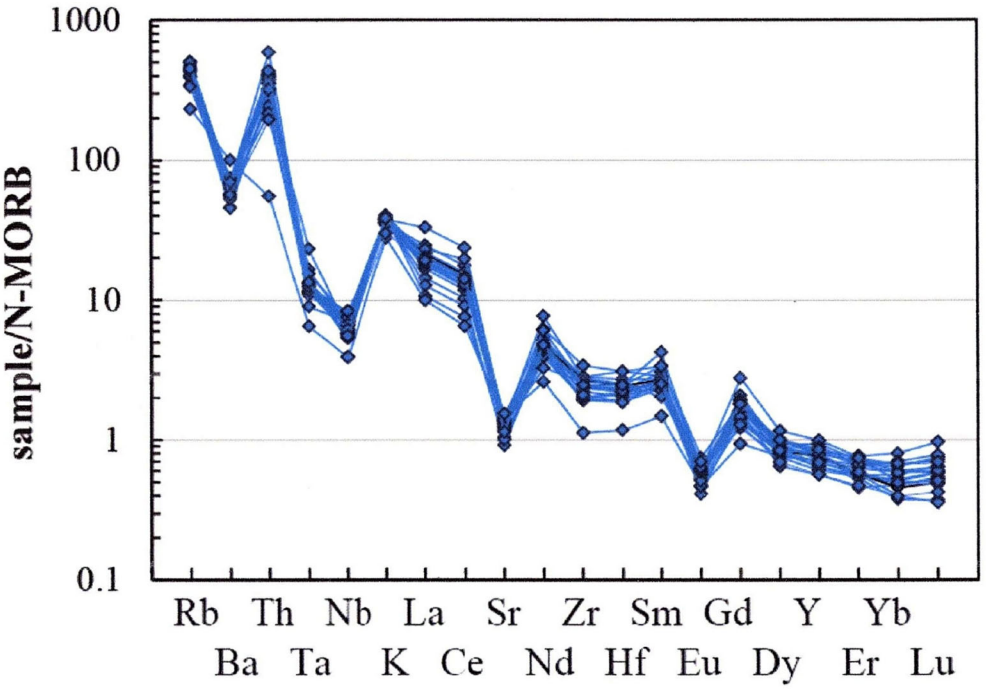

Fig. 5-3-2 Spider diagram normalized to N-MORB values for the Kibe Granite. Nomalized values are quoted for Sun and McDonough (1989).

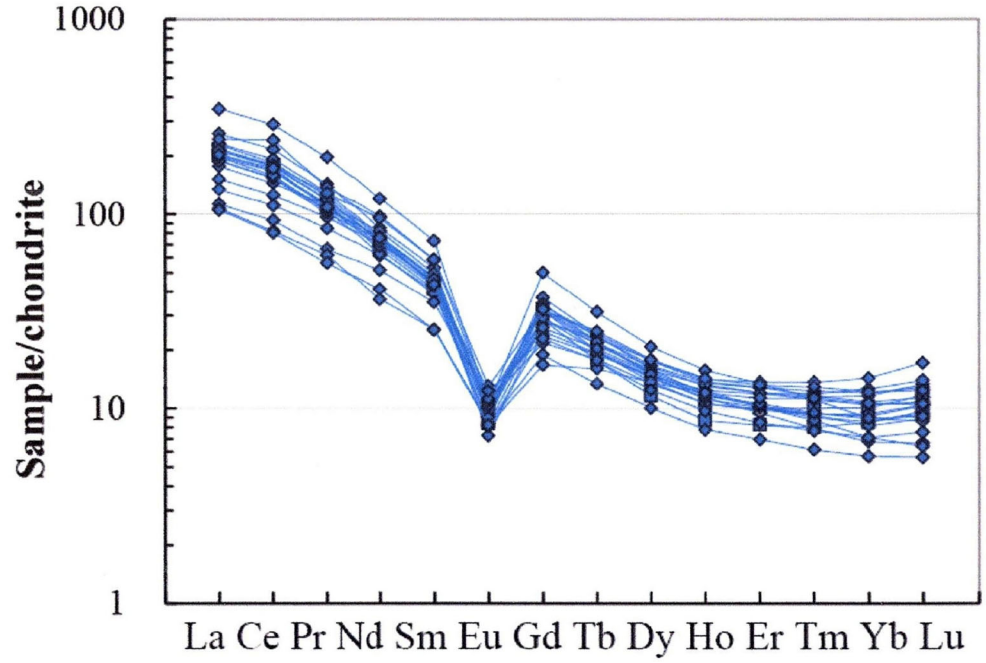

Fig. 5-3-3 Chondrite normalized REE patterns for the Kibe Granite. Nomalized values are quoted for Sun and McDonough (1989).

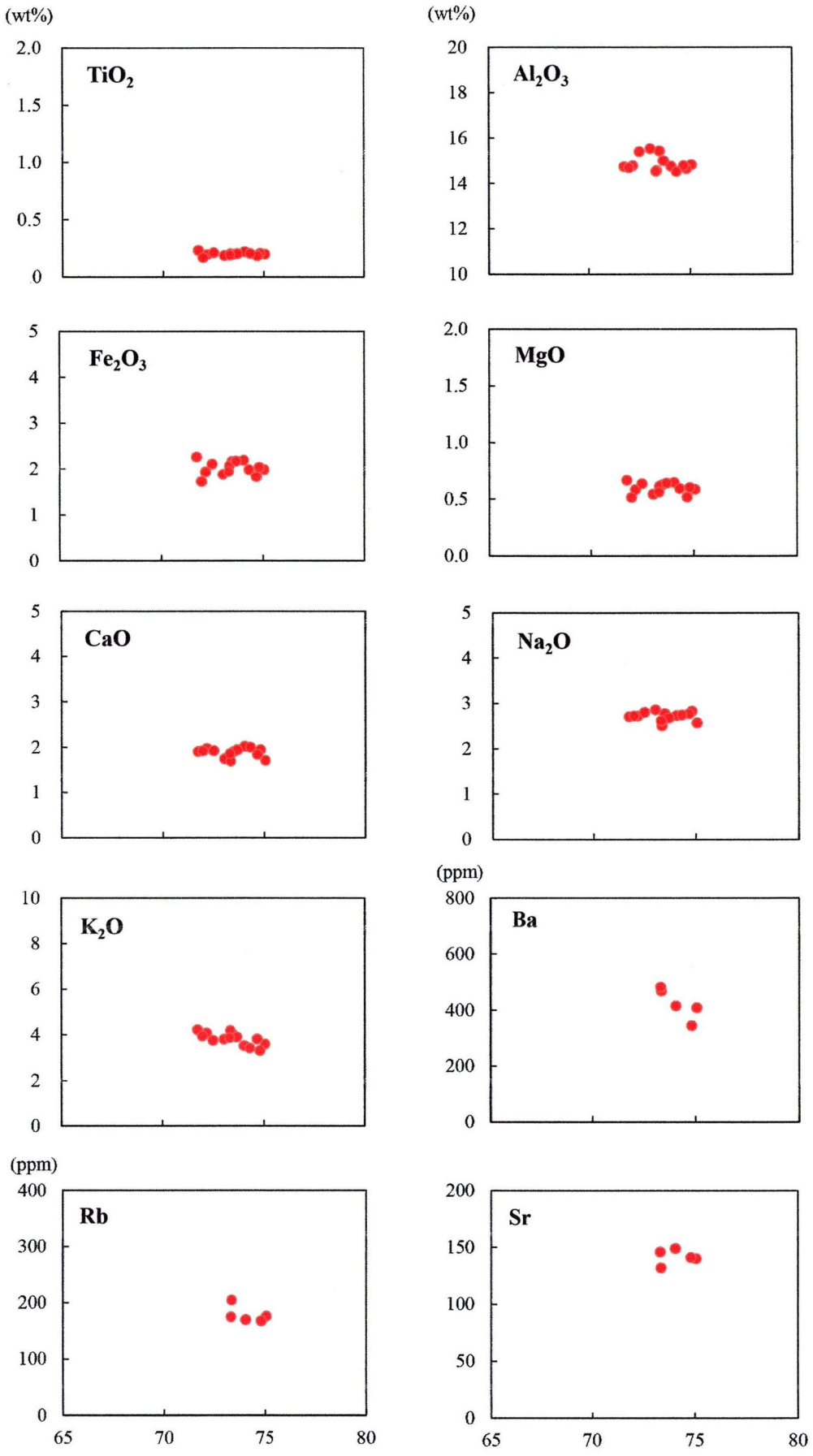

Fig. 5-4-1 Major and trace element variation diagrams of the Namera Granite.

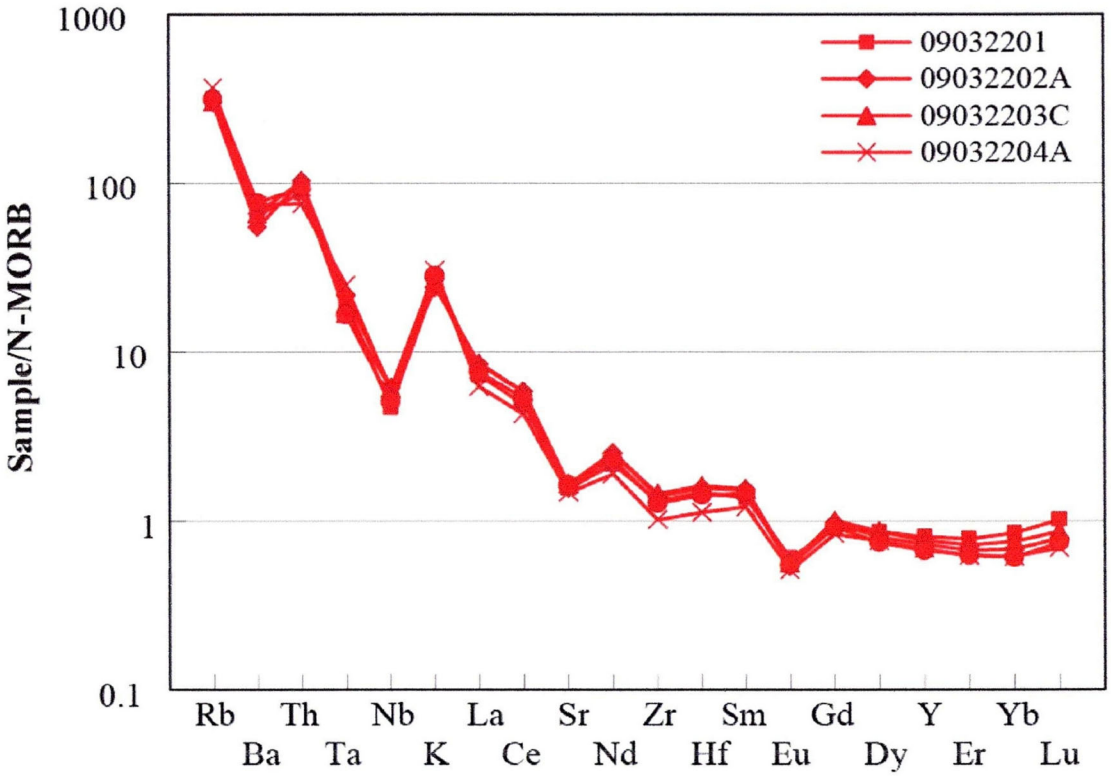

Fig. 5-4-2 Spider diagram normalized to N-MORB values for the Namera Granite. Nomalized values are quoted for Sun and McDonough (1989).

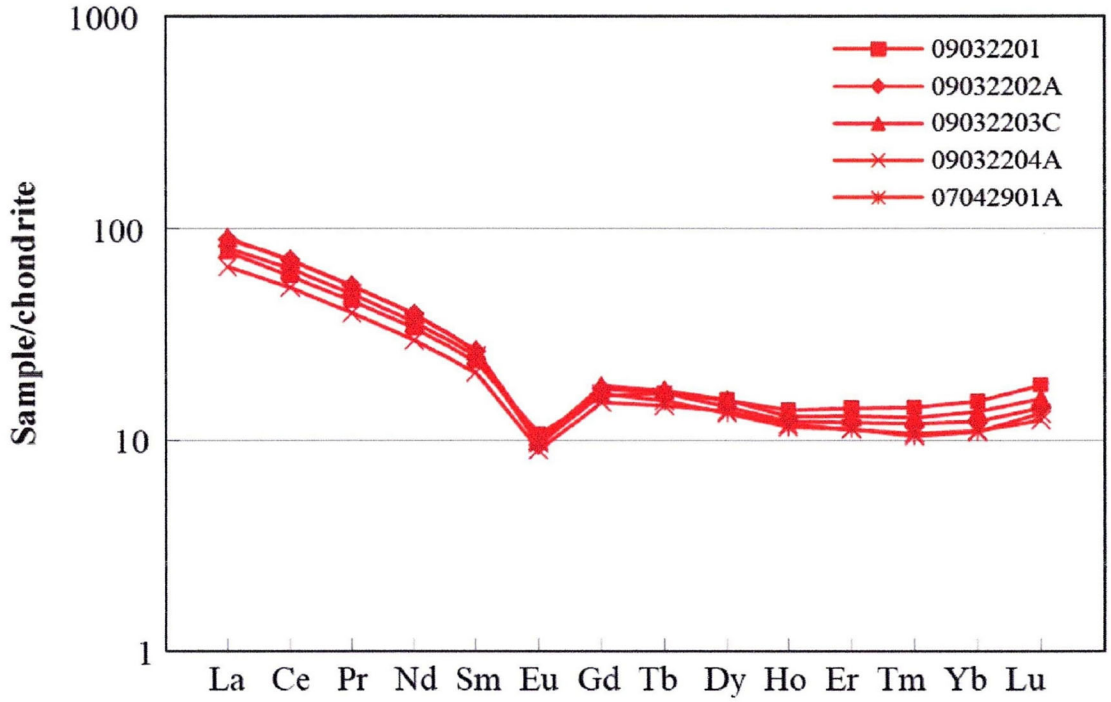

Fig. 5-4-3 Chondrite normalized REE patterns for the Namera Granite. Nomalized values are quoted for Sun and McDonough (1989).

Chapter 6. Sr and Nd isotopic compositions

Extraction of Sr and Nd from rock powders has been described by Kagami et al. (1987). Isotopic analyses are conducted with thermo-ionization mass spectrometer (TIMS, Finigan MAT MAT-262) installed at Department of Earth and Environment Sciences, Shimane University. Detailed analytical procedure is described in Iizumi (1996). Sr and Nd isotopic ratios of measured samples were normalized to 0.710241 (NIST SRM987: Yuhara, 1994; Yuhara and Kagami, 1995) and to 0.512115 (JNdi-1: Tanaka et al., 2000), respectively. Results of Sr and Nd isotopic analyses are listed in Tables 6-1 to 6-6. The isotopic initial ratios of Sr and Nd (SrI and NdI hereafter) were corrected with 91 Ma (Suzuki and Adachi, 1998). The author sometimes uses the epsilon values instead of the SrI and NdI values in some diagrams.

The SrI and NdI values of the Gamano-Obatake Granodiorite range from 0.70853 to 0.70911 and 0.51221 to 0.51227, respectively, whereas those of the Kibe Granite possess wide range, SrI = 0.70724 to 0.71165 and NdI = 0.51224 to 0.51227. The SrI values of the Kibe Granite are divided into two groups; low SrI group (low SrI) and high SrI group (high SrI), low SrI show range from 0.70706 to 0.70891, high SrI show range from 0.70984 to 0.71067. The NdI values of the low and high SrI groups are range from 0.51225 to 0.51231 and from 0.51224 to 0.51227, respectively. The isotopic compositions of the Namera Granite are different from those of the Gamano-Obatake Granodiorite and the Kibe Granite, and range from SrI = 0.70906 to 0.70927 and NdI = 0.51220 to 0.51223. The Himurodake Quartz diorite shows more depleted isotopic compositions among these Ryoke granitoids. The isotopic values show SrI = 0.70644 and NdI = 0.51233 to 0.51239.

Chapter 7. Discussion

7-1. Magma process of the Kibe Granite

The Kibe Granite is surrounded by the Gamano-Obatake Granodiorite (the Older Ryoke granite) and the high-grade pelitic gneisses, and occurs as the elliptic shape. On the other hand, the Himurodake Quartz diorite occurs as small stocks at vicinity of the Kibe Granite. In places, the Himurodake Quartz diorite is closely connected with the Kibe Granite. In this section, the author addresses geology, petrography and geochemistry including Sr and Nd isotopic ratios of the Kibe Granite, the Himurodake Quartz diorite and the host pelitic gneisses, and discusses the cause of compositional variations in the Kibe Granite, highlighting the magma processes under the open system phenomena.

7-1-1. Geochemical variations

In the variation diagrams of major and trace elements, each element clearly makes a monotonous trend although some elements are of scatter (Fig. 5-3-1). TiO_2, Fe_2O_3, MgO and CaO decrease with increasing SiO_2. K_2O, Rb, Sr and Ba roughly decrease with increasing SiO_2. In the spider diagram normalized to N-MORB values, the Kibe Granite is enrichment of LIL and depletion of high field strength (HFS) elements with distinctive Sr and Eu negative anomalies (Fig. 5-3-2). Additionally, chondorite normalized REE patterns of the Kibe Granites show negative Eu anomalies (Fig. 5-3-3). These geochemical features suggest that the compositional change of the Kibe Granite is controlled mainly by the fractional crystallization of specific minerals involving mainly plagioclase and biotite with a trace amount of K-feldspar. Figure 7-1-1-1 shows two vector diagrams using Sr (ppm) – Ba (ppm) and Zr (ppm) - TiO_2 (wt%) to verify the differentiation trend due to the effect of above described minerals. In general, Sr and Ba are distributed in plagioclase, biotite and K-feldspar in dacite to rhyolite compositions (Ewart and Griffin, 1994). The compositional trend of the Kibe Granite decreases Sr and Ba with increasing SiO_2 (Fig. 5-3-1). It is supported that

plagioclase, biotite and K-feldspar are candidate of fractionated minerals to produce the compositional variation of the Kibe Granite magma. Additionally, the Zr-TiO_2 diagram strongly supports the fractionation of biotite from the magma due to clearly decreasing TiO_2 with little changing Zr (Fig. 7-1-1-1).

If compositional variations of the Kibe Granite result from the process of simple fractional crystallization, the Kibe Granite makes an isochron. However, Sr isotopic ratios of the Kibe Granite are scattered in the Rb-Sr isochron diagram (Fig. 7-1-1-2). The Kibe Granite is divided into the low SrI and high SrI groups in the isochron diagram. Samples belonging to the high SrI group have been collected from the marginal part of suite (Fig. 3-5-1C). The Kibe Granite locally contains pelitic gneisses in the marginal part of suites, at which the granite shows the migmatitic structure (Fig. 3-5-1C). On the other hand, the low SrI group occurs in the inner side of suite. There are some MMEs in the inner side of the suite (Fig. 3-5-1D). Therefore, the reason of the Sr isotopic diversity would reflect their occurrence.

The high SrI group occurs in the marginal part of suite, and locally contains the specific texture; coarse-grained quartz grains including fine-grained minerals of plagioclase, biotite and quartz (Fig. 4-5-1B). The similar textures are also recognized in the pelitic gneisses. Moreover, phenocrysts of K-feldspar also contain corroded minerals of plagioclase, quartz and biotite. Combined with occurrence, petrography and geochemical variation, the high SrI group should be influenced by contamination of the pelitic gneiss during the differentiation of magma.

The low SrI group crops out in the inner part of suite, and is also exposed at the vicinity of the Himurodake Quartz diorite (Fig. 3-5-1D). The mineral assemblages of the low SrI group are roughly the same as those of the high SrI group but lacking garnet. In addition, the low SrI group closely appearing at the Himurodake Quartz diorite contains hornblende but lacking muscovite. On the other hand, the Himurodake Quartz diorite shows significant texture similar to that of magma mingling and mixing (Hibbard, 1995); for instance, dusty zones plagioclase, bladed biotite and acicular apatite (Fig. 4-4-1). According to occurrence, petrography and geochemistry, the low SrI group can result from the magma mingling and/or mixing between the Kibe Granite and the Himurodake Quartz diorite.

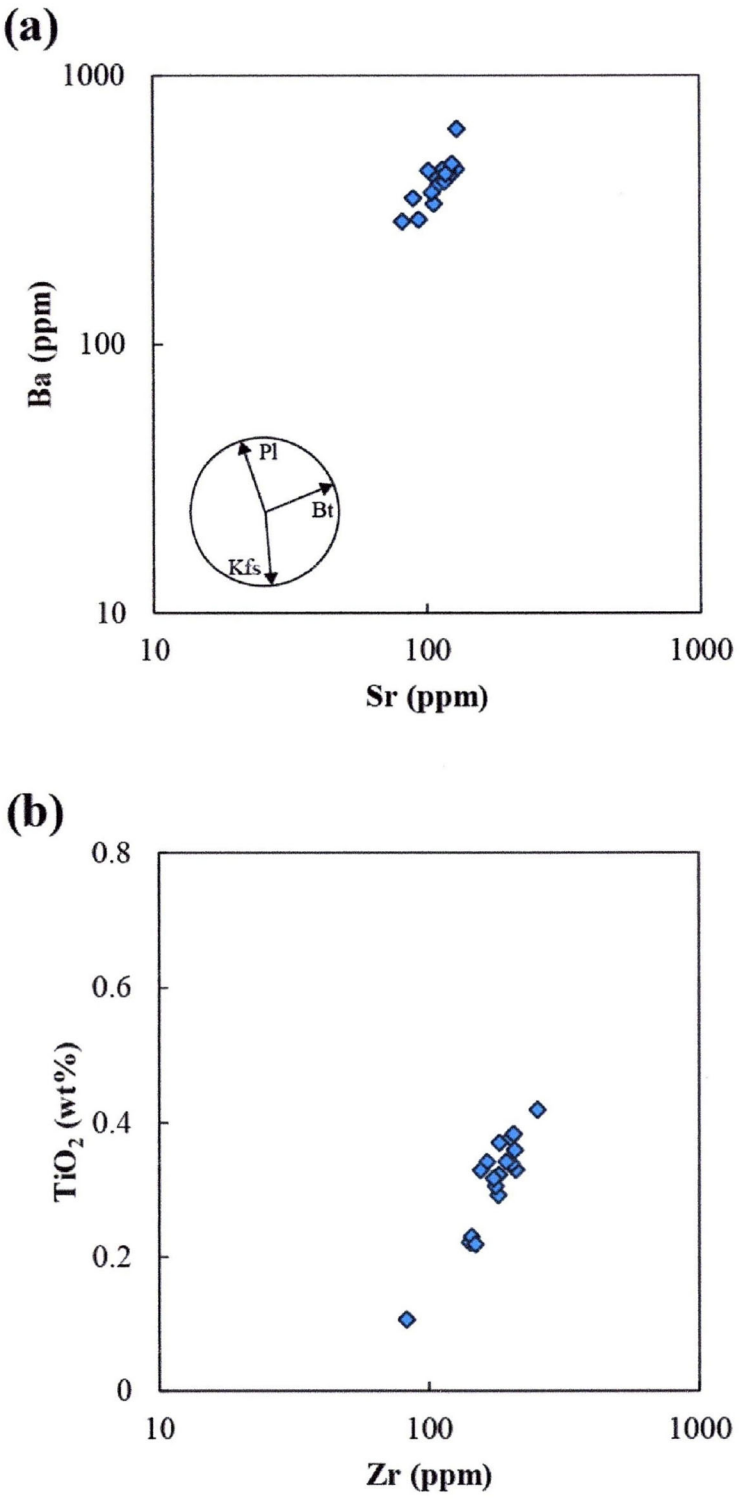

Fig. 7-1-1-1 Sr (ppm) –Ba (ppm) (a) and Zr (ppm) -TiO_2 (wt%) (b) diagrams for the Kibe Granite.

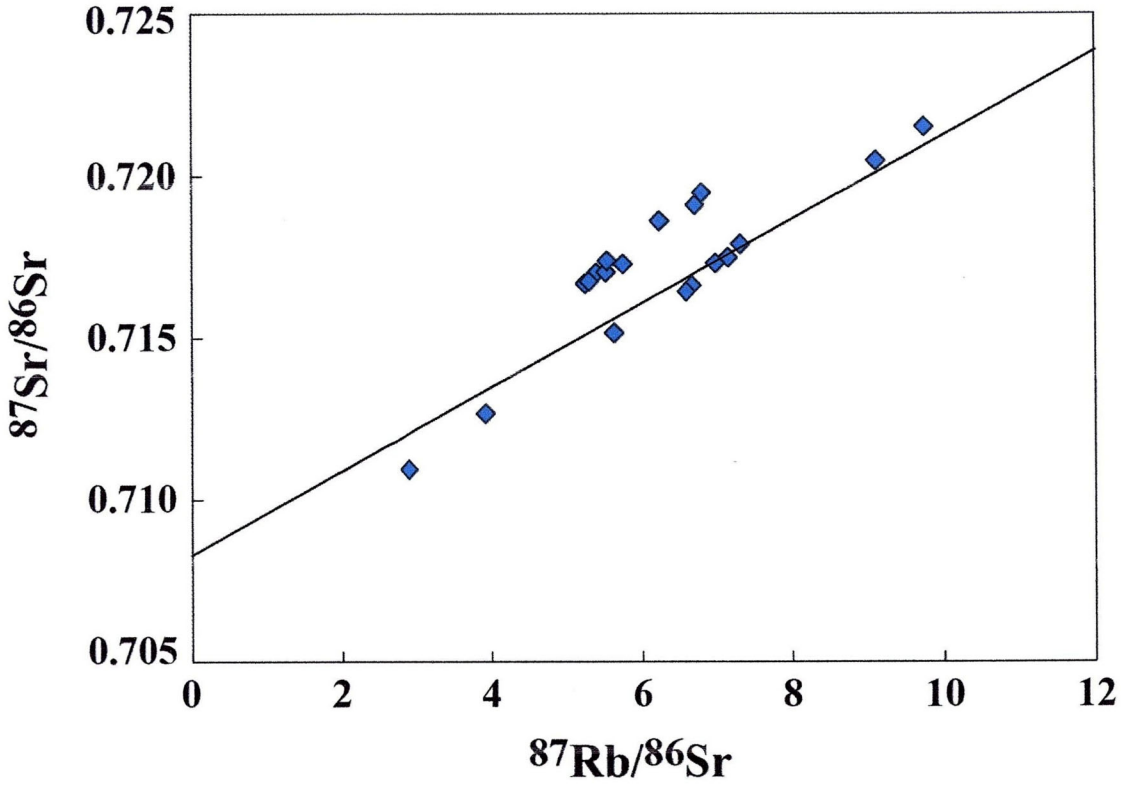

Fig. 7-1-1-2 $^{87}Sr/^{86}Sr$—$^{87}Rb/^{86}Sr$ diagram for the Kibe Granite. Solid line is a reference isochron indicating 91Ma.

7-1-2. Geochemical modeling

To verify the above assumption regarding the magma processes of the Kibe Granite, the author examines a geochemical modeling using assimilation and fractional crystallization model (AFC model; DePaolo, 1981). The formulation used for the modeling is described in the following procedure, and the results of calculated AFC trends are shown in SrI vs. reciprocal of Sr contents (1000/Sr) diagram (Fig. 7-1-2-1).

Sample 09050210 is selected as a parental magma of the Kibe Granite because this sample is collected from the inner part of suite, and possesses the average SrI values and the one of least SiO_2 contents among the studied Kibe Granite. The contaminant and mixing counterparts of this model suppose sample 10032102A (SrI = 0.71618) for the pelitic gneiss and sample 10060601B (SrI = 0.70654) for the Himurodake Quartz diorite.

As mentioned above, the fractionated minerals are regarded as plagioclase, biotite and K-feldspar. Since distribution coefficients of Sr for biotite and K-feldspar are less than 1.0 (biotite: 0.01, K-feldspar: 0.77, Bea et al., 1994), the variation of Sr contents due to the fractionation is mainly influenced by subtraction of plagioclase among such fractionated minerals. Therefore, the fractionated mineral is enough to suppose only plagioclase in this modeling. The r and Fc values represent the assimilation and fractionation ratios and the fractionation rate, respectively. The chemical compositions of the studied rocks and results of the calculated AFC trends are shown in Figure 7-1-2-1. There are two compositional variations plotted in domains A and B (Fig. 7-1-2-1). These two variations extend into the opposite directions from the inferred parental composition. The high SrI and low SrI groups are plotted within the field of domains A and B, respectively.

The high SrI group is plotted within the r-values ranging from 0.1 to 0.3 in the domain A. The variation of the high SrI group can be explained by AFC model between the Kibe Granite and the host pelitic gneisses because the r-values less than 0.3 are reasonable for the AFC process under a normal geothermal gradient in continental crusts (DePaolo, 1981). On the other hand, the low SrI group roughly exhibits the constant SrI values against the 1000/Sr values although some samples make trends controlled by the compositions of the Himurodake Quartz diorite (Fig. 7-1-2-1). The samples plotted along the r = 0.0 line are produced by

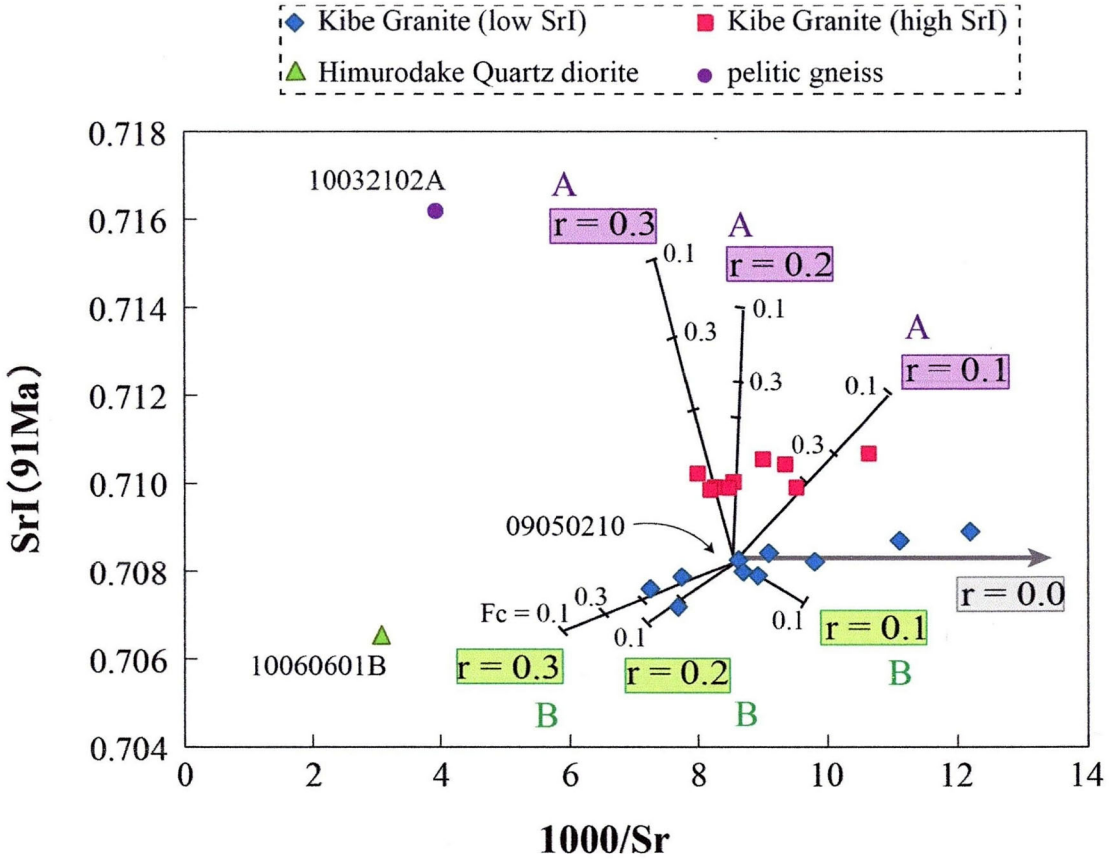

Fig. 7-1-2-1 1000/Sr-SrI (91Ma) diagram plotting the Kibe Granites, the Himurodake Quartz diorite and the pelitic gneiss. Solid lines indicate calculated trends by assimilation and fractional crystallization (AFC) model. Sample 09050210 represents a parental magma for this model. Lines (A) are of AFC trends between the Kibe Granite (sample 09050210) and pelitic gneiss (sample 10032102A). Lines (B) show both the magma mixing and fractional crystallization models (similar to AFC model) between the Kibe Granite (sample 09050210) and the Himurodake Quartz diorite (sample 10060601B). Bulk distribution coefficient for Sr (Kd = 1.25) is that of plagioclase, r: ratio of assimilation to fractional crystallization, Fc: fraction of the residual liquid.

simple fractional crystallization process, whereas the samples plotted within the r-values ~0.3 are affected by fractionation and magma mixing and/mingling with the Himurodake Quartz diorite magma. In other words, this geochemical feature suggests that the low SrI group is mainly produced through the process of mixing and/or mingling with the Himurodake Quartz diorite magma during the fractionation. The results of geochemical modeling can duplicate geochemical variations of the Kibe Granite. Consequently, the Kibe Granite is evolved with complicated magma processes involving assimilation of the pelitic gneisses and mixing of the Himurodake Quartz diorite in addition to the fractional crystallization.

7-1-3. Inferred assimilation process of the Kibe Granite

The temperature conditions of the host rocks are an important factor of the AFC process of granitic magmas (Diaz-Alcarado et al., 2011). If a granitic magma intrudes the high-temperature zone in a crust, the AFC process is easily progressed at a marginal part of suite. The Kibe Granite has been emplacement of the highest-grade zone, banded gneiss zone (Higashimoto et al., 1983) and upper structural portion of cordierite-garnet zone (Okudaira, 1996: Ikeda, 1998), of the Ryoke metamorphic rocks in the Yanai district. The intrusive age (ca. 91 Ma; Suzuki and Adachi, 1998) corresponds to the time at the immediately after peak metamorphism (ca. 95 Ma; Okudaira et al.). Okudaira et al. (2001) analyzed thermal history of the Ryoke belt in the Yanai district using numerical modeling. According to their modeling, the metamorphic rocks still preserved high temperature (> 450 °C) at the timing of emplacement of the Kibe Granite (ca. 91 Ma). Kamitomo et al. (2008) revealed that the metamorphic rocks from the highest-grade zone, the garnet-cordierite zone, initially experienced an isothermal decompression, adiabatic ascending, after the peak metamorphism. The temperature conditions of the garnet-cordierite zone have reached up to 800 °C at peak metamorphism (Ikeda, 2004). The Kibe Granite would, therefore, be emplacement in the "hot-crust". In addition, the Himurodake Quartz diorite magma also intruded as coeval magma activity with the Kibe Granite magma. As a result, the crustal temperature was elevated at the timing of emplacement of the Kibe Granite magma.

The sheeted intrusive rocks effectively provide thermal energy from intrusive suites to host rocks (Diaz-Alcarado et al., 2011). The Kibe Granite can provide the enough heat to a host rock because it occurs as the elliptic shape. On the basis of numerical study, if the host rocks has already gained the temperature conditions at least 450 °C, the partial melting can take place in the host rock and AFC processes effectively progress in the elliptic granite suite (Takahashi, 1992). Since the temperature condition of the host pelitic gneiss can expect to preserve more than 450 °C (Okudaira et al., 2001), the partial melting probably took place in the host pelitic gneiss at the timing of emplacement of the Kibe Granite. The marginal part of suite includes anhedral quartz grains that bear the fine-grained quartz and biotite (Fig. 4-5-1B). This texture is recognized in the host pelitic gneisses of the Kibe Granite (Figs. 4-1-2-1 and 4-1-2-2); thereby suggesting that the anhedral quartz grains are regarded as xenocrysts derived from the host pelitic gneiss, and the xenocrysts would be traces of the residual phases during the AFC process of the Kibe Granite. It is inferred that the AFC processes efficiently progress in the Kibe Granite at the timing of emplacement during the ascending of the Ryoke metamorphic rocks.

7-2. Cause of geochemical signatures of the Namera Granite

The Namera Granite belonging to the Younger Ryoke granite intrudes into the Ryoke metamorphic rocks and occurs at north of the Kibe Granite. The granite consists mainly of quartz, plagioclase, K-feldspar, biotite and muscovite with trace amounts of garnet and cordierite. In addition, many acicular sillimanite (fibrolite) are observed (Fig. 7-2-1). In SiO_2 vs. major and trace elements diagram, the Namera Granite is plotted on chemical trends of the Kibe Granite, but is rich in Al_2O_3 and poor in K_2O rather than the Kibe Granite (Fig. 7-2-2). The A/CNK values are higher than 1.2 (Table 5-4). However, the Sr and Nd isotopic compositions of the Namera Granite are slightly different from those of the Kibe Granite (Table 6-4). The NdI values corrected with 91 Ma of the Namera Granite show lower than those of the Kibe Granite in comparison with the same SrI values (Tables 6-3 and 6-4). Therefore, the Namera Granite probably formed the AFC process between the Ryoke pelitic

09032205

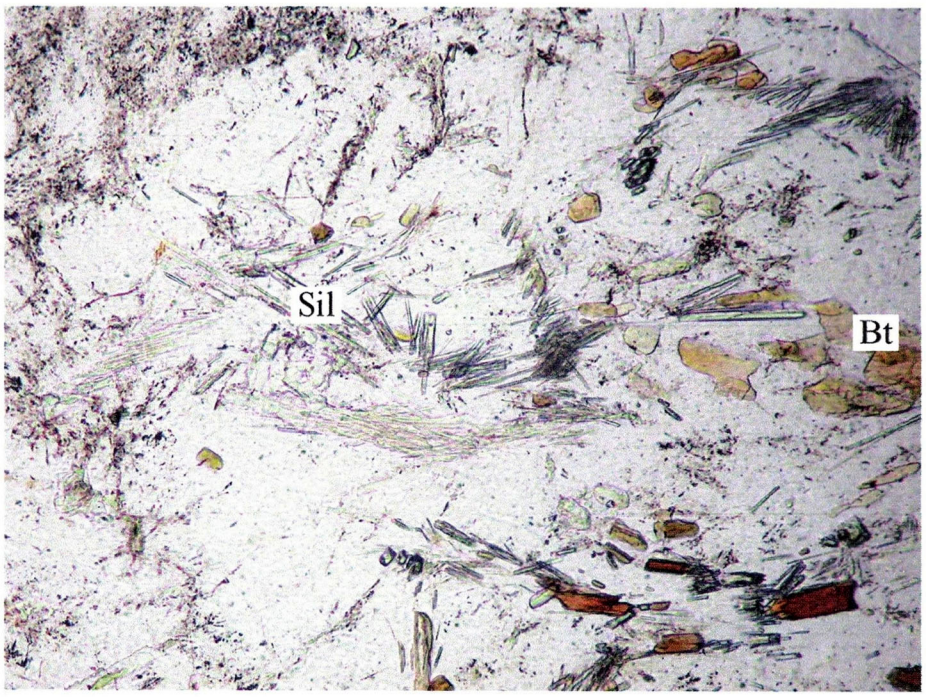

open nicol

0.3 mm

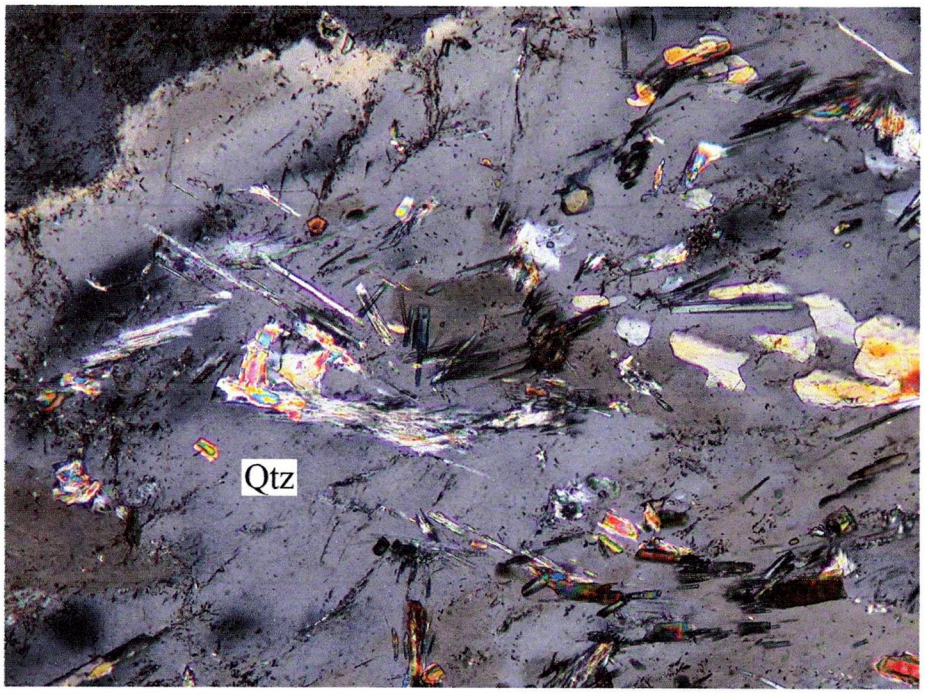

crossed nicols

0.3 mm

Fig. 7-2-1 Photomicrographs of the Namera Granite. Qtz: quartz, Bt: biotite, Sil: silimanite.

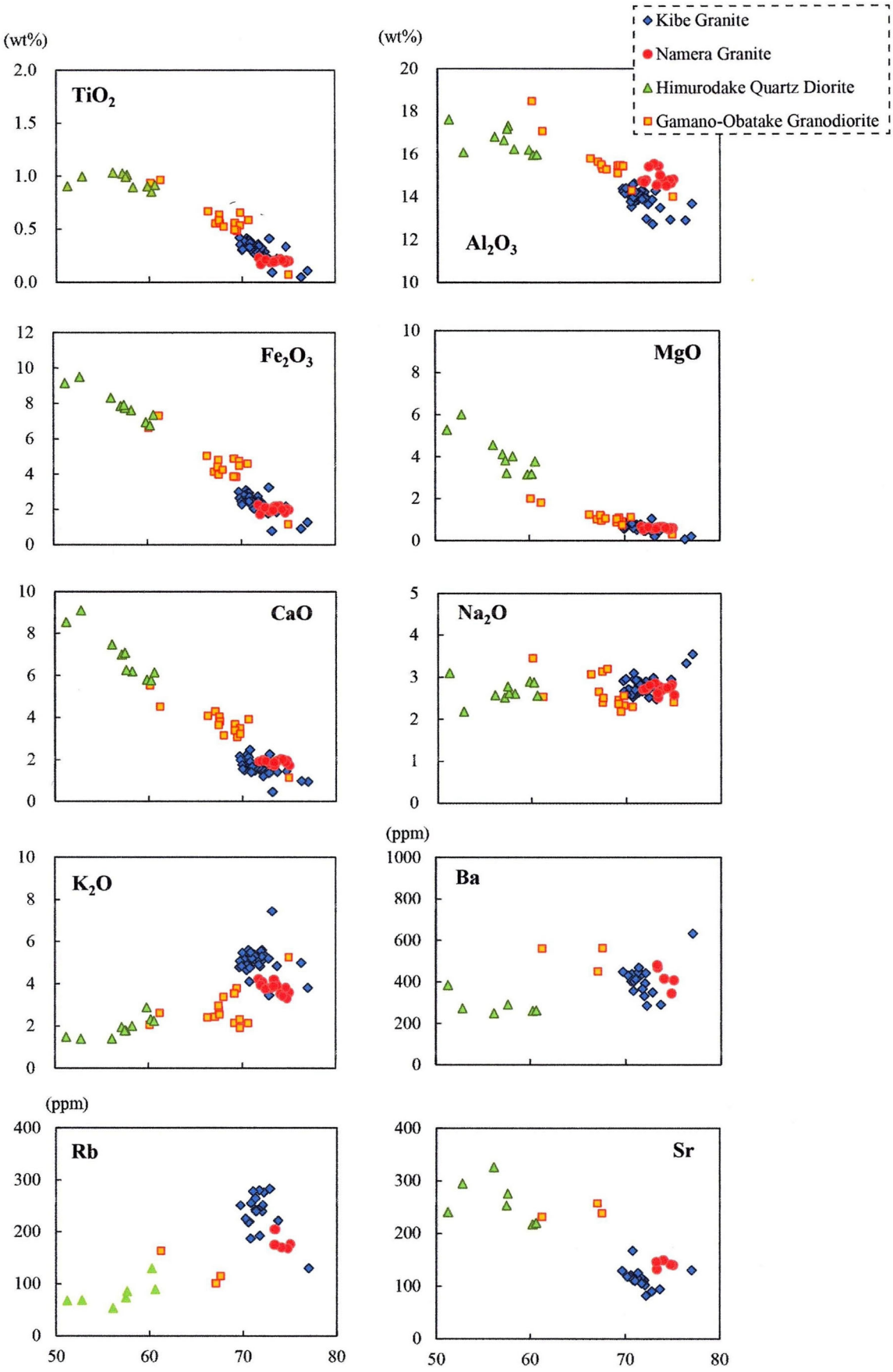

Fig. Major and trace element variation diagrams of Kibe Granite, Namera Granite, Himurodake Quartz diorite and Gamano-Obatake Granrodiorite..

gneisses possessing low Nd isotopic compositions and a granitic magma similar to the parental magma of the Kibe Granite.

7-3. Petrogenesis of the Kibe Granite

The Kibe Granite crops out in the northern part of the Gamano-Obatake Granodiorite that is the representative the Older Ryoke granite (Higashimoto et al., 1983). As mentioned previously, the intrusive boundary between two suites is obscure. Geochemical features of the Kibe Granite are similar to those of the Gamano-Obatake Granodiorite; thereby, suggesting genetic relationships between the Kibe Granite and the Gamao-Obatake Granodiorite. In this section, the author mainly addresses petrography and geochemistry of the Gamano-Obatake Granodiorite and the Kibe Granite, and discusses the petrogenesis of the Kibe Granite magma.

7-3-1. Possibility of partial melting of the Gamano-Obatake Granodiorite

The chemical trends of the Gamano-Obtake Granodiorite are different from those of the Kibe Granite in some variation diagrams (Fig. 7-2-2). These geochemical features suggest that the fractionation and/or AFC processes are unlikely adopted to explain the formation of the Kibe Granite magma. The other possibility regarding the origin of the Kibe Granite magma is a partial melting of the Gamao-Obatake Granodiorite because partial melting of granitic rocks with tonalite to granodiorite compositions is possible formation process of high-SiO_2 and -K_2O granite magma (Wedepohl, 1991; Beard and Lofgren, 1991).

It is expected that the specific textures or mineral assemblages are observed in a partially molten migmatite. The Gamano-Obatake Granodiorite is intruded by the Himurodake Quartz diorite (Fig. 3-4-2). In this part, the Gamano-Obatake Granodiorite locally shows a migmatitic structure where leucocratic patches and pools appear in the granodiorite (Fig. 3-4-2). Some plagioclase grains in the migmatite show granoblastic and corroded shapes coexisting with anhedral K-feldspar and quartz (Fig. 7-3-1-1). This texture is regarded as results of partial melting of the Gamano-Obatake Granodiorite under the eutectic situations. The corroded

09032208A

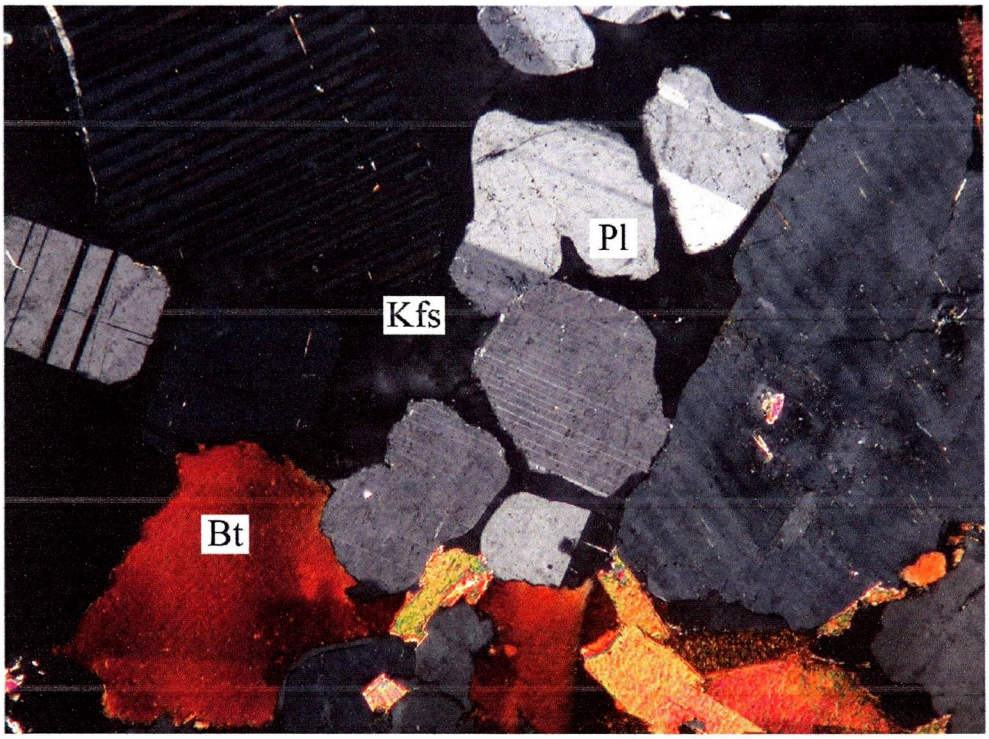

Fig. 7-3-1-1 Photomicrographs of the Gamano-Obatake Granodiorite. Plagioclase shows corroded shapes. Pl: plagioclase, Kfs: K-feldspar, Bt: biotite.

shape plagioclase is considered to be a residual mineral. In addition to this specific texture, the Gamano-Obatake Granodiorite contains a significant texture. In the boundary zone between the Gamano-Obatake Granodirote and the Kibe Granite, the granodiorite is composed mainly of plagioclase, quartz and biotite with a small amount of anhedral K-feldspar. Most of constituent minerals show subhedral to anhedral shapes. The preferred orientation of biotite grains forms pervasive foliations. On the other hand, the Kibe Granite is characterized by phenocrystic K-feldspar. It is noteworthy that preferred orientation of biotite grains and K-feldspar phenocrysts are observed in one thin section (Fig. 7-3-1-2). These two textures represent petrographical characters both of the Kibe Granite (K-feldspar phenocrysts) and the Gamano-Obatake Granodiorite (preferred orientation of biotite grains), suggesting mixture of the Gamano-Obatake Granodiorite and the Kibe Granite.

It is known that source rocks possesses low SiO_2 rather than melts derived from source rocks. The Gamano-Obatake Granodiorite possesses the low SiO_2, and shows lower REE abundances rather than the Kibe Granite (Figs. 5-1-3, 5-3-3 and 7-2-2). In addition, the SrI and NdI values corrected with 91 Ma overlap between the Gamano-Obatake Granodiorite and the Kibe Granite (Fig. 7-3-1-3). Considering petrography and geochemistry including Sr and Nd isotopic studies, the Kibe Granite magma can be produced by partial melting of the Gamano-Obatake Granodiorite.

7-3-2. Petrogenetic considerations of the Kibe Granite magma

In order to examine the above-mentioned hypothesis, model calculations have done with formulation of batch melting equation using trace element compositions and partitioning coefficient. The Gamano-Obatake Granodiorite and the Kibe Granite is regarded as a source rock and a partial molten product released from a source rock. Tables 7-3-2-1 and 7-3-2-2 show the inferred source composition, calculated melt compositions and partitioning coefficients of each mineral. The results are shown in the spider diagram normalized to values (Fig. 7-3-2-1).

Figure 7-3-2-1 shows the spider diagram normalized to N-MORB plotting the Kibe

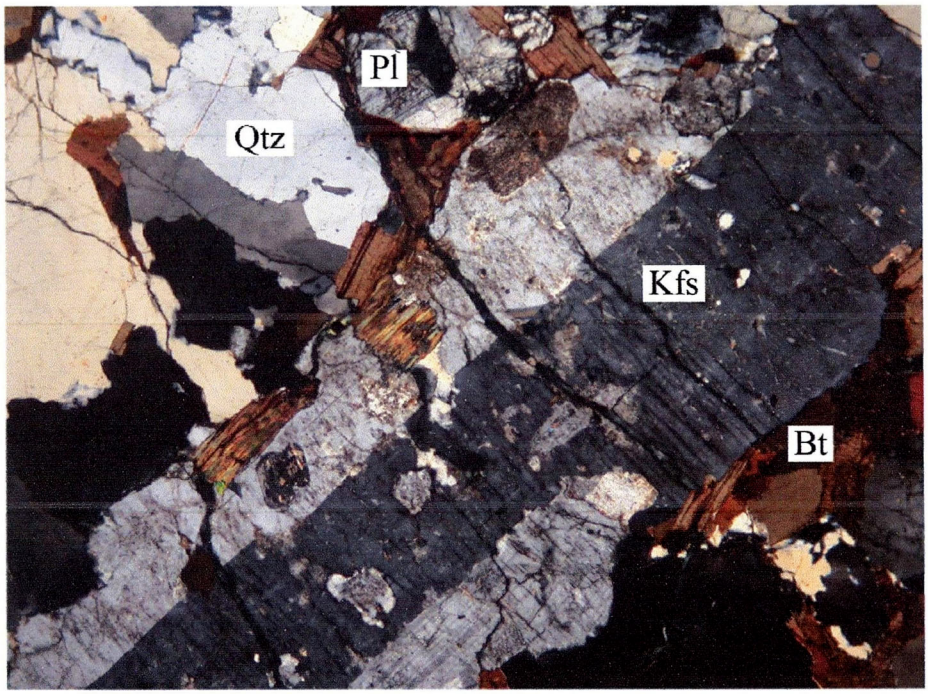

crossed nicols

1.5 mm

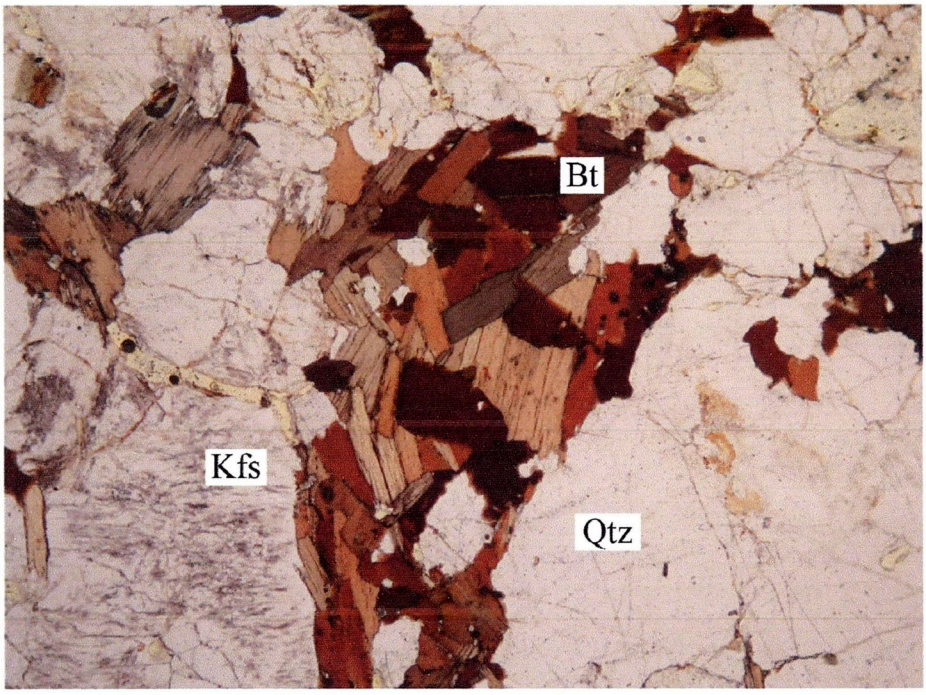

open nicol

1.5 mm

Fig. 7-3-1-2 Photomicrographs of the Kibe Granite. Note that K-feldspar phenocrysts and preferred orientation of biotite grains can be observed in the same thin section. Kfs: K-feldspar, Pl: plagioclase, Qtz: quartz, Bt: biotite.

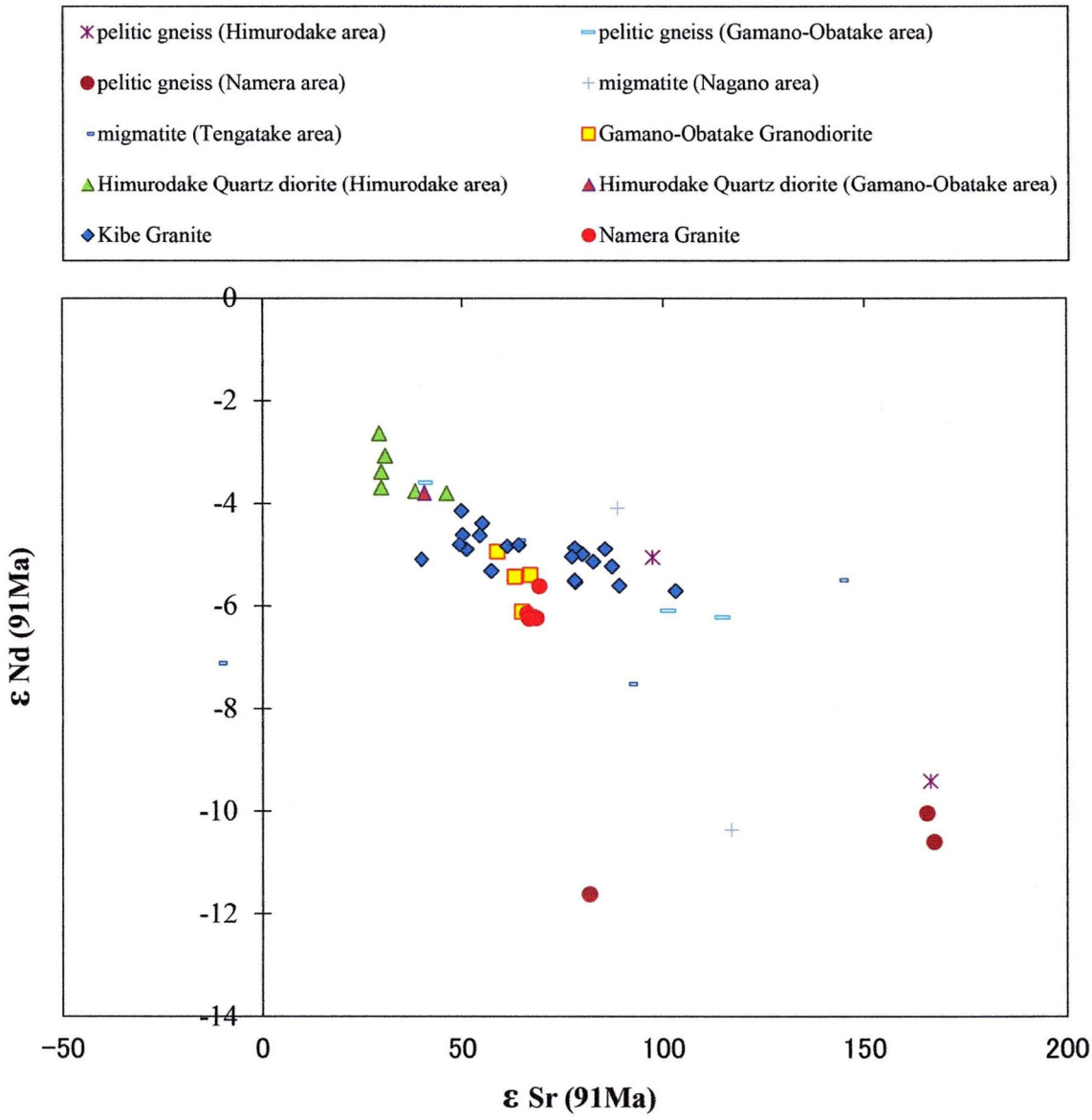

Fig. 7-3-1-3 εSr (91Ma) –εNd (91Ma) diagram for all samples of study area.

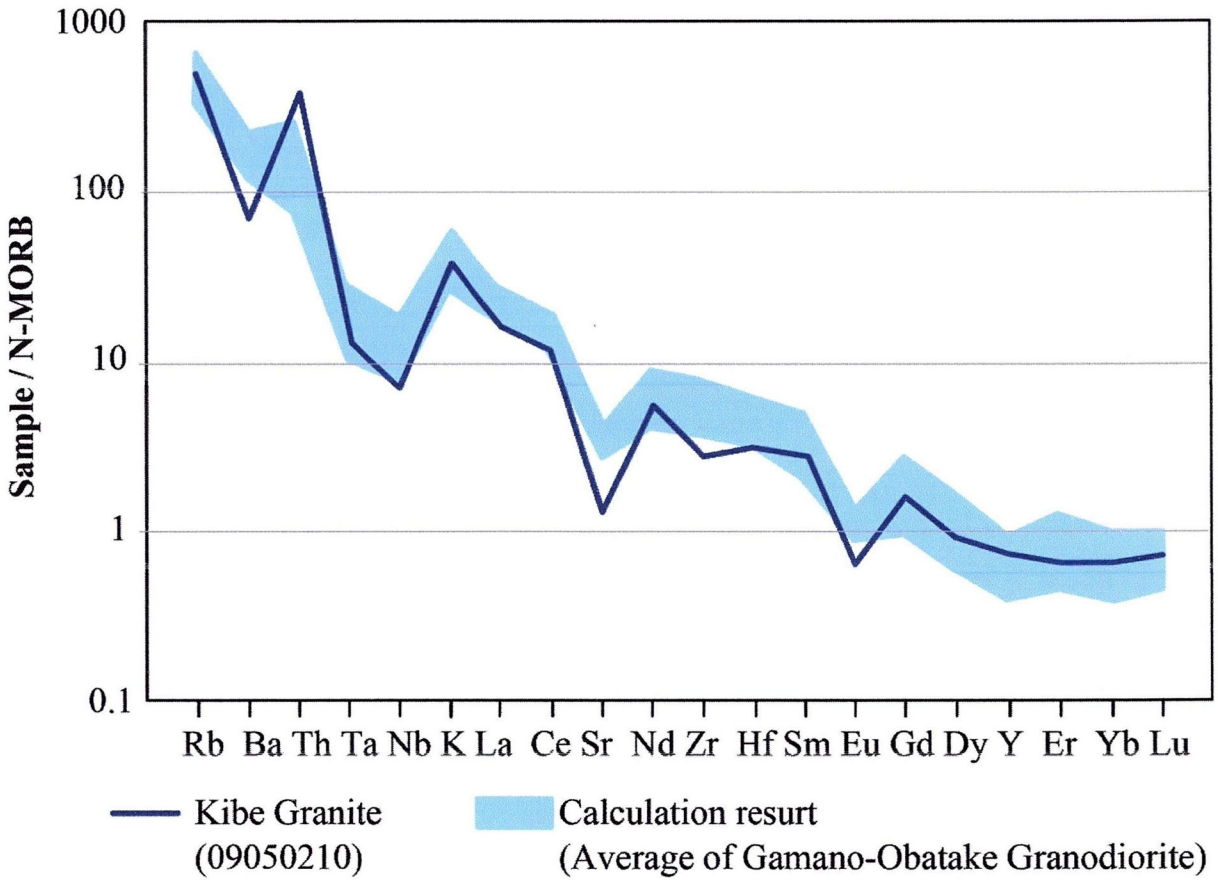

Fig. 7-3-2-1 Spider diagram plotting the Kibe Granite and calculated melt compositions utilizing the batch melting equation.

Granite and inferred melt compositions. The pattern for the inferred melt compositions is similar to that of the Kibe Granite although Sr and Eu contents of the Kibe Granite are lower than those of the calculated melts. It is assumed that the Kibe Granite documented here has already subtracted plagioclase from the inferred parental magma. Therefore, taking petrography and geochemical modeling into account, the parental magma of the Kibe Granite, the Younger Ryoke granite, can be derived from the partial melting of the Gamao-Obatake granodiorite representing the Older Ryoke granite in the Yanai district.

7-4. Igneous activity of the Ryoke granitoids

In the western part of Southwest Japan, the Yanai district is one of the typical areas of the Ryoke metamorphic belt. In this district, the Ryoke granitoids both the Older and Younger Ryoke granites are widely exposed. An understanding igneous activity in this district can, therefore, be an be establishment of typical magma processes in the Ryoke metamorphic belt. In addition to the major conclusions described in the previous sections, the author proposes a schematic model regarding igneous activity of the Ryoke metamorphic belt.

The pictorial summary is shown in the εSrI vs. εNd diagram with calculation trends of the AFC model (Fig. 7-4-1). The Gamano-Obatake Granodiorite is regarded as the source material of the parental magma of the Kibe Granite. According to the above-mentioned scenario, the SrI and NdI values of parental magma must show the same as those of the Gamano-Obatake Granodiorite. Some samples of the low SrI group of the Kibe granite overlap with the Gamano-Obatake Granodiorite in the εSrI vs. εNd diagram (Fig. 7-4-1). On the other hand, most of the high SrI and low SrI groups are plotted along the different AFC trends. On the basis of this diagram, the high SrI and low SrI groups are influenced by the geochemical features of the pelitic gneiss and of the Himurodake Quartz diorite, respectively. The results of this diagram support the magma process of Kibe Granite as discussed in the previous section.

Finally, the following petrogenetic scenarios of the Ryoke granitoids are proposed (Fig. 7-4-2). The Gamano-Obatake Granodiorite magma belonging to the Older Ryoke granite

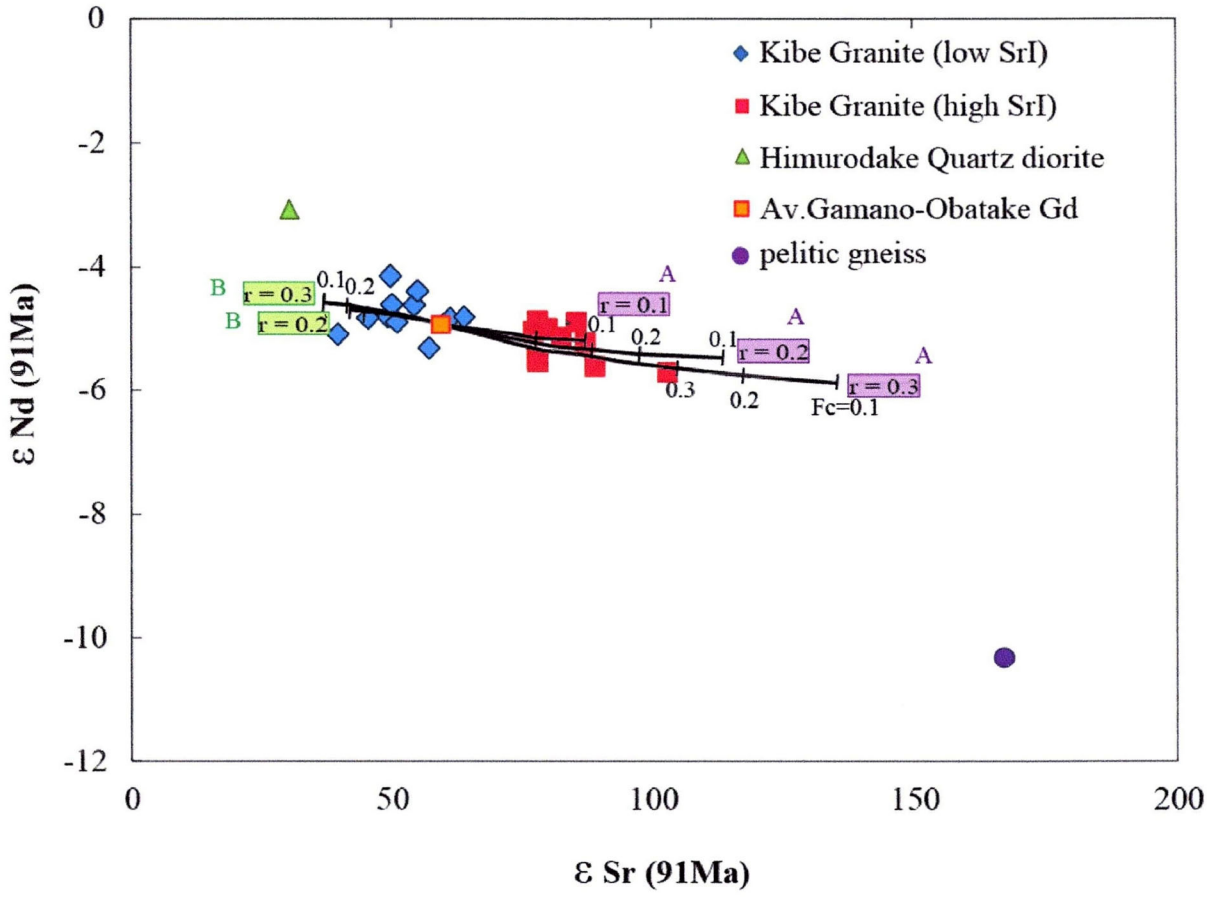

Fig. 7-4-1 ε Sr (91Ma)-ε Nd (91Ma) diagram plotting the Kibe Granites, the Himurodake Quartz diorite and the pelitic gneiss. Lines (A) are of AFC trends between the Kibe Granite (sample 09050210) and pelitic gneiss (sample 10032102A). Lines (B) show both the magma mixing and fractional crystallization models (similar to AFC model) between the Kibe Granite (sample 09050210) and the Himurodake Quartz diorite (sample 10060601B). Note that the Gamano-Obatake Granodiorite is plotted within the low SrI group of the Kibe Granite. r: ratio of assimilation to fractional crystallization, Fc: fraction of the residual liquid.

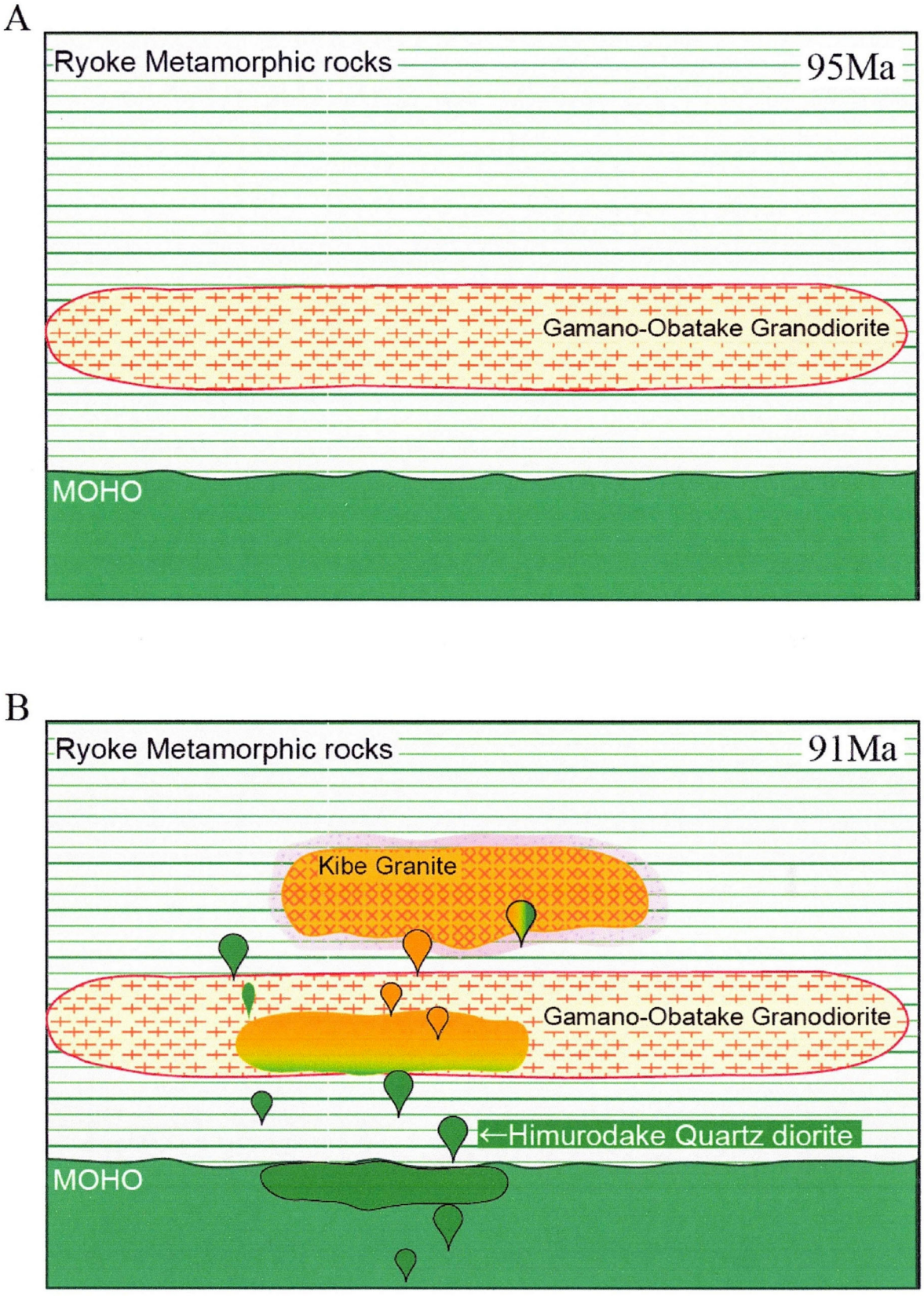

Fig. 7-4-2 Schematic the model of magma processes of the Ryoke granitoids. Detailed explanation can be seen in the text.

concordantly intruded the Ryoke metamorphic rocks close to the timing of peak metamorphism (95 ± 6 Ma) in the high-grade zone (Fig. 7-4-2A). After peak metamorphism, the Ryoke metamorphic rocks together with the Gamano-Obatake Granodiorite tectonically ascended (Okudaira et al., 2001); however, the magma activities of Ryoke granitoids still continued at this stage. According to Suzuki and Adachi (1998), the intrusive age of the Gamano-Obatake Granodiorite and the Kibe Granite are 95 ± 6 Ma and 91 ± 2 Ma, respectively. These ages overlap within the analytical error. Before the Gamano-Obatake Granodiorite was completely cooled down, the Himurodake Quartz diorite equivalent to the Younger Ryoke granite intruded the Gamano-Obatake Granodiorite (Fig. 7-4-2B). The Himurodake Quartz diorite magma supplied the thermal energy to the "hot" Gamano-Obatake Granodiorite suite. As a result, the partial melting took place in the Gamano-Obatake Granodiorite, giving rise to the parental magma of the Kibe Granite (91 ± 2 Ma). The Kibe Granite magma was evolved with complicated magma processes involving assimilation of the pelitic gneisses and mixing of the Himurodake Quartz diorite magma in addition to the fractional crystallization. According to this scenario, the Ryoke granitoid magmas continuously intrude the crust from the Older Ryoke granite to the Younger Ryoke granite with strong connection regarding their petrogenesis. Therefore, the Ryoke granitoids cannot be divided into the "Older" and "Younger" Ryoke granites. The author proposes to use the "Ryoke granite" instead of "Older and Younger Ryoke granites". An understanding of the evolution of continental crust is thought to be the magma process in the continental crust from a mantle-input basaltic magma to a granitic magma. In this paper, the author climes that the Kibe Granite, the Younger Ryoke granite, can be produced by partial melting of the Gamano-Obatake Granodiorite, the Older Ryoke granite. The formation of evolve granitic magma needs the process of a re-melting of granitic materials, which is probably derived from the basaltic lower crust. This should be the essential and general processes of the formation of the continental crust at the active continental margin.

Chapter 8. Concluding remarks

(1) The Kibe granite is geochemically divided into the high SrI and low SrI groups. The high SrI group should be influenced by contamination of the pelitic gneiss during the differentiation of magma. On the other hand, the low SrI group can result from the magma mingling and/or mixing between the Kibe Granite and the Himurodake Quartz diorite.

(2) On basis of field observations, petrographical features and a geochemical modeling, the Kibe Granite is evolved with complicated magma processes involving assimilation of the pelitic gneisses and mixing of the Himurodake Quartz diorite in addition to the fractional crystallization.

(3) The Namera Granite probably formed the AFC process between the Ryoke pelitic gneisses possessing low Nd isotopic compositions.

(4) The Gamano-Obatake Granodiorite locally shows a migmatitic structure. Some plagioclase grains in the migmatite show granoblastic and corroded shapes coexisting with anhedral K-feldspar and quartz. This texture is regarded as results of partial melting of the Gamano-Obatake Granodiorite under the eutectic situations.

(5) The SrI and NdI values corrected with 91 Ma overlap between the Gamano-Obatake Granodiorite and the Kibe Granite.

(6) Considering petrography and geochemistry including Sr and Nd isotopic studies, the Kibe Granite magma can be produced by partial melting of the Gamano-Obatake Granodiorite.

(7) The Ryoke granitoid magmas continuously intrude the crust from the Older Ryoke granite to the Younger Ryoke granite with strong connection regarding their petrogenesis. Therefore, the Ryoke granitoids cannot be divided into the "Older" and "Younger" Ryoke granites. The

author proposes to use the "Ryoke granite" instead of "Older and Younger Ryoke granites".

Acknowledgement

The author would like to express my deep gratitude to Prof. Masaaki Owada, for his warm encouragement and constant direction throughout this study, and his helpful and valuable suggestions. Prof. Teruyoshi Imaoka has done a great deal many advices and analytical support of isotopic study. Prof. Takashi Kano has also done a great deal many advices, especially field works. I gratefully acknowledge constrictive comments and reviews of this manuscript and to help the isotopic measurements by Dr. Atsushi Kamei (Shimane University). Thanks also go to Prof. Kazuhiro Tanaka, Drs. Toshiya Abe and Kiichiro Kawamura for critical reading of the manuscript. I wish to thank to Dr. Itsuki Kamitomo, Mrs. Dai Nishiduka, Kengo Takizawa, Daisuke Hyodo and Takahiro Midorikawa, and Mss. Erika Yamawaki, Chika Iwata, Yuki Hara and Madoka Terao for the laboratory work.

Finally, I am deeply grateful to all people who support me in this study.

References

Bea, F., Pereira, M.D. and Stroh, A. (1994) Mineral/leucosome trace-element partitioning in a peraluminous migmatite (a laser ablations-ICP-MS study). Chem. Geol., 117, 291-312

Beard, J. S. and Lofgren, G. E. (1991) Dehydration melting and water-saturated melting of basaltic and andesitic greenstones and amphibolites at 1, 3 and 6.9 kb. Jour. Petrol., 32, 365-401.

DePaolo, D.J. (1981) Trace element and isotopic effects of combined wallrock assimilation and fractional crystallisation. Earth Plan. Sci. Lett., 53, 189-202.

Diaz-Alvarado, J., Castro, A., Fernandez, C. and Moreno-Ventas, I. (2011) Assessing bulk assimilation in cordierite-bearing granitoids from the Central System Batholith, Soain; expelimental, geochemical and geochronological constraints. Jour. Petrol., 52, 223-256.

Ewart, A. and Griffin, W.L (1994) Application of Proton-Microprobe data to trace-element partitioning in volcanic rocks. Chem. Geol., 117, 251-284.

Gill, J. B. (1991) Orogenic Andesites and Plate tectonics. Springer-Verlag, Berlin Heidelberg, 390p.

Gromet, L. P. and Silver, L. T. (1987) REE variations across the Peninsular Range batholith: implications for Batholithic petrogenesis and crustal growth in magmatic arcs. Jour. Petrol., 28, 75-125.

Harayama, S., Koido, Y., Ishizawa, K., Nakai, Y. and Kutsukake, T. (1985) Cretaceous to Paleogene Magmatism in the Chubu District, Japan. Earth Sci., 39, 345-357.

Hibbard, M. J. (1995) Petrography to Petrogenesis. pp. 587, Prentice Hall, New Jersey.

Higashimoto, S., Nureki, T., Hara, I., Tsukuda, E., Nakajima, T. (1983) Geology of the Iwakuni district. pp. 79, Geol. Surv. Japan.

Iizumi, S. (1996) Sr and Nd isotopic analyses, using a thermal ionization mass spectrometer MAT262. Geosci. Rept. Shimane Univ., 15, 153-159.

Ikeda, T. (1998) Progressive sequence of reactions of the Ryoke metamorphism in the Yanai district, southwest Japan: the formation of cordierite. Jour. Meta. Geol., 16, 39-52.

Ikeda, T. (2004) Pressure- temperature conditions of the Ryoke metamorphic rocks in Yanai

district, SW Japan. Contrib Mineral Petrol., 146, 577-589.

Imaoka, T., Ohira, T., Sawada, Y. and Itaya, T. (1994) Radiometric ages of Cretaceous to Tertiary igneous rocks from Chugoku and Shikoku districts, Southwest Japan. Bull. Res. Inst. Natul. Sci. Okayam Univ. Sci., 20, 3-57.

Ishihara, S. (1971) Modal and chemical composition of the granitic rocks related to the major molybdenum and tungsten deposits in the Inner Zone of Southwest Japan. Jour. Geol. Soc. Japan, 77, 441-452.

Jahn, B.M., Capdevila, R., Liu, D., Vernon, A. and Badarch, G. (2004) Sources of Phanerozoic granitoids in the transect Bayanhongor-Ulaan Baatar, Mongolia: geochemical and Nd isotopic evidence, and implications for Phanerozoic crustal growth. Jour. Asian Earth Sci., 23, 629-653.

Kagami, H., Iizumi, S., Tainosho, Y. and Owada, M. (1992) Spatial variations of Sr and Nd isopote ratios of Cretaceous – Paleogene granitoid rocks, Southwest Japan Arc. Contrib. Mineral. Petrol., 112, 165-177.

Kagami, H., Kawano, Y., Ikawa, T., Ishioka, J., Kagashima, S., Yuhara, M., Shuto. K., Iizumi, S., Imaoka, T., Owada, M., Osanai, Y., and Tainosho, Y. (1999) Tranisitoin of space and time Cretaceous to Tertiary igneous activity and lower crust of Honshu Arc –Examination based on Rb-Sr whole rock isochron ages and Sr and Nd isotopes–. Mem. the Geol. Soc. Japan., no. 53, 1-19.

Kagami, H., Okano, O., Sudo, H. and Honma, H. (1987) Sr and Nd isotopic compositions and Rb, Sr, Sm and Nd concentrations of standard samples. Tech. Rep. ISEI Okayama Univ. Ser. B, 4, 1-16.

Kamei, A. (2002); Petrogenesis of cretaceous peraluminous granite suites with low initial Sr isotopic ratios, Kyusyu Island, Southwest Japan arc. Gondwana Res., 5, 813-822.

Kamitomo, I., Imaoka, T. and Owada, M. (2008) Decompressional microstructure from garnet-bearing mafic granulite in Yanai district, Ryoke belt, Southwest Japan. Jour. Geol. Soc. Japan, 114, 88-91.

Koide, H (1958) Dando granodioritic intrusives and their associated metamorphic complex. pp. 311, Japan Soc.Prom. Sci.

Kutsukake, T. (1993) An initial continental margin plutonism Cretaceous Older Ryoke granitoids, southwest Japan. Geological Magazine. 130, 15-28

Kutsukake, T. (1997) Petrology and geochemistry of a calcic and ferrous granitoid pluton : the Mitsuhashi Granite in the Ryoke Belt, southwest Japan. Journal of mineralogy, petrology and economic geology 92(6), 231-244.

Kutsukake, T. (2002) Geochemical characteristics and variations of the Ryoke granitoids, Southwest Japan: Petrogenetic implications for the plutonic rocks of a magmatic arc. Gondwana Res., 5, 355-372.

Martin, H. (1987) Petrogenesis of Archaena trondhjemites, tonalities, and granodiorites from eastern Finland: major and trace element geochemistry. Jour. Petrol., 28, 921-953.

Moutte, J. (1990) Geochemical study of Cretaceous granitic rocks from Yanai district, Southwest Japan. Univ. Mus. Univ. Tokyo, Natur. Cult., no. 2, 49-66.

Moutte, J., and Iiyama, J.T. (1984) The Ryoke-Sanyo granite series in the Iwakuni-Yanai district, Southwest Honshu, Japan. Min. Geol., 34, 425-436.

Nureki, T. (1974) Contact metamorphism in the So-o district, Yamaguchi Prefecture, Japan-with special reference to the occurrence of sillimanite. Mem. Geol. Soc. Japan, no. 11, 251-281.

Okamura, Y. (1957) Structure of the Ryoke Metamorphic and Granodioritic Rocks of the Yanai District, Yamaguchi Prefecture. Jour. Geol. Soc. Japan, 63, 684-697.

Okano, O. and Honma, H. (1983) Sr isotopic ratios of the Ryoke granite and Hiroshima granite in Yanai district. MAGMA, no. 67, 123-128.

Okudaira, T. (1996) Thermal evolution of the Ryoke metamorphic belt, southwest Japan: Tectonics and numerical modeling. Island Arc, 5, 373-385.

Okudaira, T., Hara, I., Sakurai, Y. and Hayasaka, Y. (1993) Tectono-metamorphic processes of the Ryoke belt in the Iwakuni-Yanai district, Southwest Japan. Mem. Geol. Soc. Japan, no. 42, 91-120.

Okudaira, T. and Seo, T. (1996) Granitization processes in the Tengatake migmatite zone of the Ryoke metamorphic belt in the Yanai district, southwest Japan. Tectonics and Metamorphism (The Prof. I. Hara Volume). 157-163.

Okudaira, T., Hayasaka, Y., Himeno, O., Watanabe, K., Sakurai, Y. and Ohtomo, Y. (2001) Cooling and inferred exhumation history of the Ryoke metamorphic belt in the Yanai district, south-west Japan: Constraints from Rb-Sr and fission-track ages of gneissose granitoid and numerical modeling. Island Arc, 10, 98-115.

Pearce J. A. and Norry, M. J. (1979) Petrogenetic implications of Ti, Zr, Y and Nb variations in volcanic rocks. Contrib. Mineral. Petrol., 69. 33-47.

Pearce J. A., Harris N. B. W. and Tindle A. G. (1984) Trace element discrimination diagrams for the tectonic interpretation of granitic rocks. Jour. Petrol., 25, 956-983.

Rollinson, H. (1993) Using geochemical date: evaluation, presentation, interpretation. Longman, London, 352p.

Ryoke Research Group. (1972) The Mutual Relations of the Granitic Rocks of the Ryoke Metamorphic Belt in Central Japan. Earth Sci., 26, 205-216.

Sakai, E., Otani, M., Sugioka, K., Hayakawa, M., Mizutani, T., Noda, I., Miyoshi, K., Miura, H., Matsuoka, S., Hattori, Y. and Ito, T. (1965) Preliminary Notes on the Order of Intrusion of the Mesozoic Igneous Rocks in the three cities of Mizunami, Ena, and Nakatsugawa, and in the Ena District, Gifu Prefecture, Central Japan. Rep. Aichi Univ. Edu., Natl. Sci., 14, 61-71.

Sun, S. S., McDonough, W. F. (1989) Chemical and isotopic systematics of oceanic basalts: implications for mantle composition and processes. In: Saunders, A. D. and Norry, M. J. (Eds) Magmatism in oceanic basins. Geol. Soc. London, Spe. Pub., no. 42, 313-345.

Suzuki, K. and Adachi, M. (1998) Denudation history of the high T/P Ryoke metamorphic ages of gneisses and granitoids. Jour. Meta. Geol., 16, 23-37.

Suzuki, K., Adachi. M. and Nureki, T. (1996) CHIME age dating of monazites from metamorphic rocks and granitic rocks of the Ryoke belt in the Iwakuni area, Southwest Japan. Island Arc, 5, 43-55.

Takahashi, Y. (1992) Petrological study of tonalitic rocks in the upper reaches of Satsunai River, Main Zone of the Hidaka Metamorphic Belt – Coexistent relation of S-type with I-type granite –. Jour. Geol. Soc. Japan, 98, 295-308.

Tanaka, T., Togashi, S., Kamioka, H., Amakawa, H., Kagami, H., other 14 authors (2000)

JNdi-1: a neodymium isotopic reference in consistency with La Jolla neodymium. Chem. Geol., 168, 279-281.

Wedepohl, K. H. (1991) Chemical composition and fractionation of the continental crust. Geol. Rund., 80, 207-223

Wedepohl, K. H. (1995) The composition of the continental crust. Geochim. Cosmochim. Acta, 59, 1217-1232.

Yamada, N. (1966) Finding of a Ryoke Granite Intruding into the Nohi Phyolites, and Its Significance. Jour. Geol. Soc. Japan, 72, 355-358.

Yamada, T. (1971) Relation between the Ryoke Plutonometamorphism and the Late Mesozoic Volcanoplutonism in Central Japan. Earth Sci., 25, 97-104.

Yamasaki, T., Owada, M., Imaoka, T., Shiraki, K. (1999) Major and trace element analyses of samples by X-ray fluorescence spectrometry. Rep. Cent. Instr. Anal. Yamaguchi Univ., no. 7, 22-31.

Yokoyama, S. (2009) The Ryoke granitoids. *In: Geology of Japan, Chugoku district. Y. Nishimura and K. Kiminami (eds.)*, pp. 250-258, Asakura-shoten, Tokyo.

Yuhara, M. (1994) Timing of intrusion of the Otagiri granite with respect to the deformation and metamorphism in Ryoke belt in the Ina distrist, central Japan: Examination by Rb-Sr whole rock isochron ages. Jour. Min., Petr. Eco. Geol., 89, 269-284.

Yuhara, M. (2008) Petrochemical characteristics of the Hissori Granite in the Ina district of the Ryoke Metamorphic Belt, Southwest Japan Arc: adakitic granite in the Ryoke Metamorphic Belt. Earth Sci., 62, 221-232.

Yuhara, M. and Kagami, H. (1995) Cooling history of the Katsuma quartz diorite in the Ina district of the Ryoke belt, Southwest Japan Arc. Jour. Geol. Soc. Japan, 101, 434-442.

Yuhara, M. and Kagami, H. (1999) Chronological and isotope geological study of the Takato granite in the Ina district of the Ryoke belt, Southwest Japan Arc. Jour. Geol. Soc. Japan, 105, 181-192.

Yuhara, M., Hara. F. and Kagami, H. (2000) Rb-Sr, Sm-Nd ages and its significance of the Hiji tonalite in the Ina district of the Ryoke belt, Southwest Japan Arc. Mem. Geol. Soc. Japan, no. 56, 241-253.

Yuhara, M., Kagami, H. and Nagao, K. (2000) Geochronological characterization and petrogenesis of granitoids in the Ryoke belt, Southwest Japan Arc: constraints from K-Ar, Rb-Sr and Sm-Nd systematics. Island Arc, 9, 64-80.

Appendixes

Table 5-1 Results of major and trace element analyses for the Gamano-Obatake Granodiotite.

	Gamano-Obatake Granodiorite					
Sample No.	09022801	09032206A	09032206B	09032207A	09032207B	09032208A
XRF						
SiO_2 (wt%)	70.66	67.10	67.52	69.20	69.75	67.58
TiO_2	0.58	0.55	0.64	0.56	0.53	0.56
Al_2O_3	14.29	15.64	15.41	15.45	15.42	15.30
Fe_2O_3	4.59	4.13	4.81	4.88	4.75	3.97
MnO	0.09	0.08	0.09	0.07	0.12	0.06
MgO	1.11	1.01	1.16	0.87	0.90	0.95
CaO	3.91	4.28	4.03	3.68	3.48	3.81
Na_2O	2.29	2.65	2.39	2.45	2.32	2.50
K_2O	2.13	2.44	2.76	2.14	2.32	2.55
P_2O_5	0.08	0.07	0.09	0.11	0.09	0.08
LOI	0.60	0.55	0.57	0.62	0.55	0.52
Total	100.34	98.50	99.48	100.04	100.24	97.88
A/CNK	1.08	1.06	1.08	1.18	1.22	1.11
ICP-MS						
Rb (ppm)	—	101	—	—	—	115
Sr	—	257	—	—	—	238
Y	—	20	—	—	—	11
Zr	—	177	—	—	—	187
Nb	—	17	—	—	—	13
Ba	—	450	—	—	—	562
La	—	22	—	—	—	17
Ce	—	44	—	—	—	34
Pr	—	5.5	—	—	—	4.0
Nd	—	22	—	—	—	16
Sm	—	4.8	—	—	—	3.4
Eu	—	1.2	—	—	—	1.1
Gd	—	4.7	—	—	—	3.0
Tb	—	0.8	—	—	—	0.4
Dy	—	4.2	—	—	—	2.4
Ho	—	0.8	—	—	—	0.4
Er	—	2.0	—	—	—	1.2
Tm	—	0.3	—	—	—	0.2
Yb	—	1.8	—	—	—	1.1
Lu	—	0.3	—	—	—	0.2
Hf	—	4.6	—	—	—	4.5
Ta	—	1.3	—	—	—	1.7
Th	—	8.8	—	—	—	5.6

Table 5-1 Results of major and trace element analyses for the Gamano-Obatake Granodiotite.

	Gamano-Obatake Granodiorite					
Sample No.	09032208B	09032209A	09032210T	09071803	07100702	07120101
XRF						
SiO_2 (wt%)	69.43	75.01	61.24	69.18	69.76	67.47
TiO_2	0.48	0.07	0.96	0.49	0.65	0.58
Al_2O_3	15.47	14.00	17.07	15.10	15.43	15.50
Fe_2O_3	3.84	1.17	7.30	3.87	4.49	4.42
MnO	0.12	0.06	0.13	0.07	0.05	0.08
MgO	1.09	0.28	1.80	1.02	0.73	1.21
CaO	3.07	1.12	4.51	3.39	3.22	3.64
Na_2O	2.18	2.40	2.53	2.36	2.56	3.13
K_2O	3.79	5.25	2.62	3.55	1.91	2.96
P_2O_5	0.09	0.04	0.12	0.07	0.11	0.07
LOI	0.54	0.49	0.98	0.55	0.61	0.44
Total	100.09	99.91	99.27	99.65	99.53	99.51
A/CNK	1.17	1.20	1.12	1.09	1.27	1.04
ICP-MS						
Rb (ppm)	—	—	163	—	—	—
Sr	—	—	231	—	—	—
Y	—	—	27	—	—	—
Zr	—	—	313	—	—	—
Nb	—	—	31	—	—	—
Ba	—	—	560	—	—	—
La	—	—	47	—	—	—
Ce	—	—	92	—	—	—
Pr	—	—	11	—	—	—
Nd	—	—	42	—	—	—
Sm	—	—	8.6	—	—	—
Eu	—	—	1.2	—	—	—
Gd	—	—	7.3	—	—	—
Tb	—	—	1.1	—	—	—
Dy	—	—	5.6	—	—	—
Ho	—	—	1.0	—	—	—
Er	—	—	2.6	—	—	—
Tm	—	—	0.3	—	—	—
Yb	—	—	1.9	—	—	—
Lu	—	—	0.3	—	—	—
Hf	—	—	7.1	—	—	—
Ta	—	—	2.7	—	—	—
Th	—	—	15	—	—	—

Table 5-1 Results of major and trace element analyses for the Gamano-Obatake Granodiotite.

	Gamano-Obatake Granodiorite		
Sample No.	08031602	11100811	11100812
XRF			
SiO_2 (wt%)	60.15	66.32	68.01
TiO_2	0.93	0.67	0.52
Al_2O_3	18.48	15.79	15.28
Fe_2O_3	6.61	5.04	4.25
MnO	0.11	0.09	0.07
MgO	1.99	1.23	1.05
CaO	5.52	4.07	3.15
Na_2O	3.45	3.07	3.20
K_2O	2.06	2.41	3.39
P_2O_5	0.12	0.13	0.10
LOI	0.23	0.43	0.37
Total	99.65	99.25	99.38
A/CNK	1.03	1.05	1.04
ICP-MS			
Rb (ppm)	—	—	96
Sr	—	—	167
Y	—	—	17
Zr	—	—	135
Nb	—	—	10
Ba	—	—	482
La	—	—	28
Ce	—	—	57
Pr	—	—	6.6
Nd	—	—	25
Sm	—	—	5.1
Eu	—	—	1.0
Gd	—	—	4.1
Tb	—	—	0.6
Dy	—	—	3.4
Ho	—	—	0.6
Er	—	—	1.8
Tm	—	—	0.2
Yb	—	—	1.5
Lu	—	—	0.2
Hf	—	—	3.6
Ta	—	—	0.8
Th	—	—	9.9

Table 5-2 Results of major and trace element analyses for the Himurodake Quartz diorite.

	Himurodake Quartz diorite					
Sample No.	10060601A	10060601B	10060601E	10060601F	10060607	10060608
XRF						
SiO_2 (wt%)	52.79	56.11	58.27	57.15	57.62	59.83
TiO_2	0.99	1.03	0.90	1.02	1.01	0.90
Al_2O_3	16.09	16.83	16.24	16.66	17.35	16.21
Fe_2O_3	9.49	8.33	7.61	7.86	7.74	6.94
MnO	0.20	0.14	0.16	0.14	0.14	0.13
MgO	6.01	4.55	4.02	4.12	3.21	3.15
CaO	9.12	7.48	6.20	7.00	6.26	5.80
Na_2O	2.18	2.57	2.61	2.52	2.62	2.90
K_2O	1.40	1.41	2.00	1.96	1.79	2.89
P_2O_5	0.11	0.13	0.11	0.12	0.14	0.13
LOI	0.63	0.70	0.70	0.65	1.21	0.45
Total	99.01	99.28	98.81	99.21	99.09	99.33
A/CNK	0.74	0.87	0.92	0.88	0.98	0.88
ICP-MS						
Rb (ppm)	69	54	—	—	86	—
Sr	295	326	—	—	276	—
Y	33	26	—	—	22	—
Zr	121	132	—	—	138	—
Nb	9.2	10	—	—	11	—
Ba	272	249	—	—	291	—
La	23	25	—	—	22	—
Ce	51	53	—	—	47	—
Pr	6.0	6.0	—	—	5.2	—
Nd	25	20	—	—	21	—
Sm	6.4	4.5	—	—	4.6	—
Eu	1.1	1.0	—	—	1.2	—
Gd	6.3	5.4	—	—	4.2	—
Tb	1.1	0.7	—	—	0.7	—
Dy	6.1	4.2	—	—	4.0	—
Ho	1.2	0.8	—	—	0.8	—
Er	3.3	2.3	—	—	2.3	—
Tm	0.5	0.3	—	—	0.3	—
Yb	3.2	2.3	—	—	2.3	—
Lu	0.5	0.4	—	—	0.4	—
Hf	2.9	3.1	—	—	3.3	—
Ta	0.7	0.8	—	—	0.8	—
Th	8.8	9.9	—	—	9.3	—

Table 5-2 Results of major and trace element analyses for the Himurodake Quartz diorite.

	Himurodake Quartz diorite			
Sample No.	12050501	12050502	12050503	12050504A
XRF				
SiO_2 (wt%)	57.49	60.262	51.22	60.63
TiO_2	0.99	0.853	0.91	0.92
Al_2O_3	17.19	15.957	17.63	15.98
Fe_2O_3	7.91	6.76	9.14	7.35
MnO	0.14	0.118	0.17	0.13
MgO	3.83	3.172	5.28	3.78
CaO	7.08	5.776	8.55	6.15
Na_2O	2.78	2.875	3.10	2.56
K_2O	1.80	2.323	1.49	2.25
P_2O_5	0.13	0.118	0.13	0.12
LOI	0.85	0.70	0.99	0.61
Total	100.19	98.91	98.60	100.47
A/CNK	0.89	0.90	0.79	0.90
ICP-MS				
Rb (ppm)	74	130	68	90
Sr	253	217	240	220
Y	26	26	18	21
Zr	180	108	121	127
Nb	9.1	10	5.3	9.2
Ba	260	384	262	374
La	22	25	13	21
Ce	45	52	26	44
Pr	5.6	6.7	3.3	5.3
Nd	22	24	13	21
Sm	5.0	5.5	3.1	4.5
Eu	1.1	1.0	0.9	1.0
Gd	5.0	5.2	3.1	4.4
Tb	0.8	0.9	0.6	0.7
Dy	5.0	5.1	3.5	4.2
Ho	1.0	1.0	0.7	0.8
Er	2.8	2.9	2.0	2.4
Tm	0.4	0.4	0.3	0.4
Yb	2.7	2.7	1.9	2.3
Lu	0.4	0.4	0.3	0.4
Hf	4.5	3.1	3.3	3.4
Ta	0.7	0.9	0.3	0.8
Th	8.6	13	3.4	8.6

Table 5-3 Results of major and trace element analyses for the Kibe Granite.

	Kibe Granite					
Sample No.	09050201	09050202	09050203A	09050203B	09050203C	09050204A
XRF						
SiO_2 (wt%)	71.30	72.39	72.14	72.02	73.68	72.21
TiO_2	0.27	0.28	0.26	0.22	0.22	0.23
Al_2O_3	14.04	13.66	13.98	14.23	13.49	12.97
Fe_2O_3	2.05	2.16	1.99	1.80	1.83	1.94
MnO	0.03	0.04	0.03	0.02	0.03	0.03
MgO	0.50	0.53	0.49	0.45	0.45	0.46
CaO	1.47	1.31	1.44	1.42	1.41	1.20
Na_2O	2.63	2.52	2.65	2.89	2.71	2.72
K_2O	5.38	5.35	5.59	5.55	4.84	5.13
P_2O_5	0.08	0.09	0.08	0.07	0.07	0.07
LOI	0.50	0.54	0.40	0.36	0.43	0.55
Total	98.26	98.87	99.06	99.03	99.15	97.51
A/CNK	1.10	1.11	1.07	1.07	1.10	1.06
ICP-MS						
Rb (ppm)	—	—	—	239	221	276
Sr	—	—	—	111	94	82
Y	—	—	—	20	16	23
Zr	—	—	—	145	142	144
Nb	—	—	—	14	13	14
Ba	—	—	—	392	290	285
La	—	—	—	51	47	36
Ce	—	—	—	110	102	77
Pr	—	—	—	11	11	9.2
Nd	—	—	—	33	31	33
Sm	—	—	—	6.8	6.3	7.0
Eu	—	—	—	0.6	0.5	0.4
Gd	—	—	—	6.6	5.9	5.7
Tb	—	—	—	0.7	0.7	0.9
Dy	—	—	—	3.5	2.9	4.5
Ho	—	—	—	0.6	0.5	0.8
Er	—	—	—	1.7	1.4	2.3
Tm	—	—	—	0.3	0.2	0.3
Yb	—	—	—	1.7	1.4	2.4
Lu	—	—	—	0.3	0.2	0.4
Hf	—	—	—	3.9	3.8	4.4
Ta	—	—	—	1.5	1.8	3.1
Th	—	—	—	39	37	36

Table 5-3 Results of major and trace element analyses for the Kibe Granite.

	Kibe Granite					
Sample No.	09050204B	09050205	09050206	09050207A	09050207B	09050207T
XRF						
SiO_2 (wt%)	72.82	71.93	74.74	70.49	70.49	70.67
TiO_2	0.22	0.29	0.33	0.37	0.41	0.40
Al_2O_3	13.87	13.97	12.94	14.25	14.13	13.98
Fe_2O_3	1.76	2.36	2.17	2.73	3.09	2.92
MnO	0.03	0.04	0.04	0.04	0.05	0.04
MgO	0.44	0.59	0.59	0.83	0.92	0.86
CaO	1.36	1.53	1.44	2.08	2.24	2.11
Na_2O	2.77	2.76	2.94	2.60	2.68	2.61
K_2O	5.19	4.83	3.60	5.02	4.65	4.97
P_2O_5	0.07	0.08	0.03	0.10	0.11	0.09
LOI	0.41	0.53	0.34	0.41	0.72	0.32
Total	98.94	98.90	99.16	98.92	99.48	98.96
A/CNK	1.10	1.11	1.14	1.06	1.05	1.03
ICP-MS						
Rb (ppm)	283	248	—	254	—	—
Sr	90	107	—	125	—	—
Y	18	22	—	16	—	—
Zr	149	182	—	233	—	—
Nb	15	18	—	16	—	—
Ba	349	332	—	451	—	—
La	32	62	—	6	—	—
Ce	68	132	—	14	—	—
Pr	8.0	14	—	1.8	—	—
Nd	29	40	—	8	—	—
Sm	6.1	8.1	—	2.5	—	—
Eu	0.5	0.5	—	0.7	—	—
Gd	4.9	7.7	—	2.8	—	—
Tb	0.7	0.9	—	0.5	—	—
Dy	3.7	4.1	—	2.5	—	—
Ho	0.6	0.7	—	0.5	—	—
Er	1.7	1.7	—	1.4	—	—
Tm	0.2	0.2	—	0.2	—	—
Yb	1.6	1.5	—	1.4	—	—
Lu	0.3	0.2	—	0.2	—	—
Hf	4.5	4.7	—	6.0	—	—
Ta	2.2	2.0	—	0.9	—	—
Th	32	49	—	15	—	—

Table 5-3 Results of major and trace element analyses for the Kibe Granite.

	Kibe Granite					
Sample No.	09050208	08112202	09050209A	09050209B	09050210	09050211
XRF						
SiO_2 (wt%)	70.64	71.32	70.87	71.02	71.70	73.19
TiO_2	0.38	0.33	0.36	0.34	0.36	0.07
Al_2O_3	13.54	13.86	13.87	13.79	14.29	13.54
Fe_2O_3	2.85	2.47	2.69	2.53	2.72	0.46
MnO	0.04	0.04	0.05	0.04	0.05	0.01
MgO	0.79	0.72	0.72	0.68	0.76	0.12
CaO	1.78	1.79	1.79	1.68	1.91	0.74
Na_2O	2.57	2.90	2.57	2.59	2.66	2.15
K_2O	5.04	5.16	5.30	5.32	5.15	7.80
P_2O_5	0.11	0.10	0.10	0.09	0.09	0.06
LOI	0.55	0.60	0.40	0.51	0.38	0.24
Total	98.29	99.28	98.71	98.58	100.07	98.38
A/CNK	1.05	1.02	1.05	1.06	1.06	1.02
ICP-MS						
Rb (ppm)	219	242	—	—	280	—
Sr	121	122	—	—	116	—
Y	21	26	—	—	20	—
Zr	202	212	—	—	210	—
Nb	18	17	—	—	17	—
Ba	437	422	—	—	436	—
La	54	55	—	—	42	—
Ce	113	118	—	—	89	—
Pr	12	12	—	—	11	—
Nd	35	36	—	—	38	—
Sm	7.2	7.3	—	—	7.6	—
Eu	0.6	0.6	—	—	0.6	—
Gd	7.1	7.0	—	—	5.9	—
Tb	0.8	0.9	—	—	0.8	—
Dy	3.8	4.2	—	—	4.2	—
Ho	0.7	0.8	—	—	0.7	—
Er	1.7	2.1	—	—	2.0	—
Tm	0.2	0.3	—	—	0.3	—
Yb	1.4	2.0	—	—	2.0	—
Lu	0.2	0.3	—	—	0.3	—
Hf	5.0	5.6	—	—	6.4	—
Ta	1.5	1.7	—	—	1.7	—
Th	44	42	—	—	45	—

Table 5-3 Results of major and trace element analyses for the Kibe Granite.

	Kibe Granite					
Sample No.	09071802	07100704	08031601A	10042401	10042402T	10042403A
XRF						
SiO_2 (wt%)	70.71	70.79	70.57	70.24	71.30	72.10
TiO_2	0.36	0.39	0.34	0.38	0.34	0.32
Al_2O_3	13.91	13.83	13.78	14.27	14.02	13.94
Fe_2O_3	2.66	2.93	2.74	2.81	2.50	2.39
MnO	0.04	0.05	0.04	0.04	0.04	0.04
MgO	0.72	0.82	0.74	0.83	0.75	0.65
CaO	1.70	1.76	1.81	1.49	1.77	1.58
Na_2O	2.52	2.59	2.58	2.71	2.81	2.89
K_2O	5.59	4.82	4.89	5.18	5.29	5.29
P_2O_5	0.09	0.11	0.09	0.12	0.11	0.09
LOI	0.40	0.66	0.60	0.99	0.47	0.48
Total	98.70	98.74	98.18	99.06	99.40	99.78
A/CNK	1.05	1.09	1.07	1.12	1.03	1.04
ICP-MS						
Rb (ppm)	—	—	218	225	265	252
Sr	—	—	117	118	115	102
Y	—	—	23	28	17	24
Zr	—	—	204	208	195	183
Nb	—	—	17	16	17	14
Ba	—	—	403	430	446	442
La	—	—	45	82	27	50
Ce	—	—	95	177	57	110
Pr	—	—	10	19	6.3	12
Nd	—	—	29	56	24	45
Sm	—	—	5.9	11.2	5.4	8.9
Eu	—	—	0.5	0.6	0.6	0.6
Gd	—	—	6.0	10.3	4.5	6.6
Tb	—	—	0.7	1.2	0.7	0.9
Dy	—	—	3.7	5.3	3.4	4.5
Ho	—	—	0.7	0.9	0.6	0.8
Er	—	—	2.0	2.2	1.6	2.2
Tm	—	—	0.3	0.3	0.2	0.3
Yb	—	—	2.1	1.5	1.6	2.1
Lu	—	—	0.4	0.2	0.3	0.3
Hf	—	—	5.2	5.2	5.2	5.1
Ta	—	—	1.5	1.8	1.4	1.8
Th	—	—	47	70	29	52

Table 5-3 Results of major and trace element analyses for the Kibe Granite.

	Kibe Granite					
Sample No.	10042403C	10042404	10042405	10042406T	10042407	10042408
XRF						
SiO_2 (wt%)	77.04	69.70	73.18	71.76	70.84	71.37
TiO_2	0.11	0.42	0.09	0.34	0.37	0.30
Al_2O_3	13.68	14.39	14.29	13.89	13.99	14.19
Fe_2O_3	1.27	2.99	0.78	2.47	2.70	2.36
MnO	0.02	0.05	0.02	0.04	0.05	0.04
MgO	0.18	0.93	0.18	0.71	0.85	0.65
CaO	0.94	2.16	0.46	1.63	1.89	1.64
Na_2O	3.55	2.91	2.47	2.80	2.95	2.84
K_2O	3.81	4.78	7.43	4.90	4.75	5.31
P_2O_5	0.03	0.12	0.09	0.11	0.10	0.10
LOI	0.67	0.65	0.96	0.70	0.40	0.51
Total	101.31	99.09	99.97	99.35	98.90	99.31
A/CNK	1.17	1.04	1.10	1.08	1.04	1.06
ICP-MS						
Rb (ppm)	130	251	245	192	255	239
Sr	130	129	100	105	112	125
Y	20	22	14	25	18	22
Zr	83	254	59	165	184	178
Nb	9.2	16	3.9	13	18	16
Ba	631	448	480	366	403	468
La	25	58	25	48	45	50
Ce	49	147	50	103	94	108
Pr	5.3	13	5.9	11	10	11
Nd	19	46	17	32	34	34
Sm	3.9	8.9	3.9	6.5	6.6	6.9
Eu	0.5	0.8	0.5	0.5	0.6	0.6
Gd	3.5	6.6	3.9	6.6	5.1	6.7
Tb	0.6	0.9	0.5	0.8	0.7	0.8
Dy	3.5	4.5	2.6	4.0	3.7	3.9
Ho	0.7	0.8	0.4	0.8	0.6	0.7
Er	1.9	2.1	1.2	2.0	1.6	1.7
Tm	0.3	0.3	0.2	0.3	0.2	0.2
Yb	1.8	1.8	1.0	1.8	1.2	1.2
Lu	0.3	0.3	0.1	0.3	0.2	0.2
Hf	2.4	6.4	1.8	4.2	4.8	4.5
Ta	0.9	1.2	0.4	1.6	1.7	1.6
Th	7	49	13	47	26	43

Table 5-3 Results of major and trace element analyses for the Kibe Granite.

	Kibe Granite					
Sample No.	10042409	100424010	100424011T	10060601C	10060601D	11082603
XRF						
SiO_2 (wt%)	76.36	71.06	70.93	72.87	70.80	69.77
TiO_2	0.05	0.32	0.31	0.41	0.33	0.35
Al_2O_3	12.91	14.23	14.63	12.72	14.57	14.25
Fe_2O_3	0.91	2.47	2.32	3.23	2.45	2.63
MnO	0.03	0.04	0.03	0.06	0.05	0.05
MgO	0.05	0.67	0.59	1.04	0.80	0.79
CaO	0.97	1.66	1.40	2.26	2.47	1.98
Na_2O	3.33	2.93	2.69	2.98	3.09	2.66
K_2O	4.98	5.19	5.48	3.46	4.10	5.07
P_2O_5	0.01	0.11	0.08	0.11	0.08	0.10
LOI	0.27	0.41	0.97	0.44	0.45	0.43
Total	99.87	99.09	99.42	99.58	99.21	98.08
A/CNK	1.02	1.06	1.13	1.00	1.04	1.06
ICP-MS						
Rb (ppm)	—	278	—	—	187	—
Sr	—	110	—	—	138	—
Y	—	19	—	—	16	—
Zr	—	175	—	—	156	—
Nb	—	19	—	—	13	—
Ba	—	412	—	—	356	—
La	—	47	—	—	48	—
Ce	—	97	—	—	106	—
Pr	—	10	—	—	10	—
Nd	—	36	—	—	35	—
Sm	—	7.1	—	—	6.7	—
Eu	—	0.6	—	—	0.7	—
Gd	—	5.3	—	—	4.7	—
Tb	—	0.8	—	—	0.7	—
Dy	—	3.8	—	—	3.2	—
Ho	—	0.7	—	—	0.6	—
Er	—	1.8	—	—	1.4	—
Tm	—	0.2	—	—	0.2	—
Yb	—	1.5	—	—	1.2	—
Lu	—	0.2	—	—	0.2	—
Hf	—	4.6	—	—	3.8	—
Ta	—	1.6	—	—	1.8	—
Th	—	39	—	—	23	—

Table 5-3 Results of major and trace element analyses for the Kibe Granite.

	Kibe Granite	
Sample No.	11100809	11100810
XRF		
SiO_2 (wt%)	69.96	70.04
TiO_2	0.30	0.31
Al_2O_3	14.16	14.41
Fe_2O_3	2.45	2.28
MnO	0.05	0.04
MgO	0.55	0.64
CaO	1.75	1.55
Na_2O	2.96	2.58
K_2O	4.84	5.46
P_2O_5	0.19	0.08
LOI	0.43	0.91
Total	97.63	98.29
A/CNK	1.07	1.11
ICP-MS		
Rb (ppm)	—	—
Sr	—	—
Y	—	—
Zr	—	—
Nb	—	—
Ba	—	—
La	—	—
Ce	—	—
Pr	—	—
Nd	—	—
Sm	—	—
Eu	—	—
Gd	—	—
Tb	—	—
Dy	—	—
Ho	—	—
Er	—	—
Tm	—	—
Yb	—	—
Lu	—	—
Hf	—	—
Ta	—	—
Th	—	—

Table 5-4 Results of major and trace element analyses for the Namera Granite.

	Namera Granite					
Sample No.	08112201	09032201	09032202A	09032202B	09032203A	9032203B
XRF						
SiO_2 (wt%)	73.49	75.06	74.81	74.67	73.03	71.75
TiO_2	0.20	0.20	0.20	0.19	0.19	0.23
Al_2O_3	15.43	14.81	14.64	14.78	15.54	14.73
Fe_2O_3	2.16	1.99	2.04	1.83	1.88	2.27
MnO	0.11	0.06	0.06	0.06	0.05	0.06
MgO	0.63	0.59	0.60	0.52	0.54	0.67
CaO	1.90	1.71	1.94	1.84	1.75	1.91
Na_2O	2.77	2.57	2.83	2.77	2.86	2.71
K_2O	4.03	3.59	3.31	3.82	3.81	4.22
P_2O_5	0.07	0.05	0.06	0.06	0.05	0.06
LOI	0.61	0.98	0.55	0.52	0.98	0.60
Total	101.38	101.61	101.05	101.05	100.67	99.19
A/CNK	1.25	1.32	1.24	1.23	1.29	1.18
ICP-MS						
Rb (ppm)	—	176	168	—	—	—
Sr	—	140	141	—	—	—
Y	—	23	20	—	—	—
Zr	—	97	103	—	—	—
Nb	—	11	14	—	—	—
Ba	—	408	344	—	—	—
La	—	18	21	—	—	—
Ce	—	36	43	—	—	—
Pr	—	4.3	5.1	—	—	—
Nd	—	16	18	—	—	—
Sm	—	3.6	4.0	—	—	—
Eu	—	0.6	0.5	—	—	—
Gd	—	3.3	3.6	—	—	—
Tb	—	0.6	0.6	—	—	—
Dy	—	3.9	3.6	—	—	—
Ho	—	0.8	0.7	—	—	—
Er	—	2.3	2.0	—	—	—
Tm	—	0.4	0.3	—	—	—
Yb	—	2.6	2.1	—	—	—
Lu	—	0.5	0.4	—	—	—
Hf	—	3.0	3.2	—	—	—
Ta	—	2.6	2.9	—	—	—
Th	—	11	12	—	—	—

Table 5-4 Results of major and trace element analyses for the Namera Granite.

	Namera Granite					
Sample No.	09032203C	09032204A	09032204B	09032204C	09032205	09071801
XRF						
SiO_2 (wt%)	74.05	73.36	73.68	74.31	72.17	71.98
TiO_2	0.22	0.20	0.20	0.20	0.20	0.17
Al_2O_3	14.75	14.56	15.00	14.51	14.78	14.68
Fe_2O_3	2.19	2.07	2.18	1.99	1.94	1.73
MnO	0.06	0.07	0.09	0.06	0.06	0.05
MgO	0.65	0.61	0.64	0.59	0.58	0.51
CaO	2.02	1.70	1.94	2.00	1.97	1.92
Na_2O	2.73	2.51	2.68	2.75	2.72	2.72
K_2O	3.52	4.19	3.91	3.42	4.08	3.95
P_2O_5	0.07	0.08	0.06	0.06	0.06	0.07
LOI	0.57	0.62	0.55	0.54	0.49	0.55
Total	100.84	99.97	100.93	100.45	99.06	98.34
A/CNK	1.23	1.24	1.23	1.22	1.18	1.20
ICP-MS						
Rb (ppm)	170	205	—	—	—	—
Sr	149	132	—	—	—	—
Y	21	19	—	—	—	—
Zr	107	75	—	—	—	—
Nb	14	14	—	—	—	—
Ba	415	468	—	—	—	—
La	21	16	—	—	—	—
Ce	43	32	—	—	—	—
Pr	5.1	3.8	—	—	—	—
Nd	18	14	—	—	—	—
Sm	4.1	3.2	—	—	—	—
Eu	0.6	0.5	—	—	—	—
Gd	3.7	3.1	—	—	—	—
Tb	0.6	0.5	—	—	—	—
Dy	3.9	3.5	—	—	—	—
Ho	0.7	0.7	—	—	—	—
Er	2.1	1.9	—	—	—	—
Tm	0.3	0.3	—	—	—	—
Yb	2.3	1.9	—	—	—	—
Lu	0.4	0.3	—	—	—	—
Hf	3.3	2.3	—	—	—	—
Ta	2.2	3.3	—	—	—	—
Th	12	9.0	—	—	—	—

Table 5-4 Results of major and trace element analyses for the Namera Granite.

	Namera Granite	
Sample No.	09071805	07042901A
XRF		
SiO_2 (wt%)	72.49	73.32
TiO_2	0.21	0.19
Al_2O_3	15.40	14.53
Fe_2O_3	2.11	1.95
MnO	0.07	0.06
MgO	0.64	0.56
CaO	1.93	1.86
Na_2O	2.80	2.61
K_2O	3.76	3.88
P_2O_5	0.06	0.05
LOI	0.61	0.44
Total	100.08	99.45
A/CNK	1.26	1.22
ICP-MS		
Rb (ppm)	—	175
Sr	—	146
Y	—	19
Zr	—	94
Nb	—	12
Ba	—	481
La	—	19
Ce	—	39
Pr	—	4.6
Nd	—	17
Sm	—	3.8
Eu	—	0.6
Gd	—	3.4
Tb	—	0.6
Dy	—	3.4
Ho	—	0.7
Er	—	1.9
Tm	—	0.3
Yb	—	1.9
Lu	—	0.3
Hf	—	2.9
Ta	—	2.2
Th	—	11

Table 5-5 Results of major and trace element analyses for the Ryoke metamorphic rocks.

	Ryoke metamorphic rocks			
	Gamano-Obatake area			
Sample No.	09032207C	09032208C	09032209B	09032209C
XRF				
SiO_2 (wt%)	63.72	70.45	57.91	97.31
TiO_2	1.02	0.53	1.42	0.14
Al_2O_3	15.78	14.64	18.22	2.93
Fe_2O_3	6.35	3.92	8.94	1.23
MnO	0.09	0.05	0.13	0.02
MgO	2.52	1.39	2.68	0.40
CaO	3.87	2.78	7.75	0.07
Na_2O	2.28	2.28	1.35	0.45
K_2O	2.44	2.98	1.33	1.04
P_2O_5	0.14	0.05	0.15	0.02
LOI	1.11	0.52	0.25	0.31
Total	99.32	99.60	100.14	103.91
A/CNK	1.17	1.22	1.03	1.48
ICP-MS				
Rb (ppm)	130	135	155	—
Sr	344	221	317	—
Y	26	11	21	—
Zr	252	213	158	—
Nb	43	13	12	—
Ba	325	757	346	—
La	46	26	19	—
Ce	92	53	41	—
Pr	11	6.3	5.2	—
Nd	40	24	21	—
Sm	7.6	4.7	4.8	—
Eu	1.6	1.3	1.7	—
Gd	6.4	3.7	4.8	—
Tb	1.0	0.5	0.8	—
Dy	5.3	2.5	4.4	—
Ho	0.9	0.4	0.8	—
Er	2.5	1.1	2.1	—
Tm	0.4	0.2	0.3	—
Yb	2.2	1.0	1.7	—
Lu	0.4	0.2	0.2	—
Hf	6.2	5.4	3.8	—
Ta	3.7	1.3	0.6	—
Th	16	13	1.6	—

Table 5-5 Results of major and trace element analyses for the Ryoke metamorphic rocks.

	Ryoke metamorphic rocks				
	Himurodake area			Namera area	
Sample No.	10060602	10060606	10060609	10032101	10032102A
XRF					
SiO_2 (wt%)	64.86	64.95	81.48	66.32	66.22
TiO_2	1.20	0.83	0.36	0.69	0.69
Al_2O_3	14.04	15.84	8.21	16.18	15.16
Fe_2O_3	4.14	6.12	3.04	5.25	5.29
MnO	0.12	0.11	0.20	0.05	0.05
MgO	2.98	2.46	0.95	1.65	1.73
CaO	1.77	2.24	0.38	0.55	2.85
Na_2O	1.68	2.57	1.85	1.00	3.04
K_2O	3.82	3.05	2.16	4.70	2.17
P_2O_5	0.21	0.13	0.03	0.07	0.07
LOI	4.04	1.68	0.96	1.75	1.21
Total	98.87	99.98	99.62	98.22	98.48
A/CNK	1.39	1.36	1.35	2.09	1.21
ICP-MS					
Rb (ppm)	123	—	113	208	137
Sr	181	—	47	76	254
Y	28	—	21	37	13
Zr	178	—	100	124	183
Nb	31	—	9.3	22	11
Ba	1670	—	530	1000	212
La	40	—	25	39	27
Ce	80	—	59	77	53
Pr	8.8	—	5.3	9.3	6.1
Nd	33	—	19	35	22
Sm	6.7	—	4.1	8.6	4.3
Eu	1.3	—	0.7	0.9	1.1
Gd	5.9	—	3.6	7.0	3.3
Tb	0.9	—	0.6	1.2	0.5
Dy	5.1	—	3.5	6.9	2.6
Ho	1.0	—	0.7	1.3	0.5
Er	2.8	—	2.1	3.6	1.4
Tm	0.4	—	0.3	0.5	0.2
Yb	2.8	—	2.3	3.4	1.6
Lu	0.5	—	0.4	0.5	0.3
Hf	4.2	—	2.4	3.5	5.0
Ta	1.9	—	0.6	1.3	1.1
Th	12	—	11	15	13

Table 5-5 Results of major and trace element analyses for the Ryoke metamorphic rocks.

	Namera area	
Sample No.	10032102B	10032104A
XRF		
SiO_2 (wt%)	65.43	66.08
TiO_2	0.75	0.64
Al_2O_3	16.48	15.73
Fe_2O_3	5.36	4.80
MnO	0.04	0.05
MgO	1.42	1.61
CaO	0.94	1.20
Na_2O	1.54	1.93
K_2O	4.21	3.50
P_2O_5	0.09	0.06
LOI	2.10	2.50
Total	98.37	98.10
A/CNK	1.87	1.72
ICP-MS		
Rb (ppm)	—	—
Sr	—	—
Y	—	—
Zr	—	—
Nb	—	—
Ba	—	—
La	—	—
Ce	—	—
Pr	—	—
Nd	—	—
Sm	—	—
Eu	—	—
Gd	—	—
Tb	—	—
Dy	—	—
Ho	—	—
Er	—	—
Tm	—	—
Yb	—	—
Lu	—	—
Hf	—	—
Ta	—	—
Th	—	—

Table 5-6 Results of major and trace element analyses for the Migmatite.

	Migmatite				
	Nagano Migmatite			Tengatake Migmatite	
Sample No.	10032110	06061006A	06061006B	10050101A	10050101B
XRF					
SiO_2 (wt%)	70.33	66.55	67.72	76.52	77.01
TiO_2	0.30	0.64	0.63	0.24	0.44
Al_2O_3	14.40	14.66	14.07	12.42	11.43
Fe_2O_3	3.19	5.08	4.90	1.59	2.57
MnO	0.06	0.08	0.08	0.04	0.05
MgO	0.79	1.71	1.66	0.43	0.77
CaO	1.01	0.72	0.64	1.75	1.39
Na_2O	3.53	2.78	2.55	2.88	2.30
K_2O	4.87	5.44	5.38	3.03	3.30
P_2O_5	0.06	0.06	0.05	0.02	0.03
LOI	0.36	0.69	0.72	0.49	0.59
Total	98.90	98.41	98.38	99.41	99.88
A/CNK	1.11	1.25	1.26	1.11	1.16
ICP-MS					
Rb (ppm)	165	—	214	78	96
Sr	146	—	106	232	198
Y	23	—	26	7.8	8.6
Zr	244	—	184	111	155
Nb	28	—	15	5.9	12
Ba	725	—	848	1510	1750
La	43	—	41	33	40
Ce	84	—	79	62	73
Pr	10	—	9.4	6.8	8.3
Nd	34	—	33	23	29
Sm	7.0	—	6.5	3.7	4.7
Eu	1.2	—	1.0	1.5	1.5
Gd	5.5	—	5.0	2.6	3.2
Tb	0.9	—	0.8	0.3	0.4
Dy	4.7	—	4.7	1.6	2.0
Ho	0.9	—	0.9	0.3	0.3
Er	2.3	—	2.6	0.8	0.8
Tm	0.3	—	0.4	0.1	0.1
Yb	2.2	—	2.6	0.8	0.8
Lu	0.4	—	0.4	0.1	0.1
Hf	6.5	—	5.0	3.1	4.3
Ta	3.6	—	2.4	0.7	1.0
Th	13	—	16	10	11

Table 5-6 Results of major and trace element analyses for the Migmatite.

	Migmatite	
	Tengatake Migmatite	
Sample No.	10050102A	10050102B
XRF		
SiO_2 (wt%)	84.88	82.75
TiO_2	0.19	0.29
Al_2O_3	7.54	8.32
Fe_2O_3	2.03	2.61
MnO	0.12	0.14
MgO	0.85	0.99
CaO	0.65	0.54
Na_2O	1.35	1.09
K_2O	1.35	1.94
P_2O_5	0.04	0.04
LOI	1.03	1.07
Total	100.02	99.79
A/CNK	1.55	1.71
ICP-MS		
Rb (ppm)	76	101
Sr	71	66
Y	31	28
Zr	71	92
Nb	4.6	5.8
Ba	410	691
La	26	25
Ce	50	51
Pr	6.6	6.3
Nd	25	23
Sm	5.5	5.0
Eu	0.8	0.7
Gd	4.8	4.3
Tb	0.8	0.7
Dy	4.8	4.4
Ho	1.0	0.9
Er	2.9	2.7
Tm	0.4	0.4
Yb	2.8	2.7
Lu	0.4	0.4
Hf	2.1	2.8
Ta	1.0	1.2
Th	9.4	10

Table 6-1 Rb-Sr and Sm-Nd isotopic analyses for the Gamano-Obatake Granodiorite.

Sample No.	Rb (ppm)	Sr (ppm)	$^{87}Rb/^{86}Sr$	$^{87}Sr/^{86}Sr$	(2σ)	SrI (91 Ma)	εSrI (91 Ma)	Nd (ppm)	Sm (ppm)	$^{147}Sm/^{144}Nd$	$^{143}Nd/^{144}Nd$	(2σ)	NdI (91 Ma)	εNdI (91 Ma)
Gamano-Obatake Granodiorite														
09032206A	101	257	1.137	0.710307	12	0.708836	+63	22	4.8	0.1334	0.512322	13	0.512243	-5.4
09032208A	115	238	1.398	0.710771	10	0.708963	+65	16	3.4	0.1313	0.512286	14	0.512208	-6.1
09032210T	163	231	2.042	0.711749	13	0.709108	+67	42	8.6	0.1238	0.512318	13	0.512244	-5.4
11100812	96	167	1.664	0.710681	14	0.708530	+59	25	5.1	0.1214	0.512340	13	0.512268	-4.9

Table 6-2 Rb-Sr and Sm-Nd isotopic analyses for the Himurodake Quartz diorite.

Sample No.	Rb (ppm)	Sr (ppm)	$^{87}Rb/^{86}Sr$	$^{87}Sr/^{86}Sr$	(2σ)	SrI (91 Ma)	εSrI (91 Ma)	Nd (ppm)	Sm (ppm)	$^{147}Sm/^{144}Nd$	$^{143}Nd/^{144}Nd$	(2σ)	NdI (91 Ma)	εNdI (91 Ma)
Himurodake Quartz diorite														
10060601A	69	295	0.677	0.708514	12	0.707639	+46	25	6.4	0.1559	0.512419	13	0.512326	-3.8
10060601B	54	326	0.479	0.707161	11	0.706541	+31	20	4.5	0.1388	0.512446	14	0.512363	-3.1
10060607	86	276	0.902	0.707751	13	0.706585	+31	21	4.6	0.1349	0.512420	12	0.512340	-3.5
12050501	74	253	0.846	0.707567	14	0.706473	+30	22	5.0	0.1373	0.512429	14	0.512347	-3.4
12050502	130	217	1.733	0.708716	14	0.706475	+30	24	5.5	0.1366	0.512413	13	0.512332	-3.7
12050503	68	240	0.820	0.707500	14	0.706440	+29	13	3.1	0.1435	0.512471	14	0.512386	-2.6
12050504A	90	220	1.184	0.708596	14	0.707065	+38	21	4.5	0.1307	0.512406	14	0.512328	-3.8

Table 6-3 Rb-Sr and Sm-Nd isotopic analyses for the Kibe Granite.

Sample No.	Rb (ppm)	Sr (ppm)	$^{87}Rb/^{86}Sr$	$^{87}Sr/^{86}Sr$	(2σ)	SrI (91 Ma)	εSrI (91 Ma)	Nd (ppm)	Sm (ppm)	$^{147}Sm/^{144}Nd$	$^{143}Nd/^{144}Nd$	(2σ)	NdI (91 Ma)	εNdI (91 Ma)
Kibe Granite														
09050203B	239	111	6.236	0.718603	10	0.710539	+87	33	6.8	0.1240	0.512327	13	0.512253	-5.2
09050203C	221	94	6.810	0.719475	12	0.710669	+89	31	6.3	0.1235	0.512307	12	0.512233	-5.6
09050204A	276	82	9.751	0.721514	13	0.708905	+64	33	7.0	0.1292	0.512351	13	0.512274	-4.8
09050204B	283	90	9.109	0.720479	13	0.708701	+61	29	6.1	0.1296	0.512350	14	0.512273	-4.8
09050205	248	107	6.713	0.719102	11	0.710421	+86	40	8.1	0.1238	0.512344	11	0.512270	-4.9
09050207A	245	131	5.884	0.715532	12	0.708530	+50	8.5	2.8	0.1909	0.512398	13	0.512284	-4.6
09050208	219	121	5.241	0.716680	11	0.709903	+78	35	7.2	0.1238	0.512311	13	0.512237	-5.5
09050210	280	116	6.990	0.717307	9	0.708268	+55	38	7.6	0.1059	0.512359	13	0.512296	-4.4
08031601A	218	117	5.396	0.717000	12	0.710023	+80	29	5.9	0.1230	0.512338	12	0.512265	-5.0
08112202	242	122	5.744	0.717270	10	0.709842	+77	33	6.8	0.1236	0.512336	13	0.512262	-5.0
10042401	225	118	5.522	0.717030	12	0.709890	+78	56	11	0.1205	0.512310	13	0.512239	-5.5
10042402T	265	115	6.673	0.716621	12	0.707993	+51	24	5.4	0.1344	0.512350	13	0.512270	-4.9
10042403A	252	102	7.155	0.717477	12	0.708226	+54	45	8.9	0.1213	0.512358	12	0.512285	-4.6
10042403C	130	130	2.894	0.710936	11	0.707194	+40	19	3.9	0.1218	0.512334	13	0.512261	-5.1
10042404	251	129	5.634	0.715154	11	0.707870	+49	46	8.9	0.1183	0.512345	13	0.512275	-4.8
10042405	245	100	7.098	0.720831	11	0.711654	+103	17	3.9	0.1387	0.512311	10	0.512228	-5.7
10042406T	192	105	5.295	0.716745	11	0.709898	+78	32	6.5	0.1234	0.512345	13	0.512271	-4.9
10042407	255	112	6.593	0.716427	12	0.707902	+50	34	6.6	0.1018	0.512369	13	0.512308	-4.1
10042408	239	125	5.537	0.717375	12	0.710215	+83	34	6.9	0.1243	0.512331	10	0.512257	-5.1
100424010	278	110	7.319	0.717889	12	0.708425	+57	36	7.1	0.1206	0.512320	13	0.512248	-5.3
10060601D	187	138	3.922	0.712670	12	0.707598	+45	35	6.7	0.1147	0.512342	13	0.512274	-4.8

Table 6-4 Rb-Sr and Sm-Nd isotopic analyses for the Namera Granite.

Sample No.	Rb (ppm)	Sr (ppm)	$^{87}Rb/^{86}Sr$	$^{87}Sr/^{86}Sr$	(2σ)	SrI (91 Ma)	εSrI (91 Ma)	Nd (ppm)	Sm (ppm)	$^{147}Sm/^{144}Nd$	$^{143}Nd/^{144}Nd$	(2σ)	NdI (91 Ma)	εNdI (91 Ma)
Namera Granite														
09032201	176	140	3.639	0.713926	13	0.709220	+69	16	4	0.1386	0.512284	14	0.512201	-6.2
09032202A	168	141	3.449	0.713648	14	0.709188	+68	18	4	0.1325	0.512281	12	0.512202	-6.2
09032203C	170	149	3.303	0.713539	13	0.709268	+69	18	4	0.1341	0.512313	13	0.512233	-5.6
09032204A	205	132	4.496	0.714869	11	0.709055	+66	14	3	0.1393	0.512289	13	0.512206	-6.1
07042901A	175	146	3.470	0.713576	12	0.709089	+67	17	4	0.1378	0.512283	13	0.512201	-6.2

Table 6-5 Rb-Sr and Sm-Nd isotopic analyses for the Ryoke metamorphic rocks.

Sample No.	Rb (ppm)	Sr (ppm)	$^{87}Rb/^{86}Sr$	$^{87}Sr/^{86}Sr$	(2σ)	SrI (91 Ma)	εSrI (91 Ma)	Nd (ppm)	Sm (ppm)	$^{147}Sm/^{144}Nd$	$^{143}Nd/^{144}Nd$	(2σ)	NdI (91 Ma)	εNdI (91 Ma)
Ryoke metamorphic rocks														
Gamano-Obatake area														
09032207C	130	344	1.094	0.712939	12	0.711524	+101	40	8	0.1144	0.512277	14	0.512209	-6.1
09032208C	135	221	1.769	0.714777	12	0.712490	+115	24	5	0.1204	0.512274	13	0.512202	-6.2
09032209B	155	317	1.415	0.709073	14	0.707244	+40	21	5	0.1374	0.512408	12	0.512326	-3.8
Himurodake area														
10060602	123	181	1.967	0.713795	11	0.711251	+97	33	7	0.1231	0.512335	13	0.512262	-5.1
10060609	113	47	6.968	0.725132	13	0.716122	+167	19	4	0.1272	0.512114	12	0.512038	-9.4
Namera area														
10032101	208	76	7.933	0.726316		0.716059	+166	35	9	0.1501	0.512097		0.512008	-10.0
10032102A	137	254	1.562	0.718204		0.716184	+167	22	4	0.1203	0.512065		0.511993	-10.3
10032104A	151	153	2.857	0.713846		0.710152	+82	30	6	0.1169	0.511996		0.511927	-11.6

Table 6-6 Rb-Sr and Sm-Nd isotopic analyses for the Migmatite.

Sample No.	Rb (ppm)	Sr (ppm)	$^{87}Rb/^{86}Sr$	$^{87}Sr/^{86}Sr$	(2σ)	SrI (91 Ma)	εSrI (91 Ma)	Nd (ppm)	Sm (ppm)	$^{147}Sm/^{144}Nd$	$^{143}Nd/^{144}Nd$	(2σ)	NdI (91 Ma)	εNdI (91 Ma)
Migmatite														
Nagano Migmaite														
10032110	165	146	3.272	0.714870	12	0.710639	+89	34	7	0.1243	0.512387	12	0.512313	-4.1
06061006B	214	106	5.848	0.720209	6	0.712647	+117	33	7	0.1196	0.512062	11	0.511991	-10.4
Tengatake Migmatite														
10050101A	78	232	0.973	0.710146	13	0.708888	+64	23	4	0.0983	0.512339	13	0.512281	-4.7
10050101B	96	198	1.404	0.716363	11	0.714547	+114	29	5	0.0993	0.512300	9	0.512240	-5.5
10050102A	76	71	3.099	0.714858	12	0.710850	+92	25	6	0.1343	0.512217	10	0.512137	-7.5
10050102B	101	66	4.428	0.709363	11	0.703637	-11	23	5	0.1308	0.512235	8	0.512158	-7.1

Table 7-3-2-1 Melt compositions and restitic phases and their modal compositions. Data are taken from the melting experiments (Beard and Lofgren, 1991). D: dehydration melting, W: water-saturated melting. FeO* means total Fe as FeO. A/CNK-molar $Al_2O_3/(CaO+Na_2O+K_2O)$. Starting material is average of Gamano-Obatake Granodiorite: 09032206A, 09032208A, 09032210T, 11100812.

Pressure (kbar)	6.9	6.9	Starting material
Temprature (℃)	1000	800	
Condition	D	W	
Melt compositions (wt%)			
SiO_2	69.11	71.73	65.08
TiO_2	0.93	0.2	0.71
Al_2O_3	16.33	18.16	16.06
FeO*	4.2	1.16	5.49
MnO	0.04	0.07	0.10
MgO	0.5	0.1	1.35
CaO	3.8	5.01	3.87
Na_2O	3.36	2.82	2.82
K_2O	1.48	0.67	2.92
P_2O_5	0.24	0.09	0.11
A/CNK	1.16	1.25	1.08
Degree of melting (t%)			
F	27.8	44	
Restite modes (wt%)			
Plagioclase	45.7	17.9	
Clinopyroxene	39.5	0	
Oethopyroxene	12.2	0	
Amphibole	0	78.2	
Mgnetite	0	0	
Ilmenite	2.6	3.9	
Total	100	100	

Table 7-3-2-2 Mineral-melt partition coefficients using the model calculations in this dissertation. coefficients.

	Opx	Cpx	Amp	Grt	Pl	Mt	Ilm
Rb	0.022 [b]	0.013 [b]	0.04 [b]	0.01 [b]	0.053 [b]	0.01 [b]	0.01 [b]
Ba	0.013 [b]	0.04 [b]	0.1 [b]	0.02 [b]	0.155 [b]	0.01 [b]	0.01 [b]
Th	0.05 [b]	0.01 [b]	1.5 [b]	0 [b]	0.01 [b]	0.1 [b]	0.463 [d]
Ta	0.35 [b]	0.3 [b]	1.3 [b]	0 [b]	0.025 [b]	1 [b]	3.167 [d]
Nb	0.35 [a]	0.3 [a]	1.3 [a]	0 [a]	0.025 [a]	1 [b]	1 [b]
K	0.014 [b]	0.011 [b]	0.33 [b]	0.01 [b]	0.117 [b]	0.01 [b]	0.01 [e]
La	0.031 [d]	0.047 [d]	0.2 [c]	0.04 [c]	0.302 [d]	0.22 [c]	0.005 [c]
Ce	0.028 [d]	0.084 [d]	0.3 [c]	0.08 [c]	0.221 [d]	0.26 [c]	0.006 [c]
Sr	0.032 [b]	0.033 [b]	0.23 [b]	0.02 [b]	1.6 [b]	0.01 [b]	0.01 [b]
Nd	0.028 [d]	0.183 [d]	0.8 [c]	0.2 [c]	0.149 [d]	0.3 [c]	0.008 [c]
Zr	0.045 [a]	0.162 [a]	0.4 [b]	0.5 [b]	0.013 [a]	0.2 [a]	0.3 [e]
Hf	0.051 [d]	0.173 [b]	0.4 [b]	0.5 [b]	0.015 [d]	0.4 [b]	1.883 [d]
Sm	0.028 [d]	0.377 [d]	1.1 [c]	1 [c]	0.102 [d]	0.35 [c]	0.01 [c]
Eu	0.028 [d]	0.681 [d]	1.3 [c]	0.98 [c]	1.214 [d]	0.26 [c]	0.007 [c]
Gd	0.039 [d]	0.583 [d]	1.8 [c]	3.8 [c]	0.067 [d]	0.32 [c]	0.017 [c]
Dy	0.076 [d]	0.774 [d]	2 [c]	11 [c]	0.05 [d]	0.28 [c]	0.028 [c]
Y	0.45 [a]	1.5 [a]	2.5 [a]	11 [a]	0.06 [a]	0.5 [a]	0.01 [e]
Er	0.153 [d]	0.708 [d]	1.9 [c]	16 [c]	0.045 [d]	0.22 [c]	0.046 [c]
Yb	0.254 [d]	0.633 [d]	1.7 [c]	21 [c]	0.041 [d]	0.18 [c]	0.077 [c]
Lu	0.323 [d]	0.665 [d]	1.5 [c]	21 [c]	0.039 [d]	0.18 [c]	0.1 [c]

Source date: [a] Pearce and Norry (1979), [b] Gill (1981), [c] Martin (1987), [d] Rollinson (1993), [e] interpolated or extrapolated. Opx: orthopyroxene, Cpx: clinopyroxene, Amp: amphibole, Grt: garnet, Pl: plagioclase, Mt: magnetite, Ilm: ilmenite.